

Extraction and controlled functionalization of lignin for materials applications

Présentée le 17 juin 2022

Faculté des sciences de base
Laboratoire des procédés durables et catalytiques
Programme doctoral en chimie et génie chimique

pour l'obtention du grade de Docteur ès Sciences

par

Stefania BERTELLA

Acceptée sur proposition du jury

Prof. S. Gerber, présidente du jury
Prof. J. Luterbacher, directeur de thèse
Prof. O. Rojas, rapporteur
Prof. J. Ralph, rapporteur
Prof. E. Amstad, rapporteuse

Acknowledgements

My deepest gratitude goes first and foremost to my supervisor, Prof. Jeremy Luterbacher. Thank you for having given me the chance and the trust to freely explore my ideas. You guided me with patience and passion throughout this journey, had my back whenever I needed it, encouraged me at all times and most importantly taught me that no line is ever thick enough on a scientific figure! I really couldn't have wished for a better mentor, and I am truly proud of having been part of your research group.

Throughout my youth I have also had the privilege of being taught by admirable teachers, who gave me the best education and support for my next challenges, and without whom I would have never considered a career in science. Amongst them, I am endlessly grateful to my high school chemistry teacher, Prof. Bruno Neroni, the very first person who instilled in me the passion for science.

I'm lucky to have endured this journey with my labmates at the LPDC. Whilst I am really grateful to each and everyone for the time that we spent together (a bit less when I had to use my safety officer powers!), some people have been not just colleagues, but also good friends and family. Lorenz, thank you for being a patient brother and my best friend in the lab. I've always admired your enthusiasm, your endless care for people, and how great of a scientist you are. I can't really express how thankful I am for your friendship. Jess, thank you for having shared with me all the best, funniest and weirdest moments of my journey in Lausanne, for the great music suggestions, and for having introduced me to your awesome family. Claire, Jean, Max, Louisa, Chloe, Songlan, Ana, YP and Wu, thank you for all the laughter, the singing in the lab, the hikes, the rowing sessions, the coffee breaks, the cake-dates, the scientific discussions, for being patient when I had the "tête des mauvais jours", and most importantly for being incredible friends and a family far from home when I couldn't travel back to mine. I care for you more than you know.

Much of the work of this thesis would have been way harder without the help of many other brilliant scientists. Thanks to Dr. Aurelien Bornet, Dr. Vijay Kumar Rana, Dr. Peyman Karami and Gaia De Angelis for all their invaluable help, patience and suggestions. Big thanks also to Anna Bosch Rico and Malcolm Mourez, my talented master students, for all their hard work, which is partly included in this thesis. In addition to them, I'm thankful to Prof. John Ralph, Prof. Orlando Rojas, Prof. Esther Amstad and Prof. Sandrine Gerber for having examined my doctoral work and provided me with excellent feedbacks. It was an absolute privilege to be evaluated by world leading scientists whose inspiring work I've always admired.

I am very lucky that my time at EPFL was filled with the presence of so many friends. Marina, we've gone through many of each other's highs and lows (and always survived!). Your friendship has meant a lot to me during this time. Sofya, you're such a great person and I'm grateful that our paths crossed. Your sunshine and the many adventures we dragged each other into have been some of the best highlights of the past year. AK, Robbie, Gus, Charles, Amy, Yuliy, Christi, Patrick and Daisy, thanks for having let me be a part of your improv shows. You all brought me so much laughter and distraction when I needed it the most.

I can't end this journey without also acknowledging the people who have cared about me from further away. Mari, a simple thank you won't be enough to say how grateful I am for your friendship and all that you've done for me, especially for not giving up on the idea that I should pursue a PhD. Thanks also to your family for having me around so many times and of course to Hippo, the best dog on the planet, for cheering me up every time we meet. You deserve all the best sticks! Thanks to Luca, without whom I would have not been at EPFL, Taina, Laura, Andreas and to all the other friends I met in Stockholm and Helsinki that despite the distance never ceased to root and care for me. Most importantly, thanks to all my friends in my hometown Rio Saliceto, who have been a constant rock throughout my life.

Finally I thank my parents, Maria and Giuliano, and all my extended family. I'm aware of the patience and the sacrifice it took to have me far from home for many years (and some more to come!) and I would have never made it this far without your love. I dedicate this work to you.

Abstract

Lignin is a renewable aromatic polymer that due to its abundance and unique chemical structure is a promising candidate to replace aromatic materials that are currently sourced from fossil oil. The same structure of lignin poses however drawbacks for its valorization. The high temperature and strong pH that are generally used to isolate lignin, make this polymer prone to reactions of condensation during its extraction. This translates into isolated lignins where most of their native functional groups are eliminated in favour of the formation of interunit carbon-carbon linkages. The lack of control on lignin's chemical functionalities ultimately hinders the use of this polymer for the development of new materials.

Many research groups have been trying to tackle these challenges by developing new processes that could allow for the efficient isolation of lignin without compromising on its functional groups. Amongst these, the Aldehyde-Assisted Fractionation (AAF), which relies on the formation of acetal groups between lignin's β -O-4 units and an added aldehyde, was proven to be efficient in isolating high yields of lignin, that could be then quantitatively depolymerized into small aromatic monomers.

Inspired by this research, the aim of my work is to take advantage of the AAF to quantitatively isolate lignin from lignocellulose, at the same time introducing on the biopolymer scaffold new functional groups that could allow for more effective development of lignin-based materials. My work is based on a Multifunctional-AAF, in which the multifunctional aldehydes can react with the lignin via the formation of acetals, at the same time leaving on the biopolymer additional functionalities.

In the first part of my thesis, I show how the extraction and simultaneous functionalization of lignin can be achieved by using terephthalic aldehyde (TALD). In addition to successfully functionalizing the lignin, I demonstrate how the degree of functionalization can be precisely controlled and monitored via ^1H NMR, yielding a material with high reactivity towards phenolation.

In the second part, I show how the isolation and controlled functionalization of lignin can be translated to the use of other aldehydes, namely glyoxylic acid (GA), to functionalize lignin with carboxylates, quantified via ^{31}P NMR. The isolated lignin offers in this case unique avenues for the development of more sustainable surfactants.

In the last chapter of the thesis, I show that the Multifunctional-AAF can be expanded to isolate and functionalize lignin with multiple functionalities by using mixtures of aldehydes (TALD and GA), demonstrating again that each functional group can be easily quantified. These lignins, extracted with different ratios of the two functional groups, showed dissimilar properties in terms of solubility and reactivity towards gelatin. We used these lignins to develop lignin-gelatin based hydrogels, showing how the bi-functionalization was pivotal for the formation of hydrogels with improved rheological, mechanical, self-healing and adhesive properties.

In summary, this thesis shows the development of a new approach for lignin extraction and simultaneous valorization. The versatility of this process enables more efficient functionalization, allowing the obtainment of lignins which are “tailor-made” for their end use. The control over lignin’s chemical structure and functionalization will pave the way for the use of lignin in high-end applications.

Keywords

Lignin, lignocellulosic biomass, aldehydes, fractionation, nuclear magnetic resonance, hydrogels, phenolation, surfactants, bio-based materials, biorefinery.

Résumé

La lignine est un polymère aromatique renouvelable, qui, par son abondance et sa structure chimique unique, est un candidat prometteur pour le remplacement des matériaux aromatiques actuellement issus de sources fossiles. Cependant, cette même structure aromatique de la lignine est source de difficultés pour sa valorisation. En effet, les conditions sévères de pH et de température utilisées pour son extraction favorisent la condensation et la repolymérisation de la lignine. Cela conduit à l'obtention de lignines condensées, où des liaisons carbone-carbone ont remplacé la plupart des groupes fonctionnels originels. Ce manque de contrôle des fonctionnalités chimiques de la lignine freine la valorisation de ce polymère vers le développement de nouveaux matériaux.

Plusieurs groupes de recherche ont tenté de relever ces défis en développant des nouveaux procédés qui pourraient permettre d'isoler efficacement la lignine sans compromettre ses fonctionnalités chimiques. Parmi eux, le fractionnement assisté par aldéhyde (AAF), qui repose sur la formation de groupements acétal entre les liaisons β -O-4 de la lignine et un aldéhyde ajouté, s'est avéré très efficace. Il permet d'isoler de hauts rendements de lignine, qui peut ensuite être dépolymérisée en monomères aromatiques.

Inspirée par cette recherche, le but de mon projet est de tirer profit de l'AAF afin d'isoler quantitativement la lignine de la lignocellulose et d'y introduire simultanément de nouveaux groupements fonctionnels. Cela faciliterait le développement de matériaux à base de lignine. Mon travail se base sur un AAF multifonctionnel. Les aldéhydes multifonctionnels réagissent avec la lignine par la formation d'acétal, introduisant dans le même temps de nouvelles fonctionnalités sur le squelette du biopolymère.

Dans la première partie de ma thèse, je démontre comment il est possible d'extraire et de fonctionnaliser la lignine simultanément avec l'utilisation de l'aldéhyde téréphtalique

(TALD). En plus d'y parvenir, je prouve que le degré de fonctionnalisation peut être contrôlé et mesuré par ^1H RMN. Le matériau obtenu présente une grande réactivité avec les phénols.

Dans la seconde partie, j'applique ce procédé d'extraction et de fonctionnalisation de la lignine à d'autres aldéhydes, notamment l'acide glyoxylique (GA) qui permet d'introduire des carboxylates, quantifiés par ^{31}P RMN. La lignine isolée offre des possibilités uniques pour le développement de tensio-actifs bio-basés.

Dans le dernier chapitre de la thèse, je démontre que l'AAF multifonctionnel peut être étendu aux mélanges d'aldéhydes (TALD et GA) afin d'isoler et de fonctionnaliser la lignine avec plusieurs fonctionnalités chimiques facilement quantifiées. Ces lignines, extraites avec différents ratios des deux groupements fonctionnels, ont démontré des propriétés différentes de solubilité et de réactivité avec la gélatine. Nous les avons utilisées pour développer, grâce à la bi-fonctionnalisation, des hydrogels aux propriétés rhéologiques, mécaniques, d'auto-réparation et adhésives améliorées.

En résumé, cette thèse illustre le développement d'une nouvelle approche pour l'extraction et la valorisation simultanée de la lignine. Ce procédé versatile permet une fonctionnalisation plus efficace et l'obtention de lignines « sur-mesure » pour leur application finale. Ce contrôle sur la structure chimique et la fonctionnalisation de la lignine ouvre la voie au développement de produits haute performance à base de lignine.

Mots-clés

Lignine, lignocellulose, aldéhydes, fractionnement, résonance magnétique nucléaire, hydrogels, phénolation, tensio-actifs, matériaux bio-basés, bioraffinerie.

Riassunto

La lignina è un polimero aromatico rinnovabile che, grazie alla sua abbondanza e alla sua particolare struttura chimica, è considerato un candidato promettente per sostituire materiali aromatici ad oggi provenienti da petrolio.

La struttura della lignina rappresenta tuttavia il principale inconveniente per la sua valorizzazione. Le condizioni estreme in termini di temperatura e pH che vengono generalmente usate per isolare la lignina rendono questo polimero soggetto a reazioni di condensazione durante la sua estrazione. Molti dei suoi gruppi funzionali originari vengono quindi eliminati, favorendo la formazione di legami carbonio-carbonio. La mancanza di controllo sulle funzionalità chimiche della lignina ne ostacola quindi l'utilizzo nello sviluppo di nuovi materiali.

Recentemente molti gruppi di ricerca hanno cercato di affrontare le sfide dell'estrazione della lignina, sviluppando nuovi processi con l'intento di consentirne un isolamento efficace senza comprometterne le funzionalità chimiche. Il Frazionamento Assistito da Aldeidi (AAF), che si basa sulla formazione di acetali tra i legami β -O-4 della lignina e un'aldeide introdotta nella reazione, è un metodo efficace per isolare lignine che possono essere poi depolimerizzate quantitativamente in monomeri aromatici.

L'obiettivo della mia tesi di dottorato è quindi quello di sfruttare il processo AAF per isolare quantitativamente la lignina dalla biomassa, introducendo su questo polimero nuovi gruppi funzionali al fine di ottenere un migliore sviluppo di materiali aromatici. Il mio lavoro si basa sull'uso aldeidi multifunzionali. Queste molecole, infatti, da una parte formano acetali con la lignina, mentre dall'altra lasciano sul polimero nuove funzionalità.

Inizierò quindi dimostrando come la lignina possa essere estratta e funzionalizzata usando aldeide tereftalica (TALD). Oltre ad inserire sulla lignina gruppi aldeidici, dimostrerò come il

grado di funzionalizzazione possa essere controllato tramite ^1H NMR. La lignina così ottenuta presenta un'alta reattività in reazioni di fenolazione.

Successivamente dimostrerò come questa idea possa essere trasferita anche all'uso di altre aldeidi, ovvero l'acido gliossilico (GA), per funzionalizzare la lignina con acidi carbossilici, quantificati tramite ^{31}P NMR. Questa lignina offre possibilità uniche per lo sviluppo di tensioattivi sostenibili.

Infine, mostrerò come il processo di frazionamento AAF possa essere usato per isolare e modificare lignine con molteplici funzionalità utilizzando miscele di aldeidi. Anche in questo caso dimostrerò che ciascun gruppo funzionale può essere quantificato. Queste lignine, estratte con rapporti differenti tra i due gruppi funzionali, mostrano proprietà di solubilità e reattività diverse nei confronti di soluzioni contenenti gelatina. Queste lignine sono state infatti usate per sviluppare idrogel a base di lignina e gelatina, dimostrando come la doppia funzionalizzazione sia fondamentale per formare idrogel con migliori proprietà reologiche, meccaniche, adesive e autorigeneranti.

In sintesi, questa tesi mostra lo sviluppo di un nuovo processo per l'estrazione e valorizzazione di lignina. La versatilità di questo metodo permette una migliore funzionalizzazione, consentendo di ottenere di lignine “su misura” in base al loro uso finale. La possibilità di controllare la struttura chimica e la funzionalizzazione della lignina aprirà la strada al suo uso in applicazioni di materiali di fascia alta.

Parole chiave

Lignina, biomassa lignocellulosica, aldeidi, frazionamento, risonanza magnetica nucleare, idrogel, fenolazione, tensioattivi, biomateriali, bioraffineria.

Contents

Acknowledgements.....	v
Abstract.....	vii
Keywords.....	viii
Résumé	ix
Mots-clés.....	x
Riassunto	xi
Parole chiave.....	xii
List of Abbreviations.....	xvii
List of Figures.....	xx
List of Tables.....	xxv
List of Equations.....	xxvi
Chapter 1 Introduction.....	1
1.1 Climate change: challenges and opportunities	1
1.2 Sustainable sources of carbon for energy and material production.....	3
1.3 Lignocellulosic biomass: a renewable feedstock from non-edible crops.....	5
1.3.1 Cellulose	7
1.3.2 Hemicelluloses.....	8
1.3.3 Lignin.....	9
1.4 Lignin’s challenging characterization	15
1.5 Lignin extraction and its effects on structural features	17
1.6 The challenges of using isolated lignin as a raw material.....	20
1.7 Strategies for incorporating lignin into novel materials and polymers	21
1.7.1 Functionalization of the aromatic rings	22
1.7.2 Reaction of phenolic and aliphatic hydroxyl groups	24

1.7.3	Reaction of aliphatic hydroxyl groups	26
1.8	Concluding remarks	27
Chapter 2	Objectives.....	29
2.1	Objective 1: Extraction and simultaneous chemical functionalization of lignin from lignocellulosic biomass.....	29
2.2	Objective 2: Characterization of extracted lignins for their controlled chemical functionalization.	30
2.3	Objective 3: Exploiting extracted multifunctionalized lignins in materials applications.....	31
Chapter 3	One-step extraction and controlled functionalization of lignin for phenolation reactions.....	32
3.1	Introduction	32
3.2	Lignin extraction and characterization	35
3.3	Controlling and quantifying the degree of TALD functionalization on isolated lignin.....	40
3.4	Phenolation of TALD-lignin	41
3.5	Concluding Remarks	46
Chapter 4	Extraction and Surfactant Properties of Glyoxylic Acid Functionalized Lignin 48	
4.1	Introduction	48
4.2	Extraction and Characterization of Glyoxylic acid functionalized lignin.....	50
4.3	Surface Tension Measurements.....	52
4.4	Microscopy Imaging of water-Mineral Oil emulsions over time.....	54
4.5	Preparation of a hand-cream formulation using GA-lignin as surfactant.	57
4.6	Surface tension comparison of GA-lignin with other lignin-based and industrial surfactants.....	58
4.7	Concluding Remarks	60
Chapter 5	Extraction of bi-functionalized lignin for controlling properties of gelatin-based hydrogels	62
5.1	Introduction	62
5.2	Lignin Extraction and Characterization	66
5.3	Hydrogel preparation and rheological studies.....	67
5.4	Mechanical, adhesive, and self-healing properties of prepared hydrogels.....	71

5.5	Cytotoxicity and bacterial toxicity	75
5.6	Concluding remarks	75
Chapter 6	Conclusion	77
6.1	Summary of the work	77
6.2	Outlook	78
Appendix A	Appendix for Chapter 3.....	80
Appendix B	Appendix for Chapter 4.....	97
Appendix C	Appendix for Chapter 5.....	107
References		124
Curriculum Vitae		136

List of Abbreviations

1,4-DNB	1,4-Dinitrobenzene
2D-NMR	Bidimensional Nuclear Magnetic Resonance
4CL	4-Coumarate-CoA ligase
5-HMF	5-Hydroxymethyl furfural
AAF	Aldehyde assisted fractionation
APH	Acid catalysed phenolation
ATRP	Atom Transfer Radical Polymerization
BHT	Butylated hydroxytoluene
BPH	Base-Catalysed Phenolation
C3H	<i>p</i> -Coumarate 3-hydrosylase
C4H	Cinnamate 4-hydrosylase
CAD	Cinnamyl alcohol dehydrogenase
CCoAOMT	Caffeoyl-CoA <i>O</i> -methyltransferase
CCR	Cinnamoyl-CoA reductase
CEL	Cellulolytic enzyme lignin
CoA	Coenzyme A
COMT	Caffeic acid <i>O</i> -methyltransferase
DLS	Dynamic light scattering
DMSO	Dimethyl sulfoxide
DOSS	Sodium dioctyl sulfosuccinate
DOSY-NMR	Diffusion Ordered Spectroscopy nuclear magnetic resonance
DP	Degree of polymerization
DRIFT	Diffuse Reflectance Infrared Fourier Transform
F5H	Ferulate 5-hydroxylase
FA	Formaldehyde

FID	Flame-ionization detector
G	Guaiacyl unit
G'	Storage shear modulus
G''	Loss shear modulus
GA	Glyoxylic acid
GC	Gas chromatography
GHG	Greenhouse gases
GPC	Gel-permeation chromatography
GST	Global Surface Temperature
H	<i>p</i> -Hydroxyphenyl unit
HCT	Hydroxycinnamoyl-CoA shikimate/quinic acid hydroxycinnamoyltransferase
HSQC	Heteronuclear Single Quantum Coherence
HSQC ₀	Extrapolated time-zero Heteronuclear Single Quantum Coherence
IPCC	International Panel for Climate Change
IR	Infrared
KL	Kraft Lignin
LPF	Lignin-phenol-formaldehyde
LVER	Linear viscoelastic region
MALDI-MS	Matrix-Assisted Laser Desorption/Ionization mass spectrometry
MALS	Multi-angle light scattering detectors
M _n	Number average molecular weight
MTS	3-(4,5-dimethylthiazol-2-yl)-5-(3 carboxymethoxyphenyl)-2-(4-sulfophenyl)-2H- tetrazolium
M _w	Weight average molecular weight
MWL	Milled wood lignin
NHND	<i>N</i> -Hydroxy-5-norbornene-2,3-dicarboximide
NMR	Nuclear magnetic resonance
OSL	Organosolv Lignin

PA	Propionaldehyde
PAL	Phenylalanine ammonia-lyase
PAM	Polyacrylamide
PAN	Polyacrylonitrile
PBS	Phosphate-buffered saline
PEG	Polyethylene glycol
PEGDGE	Poly(ethylene)-glycol diglycidyl ether
PF	Phenol-formaldehyde
PID	Proportional–integral–derivative controller
<i>p</i> -TsOH	<i>p</i> -Toluenesulfonic acid
RAFT	Reversible addition-fragmentation chain transfer
S	Syringyl unit
SDBS	Sodium dioctyl sulfosuccinate
SDS	Sodium dodecylbenzene sulfonate
T_1	Longitudinal relaxation time
T_2	Transverse relaxation time
TALD	Terephthalic aldehyde
TALD-lignin	Terephthalic aldehyde functionalized lignin
TALDX	Terephthalic aldehyde functionalized xylose
THF	Tetrahydrofuran
TMDP	2-Chloro-4,4,5,5-tetramethyl-1,3,2-dioxaphospholane

List of Figures

Figure 1.1. Changes in Global Surface Temperature in the period 1850-2019 and in function of the Cumulative CO₂ emissions for the same period of time. The light-blue line refers to a simulated GST change by taking in consideration only natural factors. The red line indicates the simulation of GST changes considering both anthropogenic activities and natural factor. The dark blue line indicates the observed average GST changes. The grey area shows the cumulative CO₂ released in the atmosphere in GtCO₂ from 1850 to 2019. Data were extracted from the The Sixth Assessment Report published in 2021 by the International Panel for Climate Change (IPCC)⁷. . 2

Figure 1.2. Global direct primary energy consumption in 2019 (A). Global Carbon demand for chemicals and derived materials in 2020 (B) and forecast for 2050 (C). Data for pie-chart A are taken from Smil.¹⁴ Data for pie-charts B and C are taken from Vogt.¹³ 3

Figure 1.3. Schematic representation of photosynthesis in plants. 4

Figure 1.4. Overview of the structure of lignocellulosic biomass showing microfibrils and microfibrils constituted of cellulose (light blue), hemicellulose (brown) and lignin (green). 6

Figure 1.5. The pathway for the biosynthesis of p-coumaryl (grey path), coniferyl (blue path), and sinapyl (red path) alcohols. In the figure the enzyme involved in the synthesis are indicated as PAL: phenylalanine ammonia-lyase, C4H: cinnamate 4-hydrosylase, 4CL: 4-coumarate-CoA ligase, C3H: p-coumarate 3-hydroxylase, HCT: Hydroxycinnamoyl-CoA shikimate/quinic acid hydroxycinnamoyltransferase, CCoAOMT: caffeoyl-CoA O-methyltransferase, CCR: cinnamoyl-CoA reductase, F5H: ferulate 5-hydroxylase, COMT: caffeic acid O-methyltransferase, CAD: cinnamyl alcohol dehydrogenase. Figure reproduced from Vanholme et al.⁷¹ 10

Figure 1.6. Reactions and potential lignin structures arising from the lignification process. a) resonance structures of radicals formed on the p-coumaryl (H), Sinapyl alcohol (S) and Coniferyl alcohol (G). b) dimerization of radical monolignols at the β position. c) The lignification process and coupling of oligomers. d) Potential hardwood lignin structure. c) Structure of C-lignin as reported by Li et al.⁷⁹. In the figure different linkages are indicated by different colors. In particular the β -O-4 linkage is

in light blue, β - β in violet, β -5 in green, 5-5 in dark purple, 5-O-4 in orange and benzodioxanes linkages in red..... 13

Figure 1.7. Common catalysts, side-reactions and resulting chemical structures of extracted lignins. In the figure Kraft lignin is presented in the top pathway, Lignosulfonates in the light blue/grey pathway, Organosolv lignin in the light/blue and red pathway and finally the Aldehyde-stabilized lignin is obtained following the bottom pathway..... 19

Figure 1.8. Possible chemical modifications of the lignin backbone. Functionalization of the aromatic rings are presented in the blue box, functionalization concerning both phenolic and aliphatic hydroxyl groups are shown in the grey box, and finally functionalization reactions that occurs only on the hydroxyl groups of lignin are shown in the red box. 23

Figure 3.1. The structure of hardwood lignin and overview on the functionalization process of this chapter. (a) Proposed structure of native lignin in hardwood. (b) The mechanism of condensation and repolymerization reactions of lignin treated in strong acid conditions. (c) The TALD assisted fractionation mechanism and lignin structure described in this work. (d) The phenolation reactions of lignin performed in this work.35

Figure 3.2. (a) The chemical structure of the synthesized model compounds and its ^1H NMR spectrum. (b) The chemical structure of the main structural features of lignin functionalized with terephthalic aldehyde (TALD-lignin) and its ^1H NMR and (c) HSQC NMR spectra..... 37

Figure 3.3. DRIFT spectra of formaldehyde and lignin functionalized with terephthalic aldehyde (TALD-lignin). 40

Figure 3.4. Effect of initial TALD concentration over final functionalization..... 41

Figure 3.5. Acid and basic phenolation of lignin functionalized with terephthalic aldehyde (TALD-lignin). (a) Presumed reaction mechanism. Peak growth in the aromatic region of the HSQC spectra before (b) and after phenolation in acid (c) and basic (d) conditions. Peak colours in panels (b-d) correspond to functionalities depicted in (a). (e) DRIFT spectra of TALD-lignin before and after phenolation. 43

Figure 3.6. Characterization of phenolated lignins. (a) ^{31}P NMR spectra of lignin functionalized with terephthalic aldehyde (TALD-lignin) before and after acid phenolation using TMDP as phosphorylating agent. (b) Yields of phenolation for different lignins in acid and basic conditions. 45

Figure 4.1. Overview of the lignin extraction and functionalization presented in this chapter. (a) The structure of native lignin in lignocellulosic biomass. (b) the reactions of condensation and repolymerization in

traditional lignin fractionation. (c) The aldehyde-assisted fractionation with glyoxylic acid. (d) The structure of extracted GA-lignin that is used as a surfactant..... 50

Figure 4.2. Characterization of GA-lignin. a) HSQC-NMR with peaks assignment. b) Example of a ^{31}P NMR spectrum with area assigned to the P-functionalized carboxylic acids signal highlighted in red. C) Effect of initial GA concentration over the final GA-functionalization of the extracted lignin measured by ^{31}P NMR. 52

Figure 4.3. Concentration-dependent surface tension measurements of water containing GA-lignin at different pH values (pH 1 red lines, pH 7 blue lines, pH 14 green lines) and different oil phases (a. air, b. mineral oil, c. cyclohexane and d. toluene). Black dots correspond to the initial interfacial tension values (without lignin), the grey line corresponds to propionaldehyde-functionalized lignin (PA-lignin), and the yellow dot corresponds to a GA-lignin sample at pH 14 with additional NaCl. 54

Figure 4.4. Images of different water/mineral oil emulsions at different pH taken over the course of 30 days: (Top) taken with optimal microscopy with a scale bar of 50 μm and coloured dots to mark the stability of the emulsions; and (Bottom) taken with traditional photography of the full vials containing the emulsions at day 1 and day 30 (Bottom)..... 56

Figure 4.5. Photographs (top) and microscopy images with a scale bar of 50 μm (bottom) of creams prepared by using water, mineral oil, lignin, xanthan gum and citral. Sample a is a control cream prepared without lignin, Sample b contains Kraft lignin as surfactant and Sample c contains GA-lignin as surfactant..... 58

Figure 4.6. Comparison of the water/air surface tension using various surfactants. Green bars: water/air surface tension without added surfactants. Red bars: water/air surface tension with GA-lignin at different pH values. Light-blue bars: water/air surface tension with industrial or chemically modified lignin. Grey Bars: water/air surface tension with industrial fossil-based surfactants. All measurements are done at a surfactant concentration of 10 mg/mL and at pH 7 if not indicated otherwise. An asterisk (*) indicates that the values were taken from literature. Dodecyl succinic acid-grafted lignin is taken from Delgado et al.²⁰², PAM-grafted butanosolv lignin is taken from Migliore et al.²⁰⁴, PEG-grafted enzymatic lignin is taken from Shi et al.²⁰³, Sulfomethylated alkali lignin is taken from Ouyang et al.²⁰¹..... 60

Figure 5.1. Extraction and characterization of TALD/GA-lignin. a) Overview of the extraction and simultaneous functionalization of lignin with TALD and GA. b) HSQC-NMR spectrum of TALD/GA lignin extracted with an initial TALD/GA ratio of 1. c) DRIFT spectra of formaldehyde

functionalized lignin (FA-lignin), mono-functionalized GA and TALD-lignins and bi-functionalized TALD/GA lignin extracted with an initial TALD/GA ratio of 1. The peak associated with the stretch of COOH groups is highlighted in red while the peak associated with the stretch of the aldehyde carbonyl group is highlighted in green. d) Quantification of TALD and GA via ^1H NMR and ^{31}P NMR respectively in the TALD/GA-lignin samples extracted with different TALD/GA initial ratios. The resulting TALD/GA ratios on the extracted lignin as a function of the initial ratio of aldehydes and carboxylic acids in the reaction is also shown. 65

Figure 5.2. Chemical interactions between gelatin and lignin of different produced hydrogels and their rheological properties. a) Storage Moduli of TALDGA-Gel (green), GA-Gel (red) and N-Gel (black) hydrogels reported at 1% shear strain and 11.9 rad/s angular frequency. b) Loss Moduli of TALDGA-Gel (green), GA-Gel (red) and N-Gel (black) hydrogels reported at 1% shear strain and 11.9 rad/s angular frequency. c-e) Formation and chemical interaction of gelatin based hydrogels described in this work (N-Gel, GA-Gel and TALDGA-Gel). f-h) SEM images of N-Gel, GA-Gel and TALDGA-Gel. 71

Figure 5.3. Representative shear adhesion performance (a) and stress-strain curves (b) of TALDGA-Gel, GA-Gel, and N-Gel hydrogels. Pictures of TALDGA-Gel, GA-Gel, and N-Gel hydrogels before, during and after compression (c-e). Self-healing properties of N-Gel, GA-Gel and TALDGA-Gel with a total solid content of 12 wt.% (f). 73

Figure 5.4. Cytotoxicity on mammalian Vero cells (a) and bacteria toxicity of *E. coli* (b) and *S. aureus* (c) of N-Gel, GA-Gel and TALDGA-Gel. 75

Figure A.1. Mass balance of the terephthalic aldehyde-facilitated fractionation of lignocellulosic biomass for sample 1. 85

Figure A.2. T1 relaxation time estimates for the NMRs of TALD-functionalized lignin and the internal standard (1,4 DNB). 89

Figure A.3. DOSY spectra of TALD lignin (sample 1), KL-BPH and OSL-BPH. 90

Figure A.4. Depolymerization and extraction yields of TALD-functionalized lignins, OSL and KL. *For Kraft Lignin, we assumed (1) that the Klason lignin of the original biomass used to produce Kraft lignin (which we did not have access to) was the same as that of the biomass used for the other experiments and (2) that the lignin extraction yield (which was unknown) to produce this Kraft lignin was 100%. In this way, we likely overestimate yields from Klason lignin but avoid any unfair comparison with our results. 96

Figure A.5. Structure of the native guaiacyl and syringyl repeating units and their molecular weight.....	96
Figure B.1. HSQC spectrum of propionaldehyde functionalized Lignin (PA-lignin).	100
Figure B.2. DLS measurements of lignin in aqueous phases at different pH values.	104
Figure B.3. Fluorescence microscopy image of a cyclohexane/water emulsion. No fluorescence is observed inside the oil droplets confirming that this is an oil in water emulsion (as the autofluorescent lignin is in the water phase, not in the oil phase).	105
Figure B.4. Pictures of the vials containing the emulsions of water/mineral oil at different pH, taken at day 1, 7, 14 and 30.	105
Figure C.1. a) HSQC-NMR spectra of GA-lignin (sample 1) and b) TALD-lignin (sample 10).	110
Figure C.2. ^1H NMR spectrum of extracted lignin 4. In green is highlighted the signal of bound TALD, while in yellow is highlighted the signal of 1,4-DNB used for quantification.	111
Figure C.3. ^{31}P NMR spectrum of extracted TALD/GA lignin (Sample 4). In red is highlighted the signal of bound COOH groups (GA).	114
Figure C.4. Picture of the vials containing the extracted lignin after the solubility test.	116
Figure C.5. Gelation Time of hydrogels.	118
Figure C.6. Swelling of TALDGA-Gel and GA-Gel at 25 °C.....	119
Figure C.7. Amplitude sweep of prepared hydrogels.	120
Figure C.8. Frequency Sweep of prepared hydrogels.	121

List of Tables

Table 1.1. Composition of different species of lignocellulosic biomass. Data from Zhou et al. ⁴⁴	6
Table 1.2. Distribution of monolignols and linkages in different types of biomasses.	14
Table A.1. Biomass/terephthalic aldehyde ratios used during of lignin extractions	82
Table A.2. Yields of cellulose rich solids, isolated lignin and carbohydrate derivatives after pretreatment.....	84
Table A.3. Molecular weight of isolated TALD lignin and propionaldehyde stabilized lignin determined by GPC.	87
Table A.4. Molecular weight of various isolated lignins determined by GPC.....	88
Table A.5. Quantification of aliphatic, phenolic, and carboxylic hydroxyl groups on various lignins via ³¹ P NMR. The results are reported in mmol/g of effective lignin. Aliph-OH refers to the aliphatic hydroxyl groups, 5-Subst.-OH refers to phenolic groups on aromatic rings substituted at the position 5 (such as Syringol units), G-OH refers to phenolic groups of Guaiacol units, H-OH refers to phenolic groups of Hydroxyphenylpropane units and COOH refers to carboxylic acid groups.	91
Table A.6. Detailed quantities used for ¹ H NMR quantification of the functionalized lignins and quantification results.....	93
Table A.7. Structure, name and effective carbon number used (ECN) of lignin monomers obtained using THF as the GC solvent. ²²⁹	95
Table B.1. Experimental data and corresponding yields for the GA-lignin samples.....	99
Table B.2. Quantification of aliphatic, phenolic and carboxylic hydroxyl groups of extracted GA-lignins via ³¹ P NMR. Aliph-OH refers to the aliphatic hydroxyl groups, 5-Subst.-OH refers to phenolic groups on aromatic rings substituted at the position 5 (for example Syringol units), G-OH refers to phenolic groups of Guaiacol units, H-OH refers to phenolic groups of Hydroxyphenylpropane units and COOH refers to carboxylic acid groups.....	101

Table C.1 Ratios of biomass, TALD and GA used during of lignin extractions.	108
Table C.2. Data regarding sample preparation and results for ^1H NMR quantification of TALD in extracted lignin samples.....	113
Table C.3. Quantification of aliphatic hydroxyl, phenolic hydroxyl and carboxylic acid groups on extracted lignins measured via ^{31}P NMR. The results are reported in mmol/g of effective lignin. Aliph-OH indicates the aliphatic hydroxyl groups, S-OH indicates the phenolic groups of Syringol units, G-OH indicates the phenolic groups of Guaiacol units, H-OH indicates the phenolic groups of Hydroxyphenylpropane units and COOH indicates the carboxylic acid groups of GA.	115
Table C.4. Result of the solubility test for the extracted TALD/GA lignins.	116

List of Equations

Equation A.1. Effective isolated lignin.....	83
Equation A.2. Lignin Extraction Yield K_{Klason}	83
Equation A.3. Normalized 1,4-DNB integral.	92
Equation A.4. Normalized aldehyde integral.....	92
Equation A.5. mmol 1,4-DNB in NMR sample.	92
Equation A.6. mmol aldehyde in NMR sample.....	93
Equation A.7. mmol of free aldehyde in 1g of lignin.	93
Equation A.8. n_{decane}	94
Equation A.9. n_{monomer}	94
Equation A.10. Monomer Yield [wt.%]	94
Equation B.1. Effective Isolated lignin.....	98
Equation B.2. Lignin extraction yield on Klason lignin bases.	98
Equation C.1. Normalized 1,4-DNB integral.	112
Equation C.2. Normalized aldehyde integral.....	112
Equation C.3. mmol of 1,4-DNB in NMR sample.	112
Equation C.4. mmol of TALD in NMR sample.	112
Equation C.5. mmol of TALD in 1g of lignin.....	113
Equation C.6. g of TALD in 1g of lignin.	113

Equation C.7. g of GA in 1g of lignin.	115
Equation C.8. Swelling of hydrogels.....	118

Chapter 1 Introduction

This chapter was adapted from the following article with the permission of all co-authors and of the journal.

Postprint version of the article: Stefania Bertella, Jeremy S. Luterbacher. "Lignin Functionalization For The Production Of Novel Materials". Trends In Chemistry, 2020, 2, 440-453.

My contribution: Literature research and drafting of manuscript and figures.

1.1 Climate change: challenges and opportunities

Reducing climate change and shifting towards a more sustainable society is one of the most urgent challenges of the present times.¹ When the industrial and agricultural revolutions started in the second half of the 19th century, they led to tremendous technological developments and an increase in the quality and length of human life, which resulted in global population growth.²

This rapid growth, which was built on a reliance on fossil resources such as oil, coal and gas for energy and materials, has ultimately taken its toll on the environment due to the increase of greenhouse gases (GHG) emissions that are responsible for the global increase in atmospheric temperatures and consequently for climate change, extreme weather conditions^{3,4} and the loss of biodiversity.^{5,6}

The Sixth Assessment Report recently published by the International Panel for Climate Change (IPCC) has in fact shown that from 1850 to 2019 the average global surface temperature (GST) has increased by 1.2 °C (**Figure 1.1**, dark blue line). These data are in accordance with the simulation of GST changes where anthropogenic factors, such as the cumulative CO₂ emissions (**Figure 1.1**, grey area), were taken in consideration in the temperature increase (**Figure 1.1**, red line), whereas if only natural factors were to be

considered (**Figure 1.1**, light blue line), there wouldn't be a substantial difference in GST across the same time span.

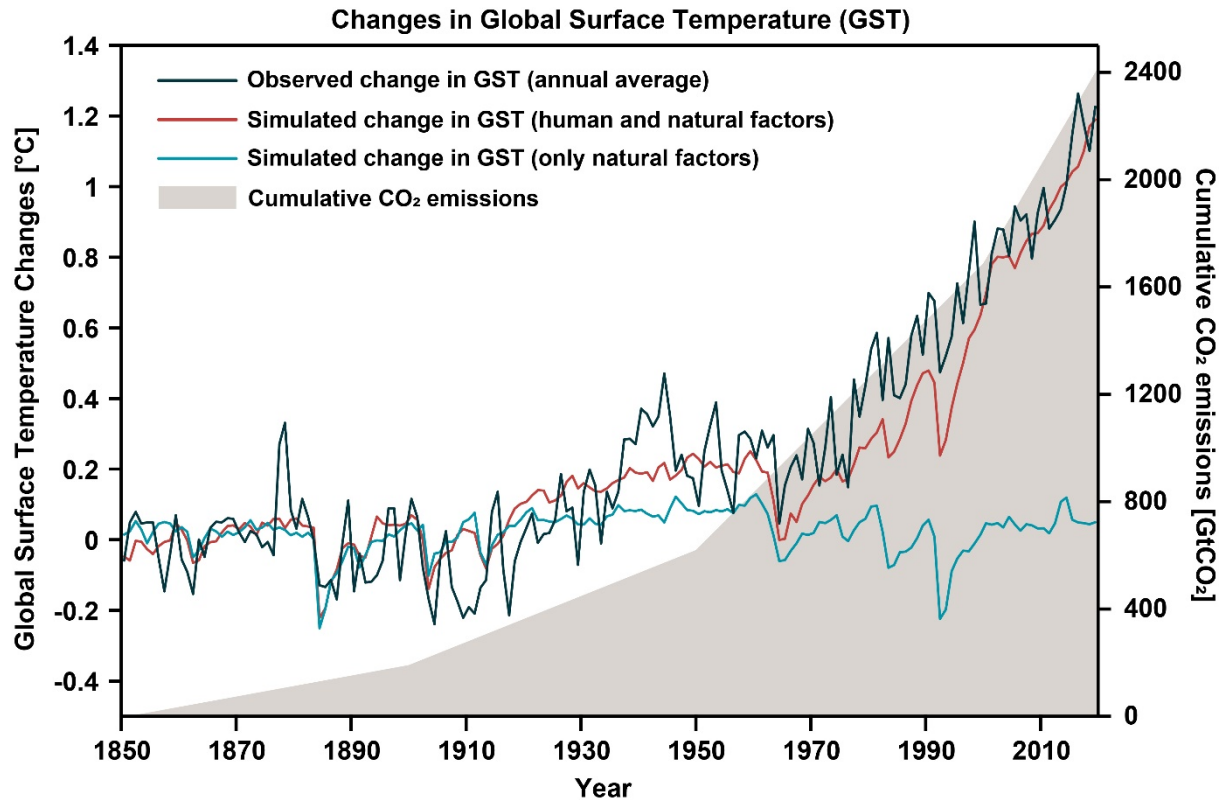


Figure 1.1. Changes in Global Surface Temperature in the period 1850-2019 and in function of the Cumulative CO₂ emissions for the same period of time. The light-blue line refers to a simulated GST change by taking in consideration only natural factors. The red line indicates the simulation of GST changes considering both anthropogenic activities and natural factor. The dark blue line indicates the observed average GST changes. The grey area shows the cumulative CO₂ released in the atmosphere in GtCO₂ from 1850 to 2019. Data were extracted from the The Sixth Assessment Report published in 2021 by the International Panel for Climate Change (IPCC)⁷.

The same IPCC report concluded that based on a business-as-usual scenario, where no concrete actions are to be taken by governments in order to decrease the emission of anthropogenic CO₂ and the other GHG, the average global temperatures are predicted to rise up to 4 °C by the end of the current century, with catastrophic consequences.⁸ This would cause an increase of sea level, ocean acidification and warming, hot temperature extremes and heavy precipitations over land as well as droughts in drying regions of the planet⁷, with consequences not only for the environment, but also for societal and political aspects such as

migration, famine and conflicts.⁹ To face these environmental and political issues, many countries are establishing programs and strategies to mitigate climate change.^{10–12}

These concerns are notably leading to an increased demand for sustainable alternatives to the use of oil, coal and natural gas, which up until the last few years have been the source of 86% of the total energy (**Figure 1.2, A**) and 90% of the carbon-based chemicals and materials (**Figure 1.2, B**) generated globally.^{13,14} Projections from the Nova Institute have also shown that with an increasing population, by the year 2050 the demand for chemicals and materials will increase by three times with an associated increase in energy consumption.¹³ The production of carbon-based chemicals and related materials will then be mainly focused on recycling of already produced materials and sustainable sources of carbon for the synthesis of new ones, completely out-phasing fossil sources (**Figure 1.2, C**).

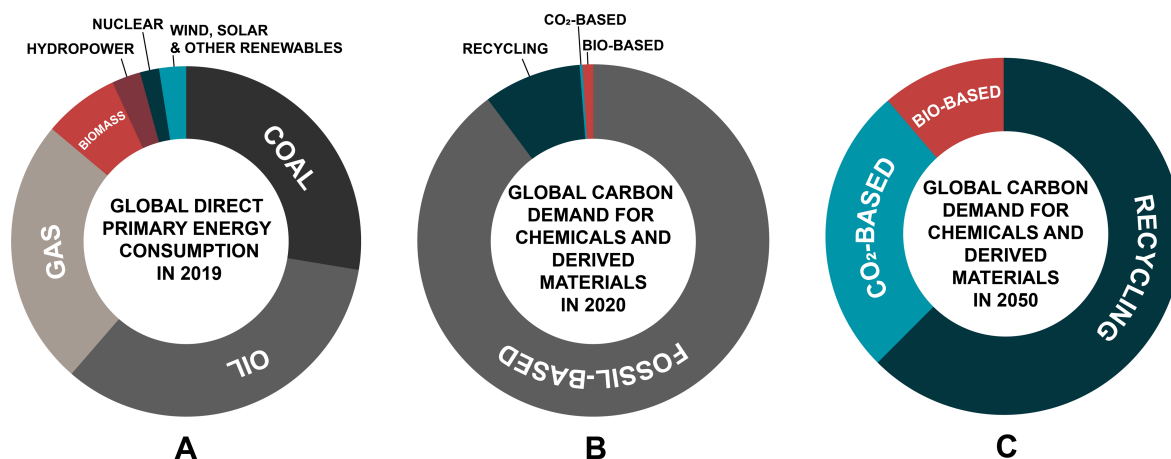


Figure 1.2. Global direct primary energy consumption in 2019 (A). Global Carbon demand for chemicals and derived materials in 2020 (B) and forecast for 2050 (C). Data for pie-chart A are taken from Smil.¹⁴ Data for pie-charts B and C are taken from Vogt.¹³

1.2 Sustainable sources of carbon for energy and material production

The scientific community is hence exploring new renewable feedstocks for producing energy and materials without an increase in GHG emissions, and possibly to develop technologies able to sequester from the atmosphere harmful chemical compounds which have been released in the past.¹⁵ Technologies such as photovoltaic and solar power¹⁶, hydropower¹⁷, geothermal¹⁸ and wind power¹⁹ are constantly being improved in order to deliver green

hydrogen and electricity for fuels, transportation, manufacturing and domestic use in high yields and in a cost competitive way.²⁰

For what concerns carbon-based chemicals, there are two main feedstocks that could be exploited for the manufacturing of materials and fuels. One of these feedstocks is the carbon dioxide already present in the atmosphere as well as that which is generated in manufacturing or fuel combustion.²¹ Currently, promising technologies are being developed for the sequestration of CO₂ from the atmosphere or from the source of generation, such as the exhaust of industrial plants.^{22,23} In these systems carbon dioxide is captured by means of membranes and it is either stored underground after mineralization²⁴ or transformed into other chemicals by means of electrochemical^{25,26} or conventional synthetic routes.^{27,28} The way that nature uses to store carbon dioxide and transform it into chemicals with higher energy resides in photosynthesis, a process where atmospheric carbon dioxide is first absorbed from the atmosphere and subsequently reacted with water in presence of sunlight as source of energy to produce glucose and oxygen, as shown in **Figure 1.3**.²⁹ Forest and agricultural crops and their residues, grasses and algae are all generated and thrive through photosynthesis, and constitute the feedstock defined as plant biomass.^{30,31}

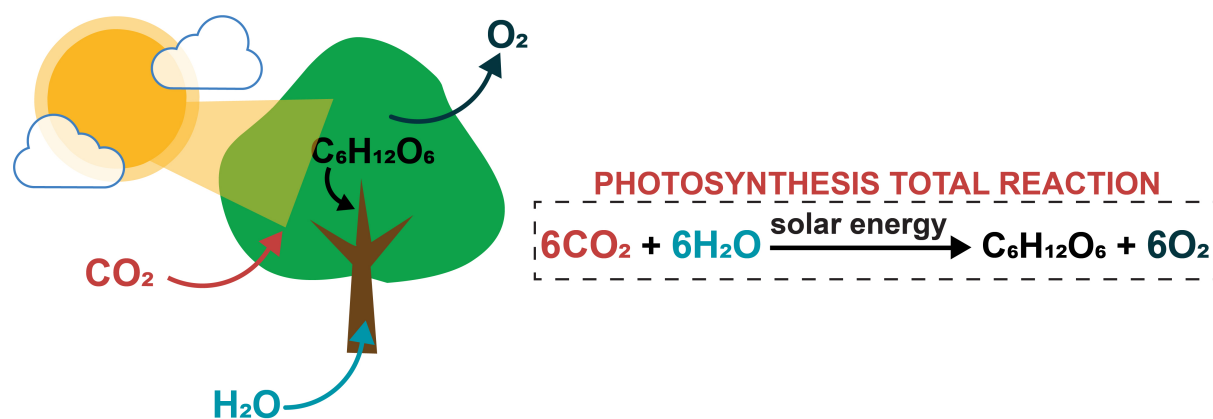


Figure 1.3. Schematic representation of photosynthesis in plants.

Due to their high energy density, different types of biomass have historically been directly burned to produce heat or converted into smaller molecules and fuel in processes known as biorefineries.³²

The so-called first generation biorefineries are based on the conversion into chemicals of starch-based and edible crops such as corn, sugar cane and wheat into bio-ethanol via fermentation with yeasts.^{33,34} Other edible and fat-rich crops such as rapeseed and soybean oil are converted into biodiesel via transesterification reaction.^{35,36} Although first-generation biorefineries have already well-established processes, there is still debate as to whether they

are truly sustainable from a social point of view. In fact, as these types of biofuels are generated from edible crops, they are potentially in competition with the production of food, affecting food prices especially in regions of the planet which are already poor.³⁷ Moreover, the extensive use of land and chemicals, such as fertilizers and pesticides, that these types of cultivation need has the potential to cause a decline in biodiversity as well as to increase problems like deforestation, causing irreversible damage to ecosystems.³⁸

To move away from these issues, new generations of biorefineries are being developed.³⁹ In particular, these new generation of biorefineries aim to use non-edible cellulose-based wastes from crops production and lignocellulosic material for their fractionation into chemicals for fuel and material applications.^{40,41} While these types of integrated biorefinery concepts could help moving away from some of the aforementioned environmental and social issues, especially in relation to food competition, their development still requires much effort due to the complexity of the chemical composition of these feedstocks.⁴²

1.3 Lignocellulosic biomass: a renewable feedstock from non-edible crops.

In the context of using sources of carbon that don't compete with food production, lignocellulosic biomass is an especially promising feedstock to replace carbon-based products, because it already contains partially reduced multi-carbon molecules.⁴³

Most of the mass of lignocellulosic biomass is found in the macro and microfibrils of the rigid walls of its plant cells, which is composed by approximately 95 wt.% of three biopolymers: cellulose, hemicelluloses, and lignin (**Figure 1.4**). The remaining 5 wt.% of lignocellulose is constituted by inorganic ashes and organic extractives such as small aromatic molecules, fats, waxes, and terpenes.

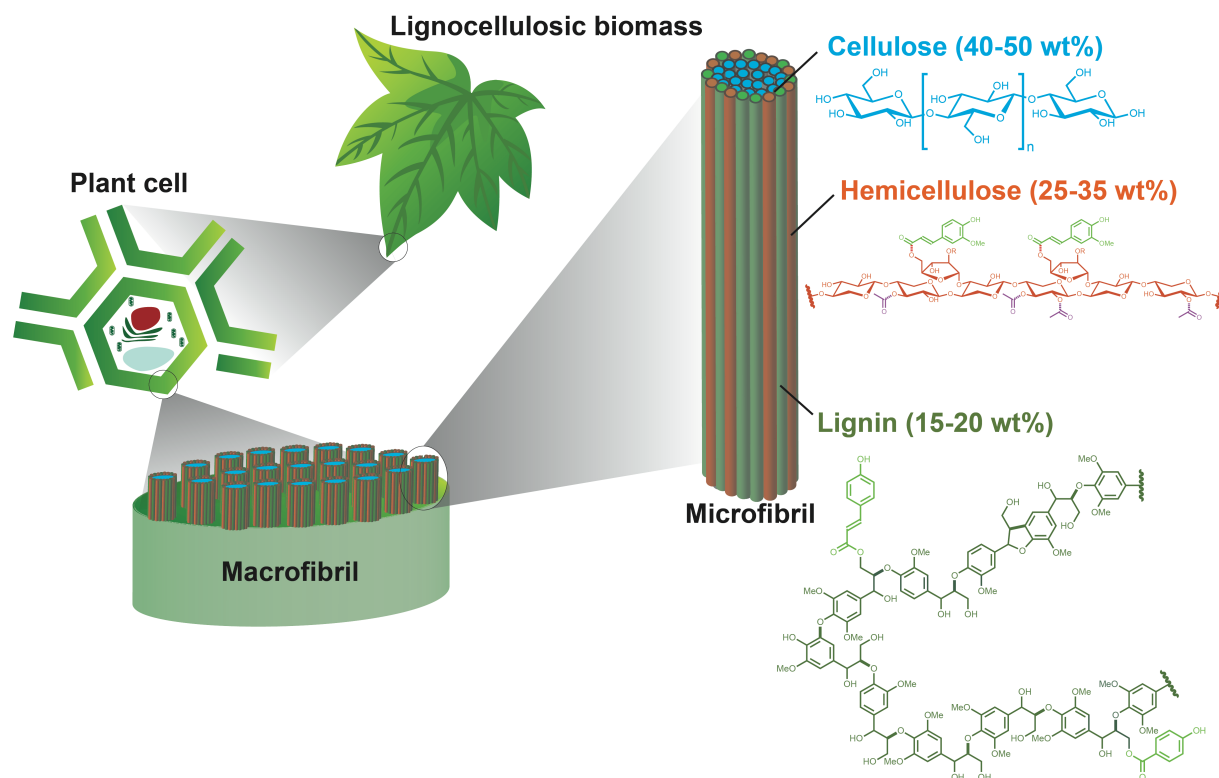


Figure 1.4. Overview of the structure of lignocellulosic biomass showing macrofibrils and microfibrils constituted of cellulose (light blue), hemicellulose (brown) and lignin (green).

The composition of the major and minor components of lignocellulosic biomass is not constant, but greatly depends on plant species. In general, softwoods and hardwoods contain a higher percentage of lignin and cellulose, while grasses and agricultural residues such as corn cobs are composed by a minor quantity of lignin and cellulose in favour of a higher amount of hemicelluloses. A summary of the composition of different plant species is summarized in **Table 1.1**.

Table 1.1. Composition of different species of lignocellulosic biomass. Data from Zhou et al.⁴⁴

Biomass	Cellulose [%]	Hemicellulose [%]	Lignin [%]	Ash [%]	Extractives [%]
Aspen	52.7	21.7	19.5	0.3	5.7
Bagasse	45.9	28	20.7	2.7	3.7
Beech	45	33	20	0.2	2
Birch	47	25.9	22	0.3	4.7

Corn Stover	35.3	28.9	19.9	4.6	6.6
Corn Straw	43.1	31.8	11	0.8	13.3
Corn cob	37.6	31.6	20.8	3.2	8.1
Pine	46.9	20.3	27.3	0.3	5.1
Poplar	49.7	24.1	23.6	0.4	2.2
Spruce	47.2	13.3	36	0.2	1.9
Sugar Cane	49.5	24.4	22.7	0.3	1.8
Wheat Straw	38.9	21.1	18	9.7	5.5

1.3.1 Cellulose

Cellulose, the most abundant biopolymer on the planet, is a linear homopolymer of glucose that accounts for about 40-50 wt.% of the total weight of lignocellulosic biomass. In this polysaccharide, the glucose units are linked together through β -1,4-glycosidic bonds at the C₁ and C₄ positions, forming linear polymeric chains (**Figure 1.4**, light blue). The molecular weight and length of the polymeric chains of cellulose, defined as degree of polymerization, or DP, greatly depends on the source of biomass but generally varies between 2000 and 15000.⁴⁵ However, as the DP of cellulose can be modified by the fractionation process used to isolate the different components of the biomass, the measured DP value of cellulose can generally only be used in a relative way.^{46,47}

The high number of free hydroxyl groups in the polymeric chains of cellulose is the driving force for their crystalline packing via the formation of hydrogen bonds and weak Van der Waals forces.⁴⁸ Cellulose crystallizes in different allomorphs based on the orientation of its polymeric chains. These allomorphs are named I _{α} , I _{β} , which are the only ones naturally present in nature in different proportion depending on the plant species, and II, III_I, III_{II}, IV_I, IV_{II}, which don't recur naturally but that can be obtain after chemical or thermal treatment of cellulose.^{49,50} The aggregation of several crystalline domains forms lignocellulosic microfibrils, while the aggregation of several microfibrils form macrofibrils. The structured orientation of the cellulose crystalline domain is one of the main factors to provide lignocellulose with its strength and mechanical properties. Due to its high abundance and

particular properties, cellulose has been exploited for millennia in the production of paper which, to this day, remains one of the main materials produced with this biopolymer.⁵¹ More recently, cellulose has also been used to develop nonwoven tissues⁵² and absorbent materials.⁵³ A new field of applications for cellulose resides in the disaggregation of cellulose fibers to obtain nanofibers of 2-4 nm diameter. Nanofibers of cellulose are a versatile material for their further chemical functionalization which, coupled with their good mechanical properties, makes them good candidates for the development of bio-based materials such as bioplastics, membranes and coatings.⁵⁴

1.3.2 Hemicelluloses

Hemicelluloses are linear or branched polysaccharides that accounts for about 25-35 wt.% of the total lignocellulose weight.⁵⁵ Generally, the main units that forms this polysaccharide include pentoses such as D-xylose and L-arabinose or hexoses such as D-mannose, D-glucose and D-galactose (**Figure 1.4**, brown). In addition to these main building blocks, hemicellulose can contain a small fraction of other compounds such as D-glucuronic acid, D-galacturonic acid, L-rhamnose and L-fucose.⁵⁶

Based on their structures and chemical compositions, hemicelluloses can be divided in several sub-categories: xylans (where the molecule of xylose are linked together through β -1,4-xylosyl bonds), xyloglucans (heteropolymers of xylose and glucose), mannans (homopolymers of mannose), glucomannans (heteropolymers of mannose and glucose), β -1,3-glucans and β -1,4-glucans (homopolymers of glucose) and galactans (homopolymers of galactose)⁵⁷. The monomeric composition, additional functionalization of residual hydroxyl groups, such as acetylation, and the polymeric structure of these polysaccharides in lignocellulosic biomass greatly depends on the plant species. Usually though, the hemicellulose fraction of hardwood and grasses is mainly composed of xylans, whereas in softwood most of the hemicelluloses are commonly found in the form of glucomannans.⁴⁴

Contrary to cellulose, the heterogeneity of hemicelluloses, in terms of monomeric composition and polymeric structure, makes these biopolymers less prone to crystallization, and consequently more easily solubilized in water and depolymerized at milder acidic conditions.^{58,59}

Due to their abundance and easier processability, hemicelluloses have also been investigated as potential candidates for the development of sustainable materials and polymers.⁶⁰ As an

example, extracted hemicelluloses have been used in their polymeric form for the synthesis of composites with other polymers or small molecules such as chitosan, poly-(ϵ -caprolactone) and citric acid.^{61–63} Alternatively, the building blocks of hemicelluloses, in particular xylose and mannose, have also been exploited as monomers in the development of new plastics.^{64,65}

1.3.3 Lignin

Lignin is an aromatic heteropolymer constituted by phenylpropanoid units that forms the remaining 15–20 wt.% of the lignocellulosic mass (**Figure 1.4**, green).⁶⁶ In the plant, lignin has the function of providing rigidity and mechanical strength to the plant cell wall. Its hydrophobic aromatic structure is also able to prevent the attack of external pathogens, preventing degradation of the organic matter and providing antibacterial properties.⁶⁷

Lignin is formed during the radical biosynthesis and coupling of several monolignols, the most abundant being *p*-coumaryl (H), coniferyl (G), and sinapyl (S) alcohols⁶⁸, which are biosynthesized in the plant in several steps starting from the amino acid phenylalanine through the phenylpropanoid pathway shown in **Figure 1.5**.^{69,70}

In this process, L-phenylalanine is first deaminated by the enzyme phenylalanine ammonia-lyase (PAL). The obtained cinnamic acid undergoes hydroxylation by cinnamate 4-hydroxylase (C4H) yielding *p*-coumaric acid as a product. *p*-Coumaric acid is then activated to form the corresponding Coenzyme A thioester via 4-coumarate:CoA ligase (4CL). The newly formed *p*-coumaroyl-CoA could then follow two different paths. The first option is for it to be first reduced to *p*-coumaraldehyde by cinnamoyl-CoA reductase (CCR) and subsequently transformed in *p*-coumaryl alcohol by the cinnamyl alcohol dehydrogenase (CAD), completing therefore the synthesis of the H monolignol (**Figure 1.5**, grey path). Alternatively, *p*-coumaroyl-CoA can undergo the action of the enzyme hydroxycinnamoyl-CoA shikimate/quinate hydroxycinnamoyltransferase (HCT) to form the corresponding shikimic or quinic acids. *p*-Coumaroyl shikimic or quinic acids are then hydroxylated in the *ortho*-position by *p*-coumarate 3-hydroxylase (C3H) to form the corresponding caffeoyl shikimic or quinic acids. These molecules can be again coupled with coenzyme A by HCT and methoxylated in the *ortho*-position by caffeoyl-CoA O-methyltransferase (CCoAOMT) to form feruloyl-CoA. The enzyme CCR then reduces feruloyl-CoA to coniferaldehyde, which is further reduced to coniferyl alcohol (the G monolignol) by CAD (**Figure 1.5**, blue path). Coniferaldehyde can be further hydroxylated to 5-hydroxy-coniferaldehyde by ferulate 5-

hydroxylase (F5H) and methoxylated to sinapaldehyde by caffeic acid O-methyltransferase (COMT). Finally, sinapaldehyde is reduced by CAD to sinapyl alcohol, the S monolignol (**Figure 1.5**, red path).

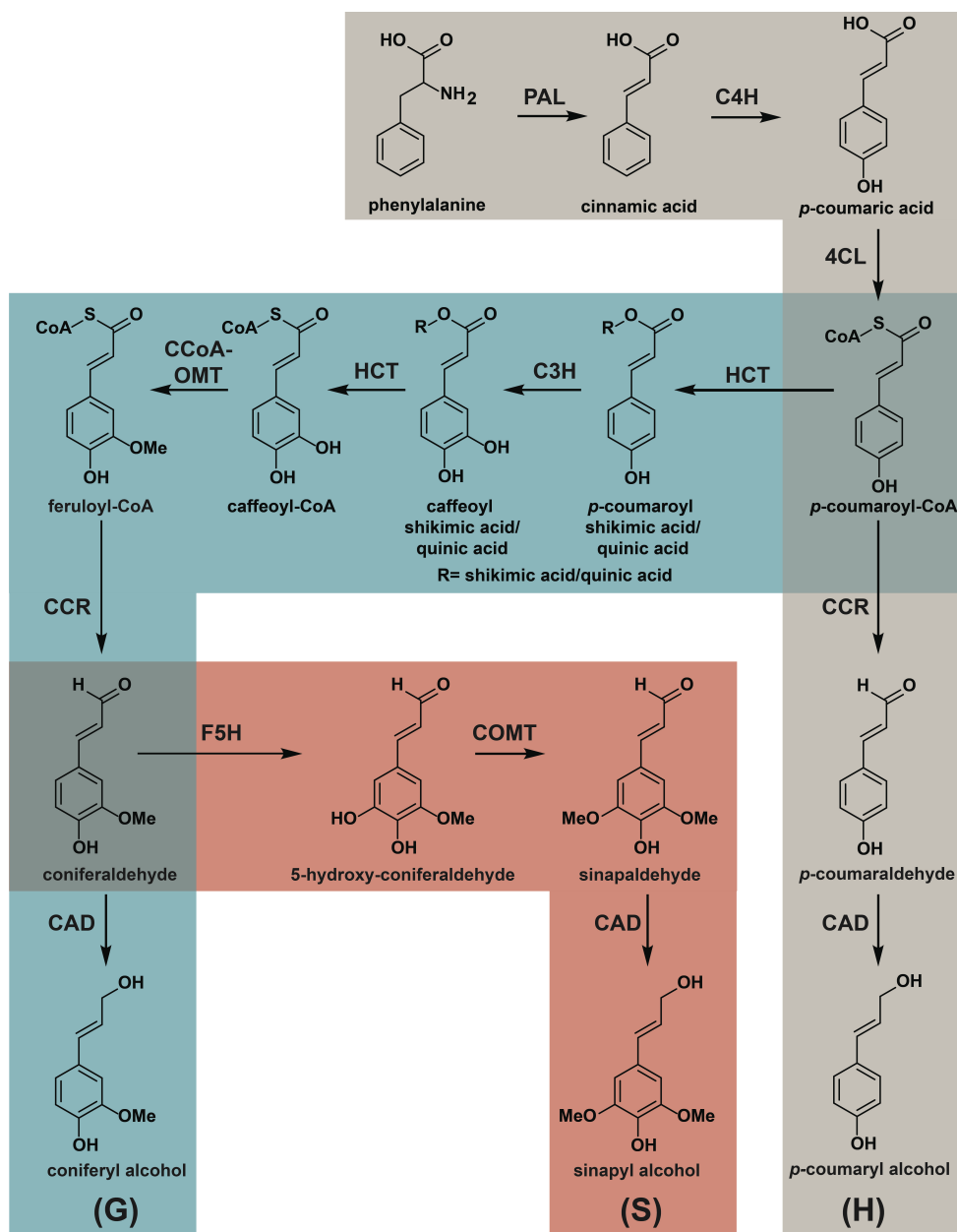


Figure 1.5. The pathway for the biosynthesis of p-coumaryl (grey path), coniferyl (blue path), and sinapyl (red path) alcohols. In the figure the enzyme involved in the synthesis are indicated as PAL: phenylalanine ammonia-lyase, C4H: cinnamate 4-hydroxylase, 4CL: 4-coumarate-CoA ligase, C3H: p-coumarate 3-hydroxylase, HCT: Hydroxycinnamoyl-CoA shikimate/quinic acid hydroxycinnamoyltransferase, CCoA-OMT: caffeoyl-CoA O-methyltransferase, CCR: cinnamoyl-CoA reductase, F5H: ferulate 5-hydroxylase, COMT: caffeic acid O-methyltransferase, CAD: cinnamyl alcohol dehydrogenase. Figure reproduced from Vanholme et al.⁷¹

Following their biosynthesis, the monolignols are transported in the plant cell wall where they undergo polymerization to form lignin. The driving force for the synthesis of the lignin oligomers is the formation of highly reactive radicals through dehydrogenation and oxidation of the monolignols from enzymes such as peroxidases or laccases.⁷² The newly formed monolignols radicals are stabilized through the delocalization of electrons in a high number of possible resonant structures (**Figure 1.6, a**) and can then polymerize towards the formation of lignin oligomers.⁷³ The creation of reactive monolignol radicals is followed by their coupling to form a dimer, a reaction which usually happens at the β position of the monolignols. As a consequence, the two monolignols involved in the coupling can only be linked through β - β , β -O-4 or β -5 linkages (**Figure 1.6, b**).

After the formation of a covalently bound dimer, this lignin precursor needs to be oxidized again into a radical in order to couple with another radical monolignol, thus forming the growing oligomeric chain in a process called lignification, that by its nature of radical coupling grows one unit at the time.⁷⁴ The reaction between a monolignol radical on the β position and a phenolic radical dimer, or short oligomeric chain, results in the formation of β -O-4 or β -5 linkages. Although with less probability, the coupling of two growing radical oligomeric chains is also possible, resulting in the formation of 5-5 and 5-O-4 bonds (**Figure 1.6, c**).^{75,76}

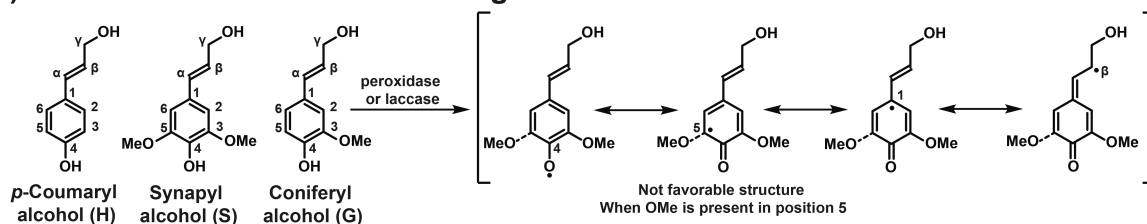
In conclusion, the final outcome of lignification is the formation of a random aromatic copolymer constituted by syringyl (S), guaiacyl (G), and *p*-hydroxyphenyl (H) subunits linked through several different C–O and/or C–C linkages.⁷⁷ The actual monomer composition and linkage distribution varies across wood species. Softwoods like pine or spruce are composed mainly of guaiacyl units, while hardwoods such as birch or eucalyptus contain both guaiacyl and syringyl monolignols, but with a higher fraction of syringyl units (see potential model structures in **Figure 1.6, d**). *para*-Hydroxyphenyl units, together with the syringyl and guaiacyl units, may be at slightly elevated levels in grass (**Table 1.2**).⁷⁸

Regarding linkage distribution, the main and most important bond for lignin upgrading which is found in hardwood, softwood, and grass lignins is the β -O-4 linkage (**Figure 1.6, b and c** light blue), which normally constitutes 40 to 85% of the total bonds between lignin's monolignols, depending on the wood species. The other types of bonds present in lignin include the β - β , which is sometimes generated during the dimerization of two monolignols radicals (**Figure 1.6, b** violet), the β -5 (**Figure 1.6, b and c**, green), which can be generated during dimerization or during the lignification process, and finally the 5-5 (**Figure 1.6, d** dark

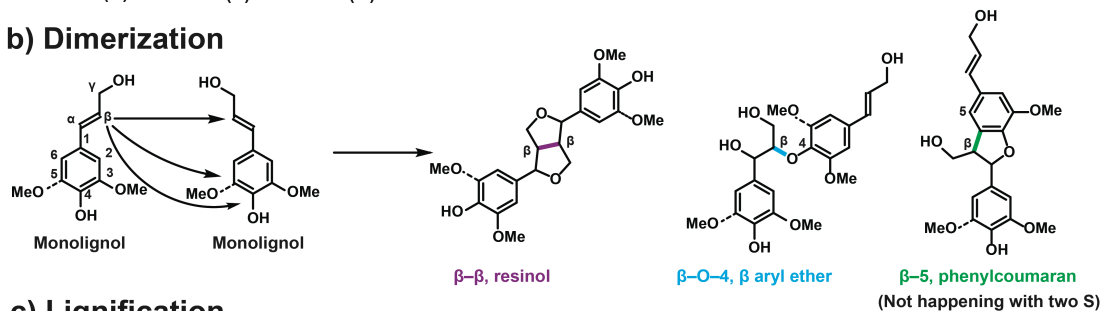
purple) and 5-O-4 (**Figure 1.6**, d orange) which are the result of coupling of two growing oligomeric chains. These additional bonds together account for the remaining 15 to 60% of interunit linkages.^{75,76} The discrepancy in the distribution of linkages across several biomass species arises from the fact that when a high proportion of monolignols is derived from sinapyl alcohol rather than coniferyl alcohol, which is for example case of hardwood and grasses, certain types of linkages, such as the 5-5 or the β -5 cannot be formed due to the presence of an additional methoxy group in the ortho position. This therefore prevents the radical coupling of monolignols in the position 5 during dimerization and coupling of oligomeric chains (**Figure 1.6**, b and c). For this reason, hardwoods and grasses present in general a higher percentage of β -O-4 ether linkages. A table covering the distribution of monolignols and linkages found in different types of biomass sample is presented in **Table 1.2**.

Exceptions to these standard linkages and monolignols can however be found in nature. An example of this was recently reported by Li and co-workers, where they showed that the lignin within vanilla seed coats is a homopolymer of caffeyl alcohol units, which are held connected together through benzodioxanes linkages (**Figure 1.6**, e red).⁷⁹

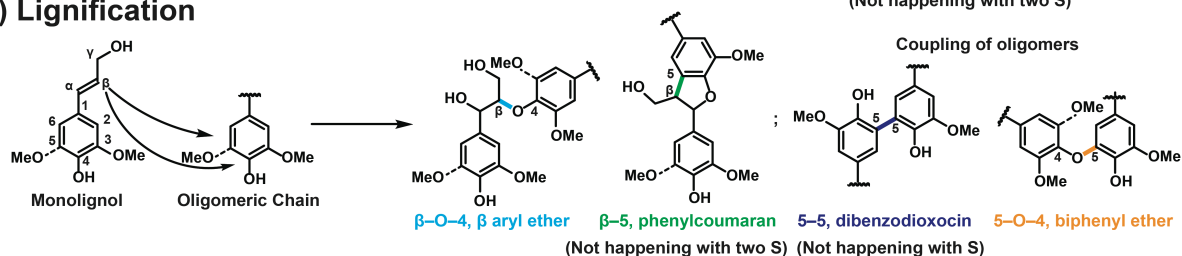
a) Resonance structures of monolignols



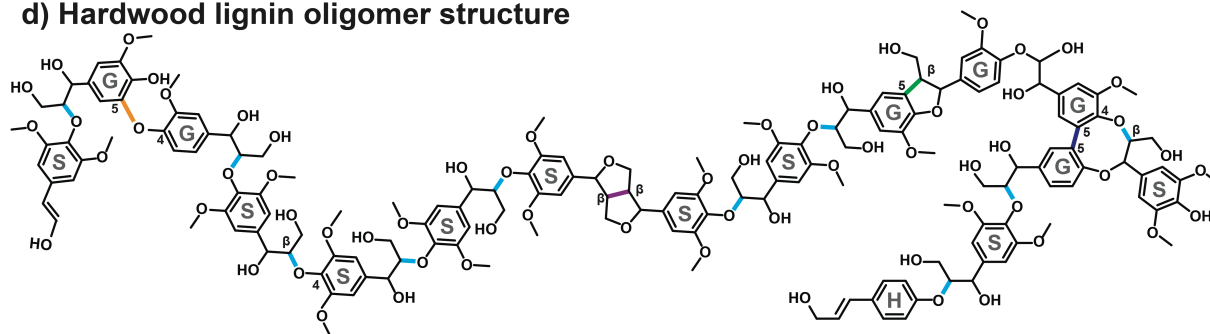
b) Dimerization



c) Lignification



d) Hardwood lignin oligomer structure



e) C-lignin oligomer structure

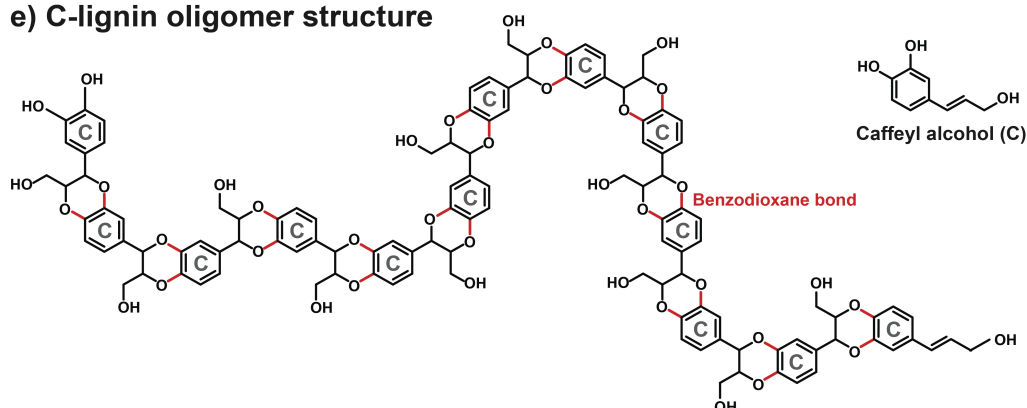


Figure 1.6. Reactions and potential lignin structures arising from the lignification process. a) resonance structures of radicals formed on the *p*-coumaryl (H), Sinapyl alcohol (S) and Coniferyl alcohol (G). b) dimerization of radical monolignols at the β position. c) The lignification process and coupling of oligomers. d) Potential hardwood lignin structure. e) Structure of C-lignin as reported by

Li et al.⁷⁹. In the figure different linkages are indicated by different colors. In particular the β -O-4 linkage is in light blue, β - β in violet, β -5 in green, 5-5 in dark purple, 5-O-4 in orange and benzodioxanes linkages in red.

Table 1.2. Distribution of monolignols and linkages in different types of biomasses.

Data from Liu et al.⁸⁰

		Softwood [%]	Hardwood [%]	Grass [%]
Monolignols	H (p-coumaryl alcohol)	<2	<2	<5
	G (coniferyl alcohol)	>95	25-50	33-80
	S (sinapyl alcohol)	0	46-75	20-54
Linkages	β -O-4	43-50	50-65	74-84
	5-O-4	5	6-7	n.d.
	5-5	5-7	<1	n.d.
	β - β	2-6	3-12	1-7
	β -5	9-12	3-11	5-11
	β -1	<2	<2	<2

Given the variety of chemical functionalizations present in the native lignin, coupled with the fact that lignin is the most abundant source of renewable aromatics on the planet, this biopolymer is a very promising starting point for the development of more sustainable aromatic materials. The use of lignin in sustainable materials is however a not easy task, given the challenges that arise starting from its extraction, characterization, and further chemical functionalization. In the next sections of this chapter, I will touch upon the major challenges regarding the upgrade of oligomeric lignin in the development of new aromatic bio-based materials, before discussing, in the next chapter, how the research work of my doctoral studies aims at overcoming several of the obstacles described here.

1.4 Lignin's challenging characterization

Due to the complexity, heterogeneity, and variety that is present in lignin, elucidating its structure and associated properties is a nontrivial task.⁸¹ One of the main recurring issues is

that lignin is difficult to isolate from its other components without modifying its structure. This leads to a trade-off where lignin must either be characterized in the presence of other biomass constituents or analysed in a modified form. One example of these recurring issues is faced during gravimetric isolation techniques, such as the Klason method, which is known to lead to significant lignin degradation due to the high acidity that is used.⁸² Moreover, the high acidity necessary for the isolation of lignin can also lead to polysaccharide degradation and the formation of humins that are sometimes erroneously included within the lignin quantification (often termed “pseudo-lignin”).

A few types of isolated lignin can overcome these challenges. Amongst the most important are milled wood lignin (MWL) and cellulolytic enzyme lignin (CEL). The first is based on finely ball-milling wood followed by extraction of the lignin using a solution of water and dioxane. The second, also begins with ball-milling, but is then followed by several treatments with cellulase enzymes that can hydrolyse the polysaccharides leaving behind the lignin as a solid residue (EL); it can then be extracted with dioxane/water, as for the MWL, to produce a CEL. However, these methods have several limitations. Notably, the extraction of lignin is less efficient compared to chemical methods, leaving some lignin behind, while the intensive ball-milling has the effect of partially depolymerizing lignin and inducing chemical modification on its structure.^{83,84}

Analysing isolated lignin can thus be complicated by these structural modifications, which make the analytical results very difficult to trace back to the native lignin structure. To overcome the need of lignin extraction, many researchers have focused on analysing native lignin embedded in plant cell walls *via* nuclear magnetic resonance (NMR) spectroscopy. However, these techniques require reducing plant material to a gel-like structure through ball-milling and then finding suitable solvents capable of solubilizing or at least swelling the whole cell walls without yielding chemical modification.⁸⁵ Due to lignin’s complex structure, the information provided by ¹H NMR is often limited because the signal of the various protons overlaps. 2D NMR, and particularly Heteronuclear Single Quantum Coherence (HSQC) NMR, leads to much more straightforward identification of the various lignin and carbohydrate functionalities, as the overlapping of peaks is completely avoided or largely minimised. The output of this NMR experiment is in fact a bidimensional spectrum where each signal corresponds to a unique C–H bond within the analysed sample.

Similar to its use for whole cell wall characterization, NMR is frequently used for analysing isolated lignin. Despite the absence or reduced signal of carbohydrates, 2D-NMR techniques

still need to be used to resolve the different functionalities that would otherwise overlap in 1D techniques. Nevertheless, advances have been made to be able to quantify chemical bonds in lignin via spectroscopy. ^{31}P NMR is a powerful tool that can be used to quantify hydroxyl and phenolic groups, but still requires a functionalization step where the hydroxyl and phenolic groups of lignin are commonly phosphitylated *via* a reaction with 2-chloro-4,4,5,5-tetramethyl-1,3,2-dioxaphospholane (TMDP).⁸⁶ Recently, Talebi Amiri and colleagues applied the HSQC₀ technique, more commonly used on proteins, to quantify chemical bonds present on the lignin backbone and predict the behaviour of the polymer under catalytical hydrolytic conditions.⁸⁷

Together with NMR methods, functional groups can also commonly be determined by infrared spectroscopy. Although powerful, both techniques are not always optimized for a complex substrate like lignin and, particularly in whole cell experiments, are commonly used to provide qualitative rather than quantitative information of the functionalities present in the biopolymer. Specifically, peak ratios can be used to provide some information on the relative ratios of the different functionalities present but not their actual amounts.

Despite the challenges and limitations, several analytical techniques have been applied in the study of the isolated biopolymer. Among the properties of isolated lignin that are commonly reported is molecular weight. Gel-permeation chromatography (GPC) is the typical tool for this kind of measurement, although it often requires functionalization to make the polymer soluble for analysis. Moreover, due to variable structures, no calibration standards for lignin exist. Although it is common to use polystyrene as a calibration standard, it cannot be considered to give an accurate measure of the molecular weight as the hydrodynamic volumes are different for the two polymers. In addition to this, an extra source of error can come from the detection systems used for the determination of molecular weights. An example of this was presented recently by Zinovyev and colleagues who reported that when size exclusion chromatography was combined with multi-angle light scattering detectors (MALS), molecular weight could be incorrectly estimated due to the autofluorescence of lignin's aromatic structure.⁸⁸ Lignin molecular weight has also been investigated by mass spectroscopy, particularly Matrix-Assisted Laser Desorption/Ionization mass spectrometry (MALDI-MS). However, the heterogenous nature of lignin and the challenge of ionizing all fractions equally severely limit the use of this technique for accurately characterizing lignin.⁸⁹

Altogether, the dramatic progress made in the last 15 years, especially with NMR techniques, has allowed the research community to have a much clearer understanding of lignin's

structure. This has translated into the ability to better relate lignin's structure with its chemical reactivity and physical properties. This has been at the root of recent progress in the ability to control and tune lignin's behaviour for specific application.

1.5 Lignin extraction and its effects on structural features

Before valorising, modifying, or incorporating lignin into materials, the biopolymer must be isolated.⁹⁰ Several processes and methods have been developed over the years to achieve this separation. The pulp and paper industry is the predominant large-scale producer of lignin, where the biopolymer comes out as a by-product of the isolation and purification of pure cellulose from wood for its further use in the production of paper, cardboard, textiles and other applications.⁹¹ The two most common and well-known pulping processes for the industrial extraction of lignin are the Kraft (**Figure 1.7**, top pathway) and the Sulfite processes (**Figure 1.7**, light blue/grey pathway).⁹²

Although these two processes allow the isolation of pure cellulose and lignin at industrial scales, the severity of the methods invariably lead to a highly condensed and chemically modified isolated lignin, due to side-reactions dependant on the catalysts used. In both cases however the harsh conditions of temperature and pH favour the formation of unstable intermediates on the lignin backbone *via* the elimination of water molecules (**Figure 1.7**). Condensation of these intermediates occurs through intra- or inter-molecular reactions with other lignin oligomers creating new highly stable C–C linkages. These intermediates can also react with other chemical species present in solution.^{93,94} The combination of all these side-reactions, as we will discuss, is one of the key factors that limits the formation of controlled chemical structures and ultimately, the use of industrial lignins.^{95,96}

In more details, the Kraft process (**Figure 1.7**, top pathway) relies on the use of a basic aqueous solution of sodium sulfide at temperatures between 150-180 °C. In these conditions quinone methide intermediate can form and react with hydrogen sulphide to form reactive thiol groups, which at high pH values keep reacting further, leading to the formation of different functional groups such as double bonds, aldehydes, ketones etc.^{93,94} Under these harsh conditions, moreover, lignin partially depolymerizes into oligomers that are substantially modified from their native structure but become soluble at pH values above 12, due to the deprotonation of the phenolic functional groups. Hemicellulose, rosin soaps, and

inorganic compounds are also solubilized in the same aqueous solution, forming so-called black liquors. The liquors (after being dried) are normally burned in the recovery boiler of the industrial plant to isolate inorganic salts, while the thermal energy that is liberated from the combustion of lignin is then recovered to fulfil the energetic demand of the pulp mills. However, when the production of lignin exceeds the need for energy, the recovery of Kraft lignin can be achieved through a process called Lignoboost, that leads to the isolation of a solid lignin after acidification with CO₂, sulfuric acid and subsequent filtration.⁹⁷

In the sulfite process (**Figure 1.7**, light blue/grey pathway) lignin is removed using an aqueous solution of different sulfites or bisulfites salts with pH values ranging from 1 to 5. During the process, lignin is dissolved into the aqueous liquor together with hemicellulose, leaving cellulose behind as a solid. As for Kraft lignin, it is possible to recover lignin from sulfite pulping. In these cases, the “Magnefite” process allows to recover magnesium lignosulfonates⁹⁸, while the Howard process allows the isolation of calcium lignosulfonates by precipitation and filtration with CaO.⁹⁹

In addition to the two industrial methods described above which use aqueous solutions for the extraction of lignin, another class of emerging pulping and lignin valorization processes use organic solvents at temperatures ranging from 80 to 250 °C to fractionate the biomass. These novel methods are usually referred to as Organosolv processes (**Figure 1.7**, red pathway). The resulting Organosolv lignins can be obtained using several solvent mixtures and conditions.¹⁰⁰ Alcohols or dioxane are the most frequently utilized organic solvent for this process and are often combined with water in concentrations generally varying from 40 to 100%. To help the delignification, inorganic acid catalysts (e.g., H₂SO₄ or HCl) or organic acids (e.g., formic acid) are added at low concentrations (0.1 to 2%).^{101–103}

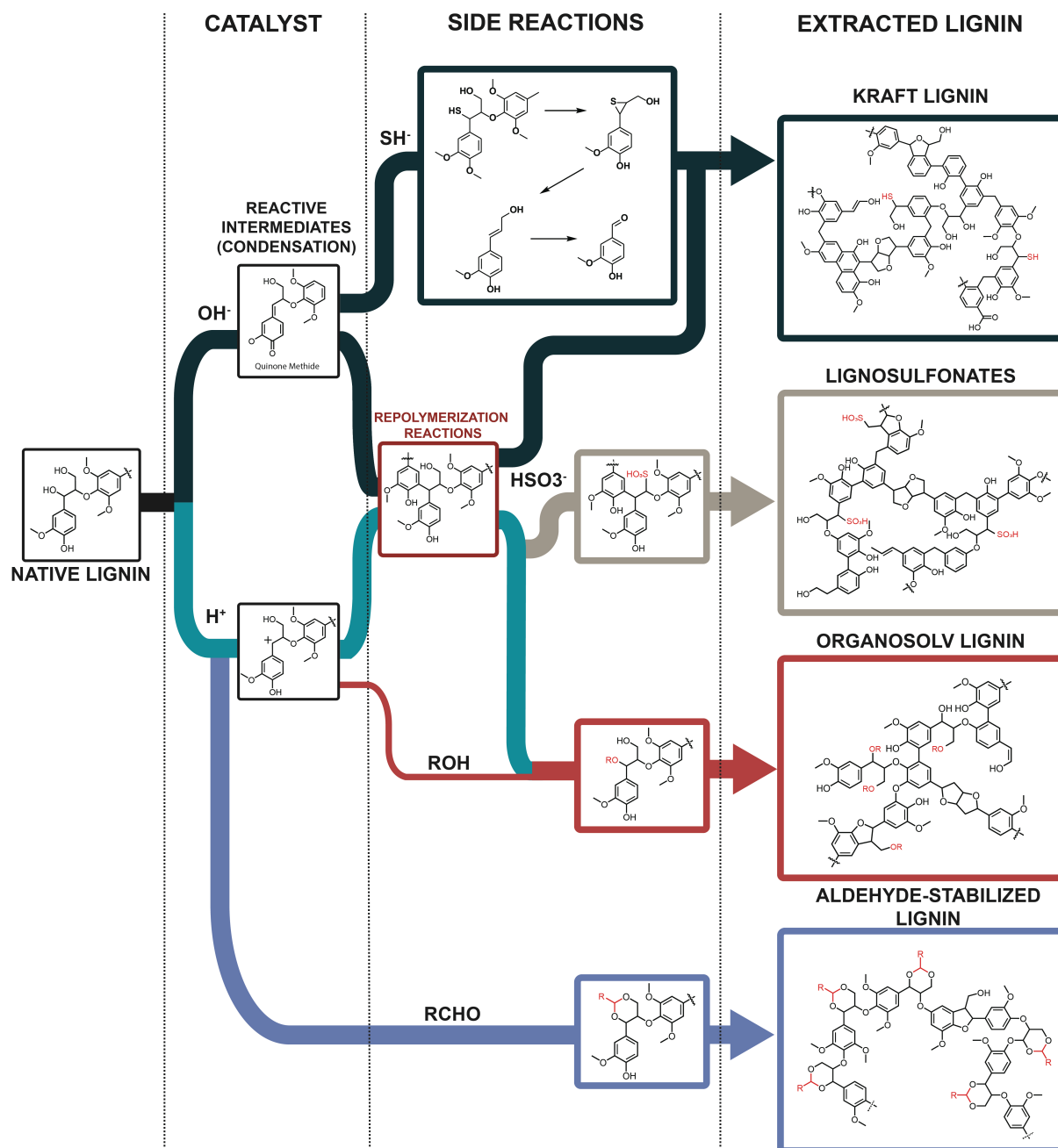


Figure 1.7. Common catalysts, side-reactions and resulting chemical structures of extracted lignins. In the figure Kraft lignin is presented in the top pathway, Lignosulfonates in the light blue/grey pathway, Organosolv lignin in the light/blue and red pathway and finally the Aldehyde-stabilized lignin is obtained following the bottom pathway.

Organosolv lignins follow a similar path to the previous process for what concerns the formation of cationic intermediates and condensation and repolymerization reactions, hindering lignin's subsequent upgrading or use.¹⁰⁴ However, in some of these processes, the alcohols that are present can react with the aforementioned cationic intermediates, forming

new ether bonds that can partially avoid the subsequent repolymerization and thus the formation of new C–C linkages.

Recently, our research group reported that a modified acid-catalysed Organosolv process with the addition of aldehydes such as formaldehyde (the Aldehyde Assisted Fractionation, AAF) could greatly improve the quality and upgradeability of the resulting lignin. In the AAF (**Figure 1.7**, bottom pathway), the presence of aldehydes in the reaction media prevents the condensation and repolymerization of lignin by blocking the reactivity of the hydroxyl groups in the α and γ positions of the monolignols *via* the formation of a 1,3-dioxane ring.

Acetal formation is highly favourable and maintains intact a large majority of the ether bonds originally present in the lignin. Because of this functionalization, the lignin obtained can be catalytically depolymerized to monomers at near-theoretical yields (i.e., based on the cleavage of the number of β -O-4 linkages originally present in the lignin), which demonstrated near complete functionalization.¹⁰⁵

1.6 The challenges of using isolated lignin as a raw material

Substituting aromatic materials derived from synthesis of individual fossil-based building blocks with extracted lignin poses several challenges, most of which come from the fact that many of the reviewed extraction techniques, especially those used at an industrial scale, have little to no control over the lignin's final structure. As characterized during hydrothermal biomass pretreatment, and as described before, lignin tends to depolymerize and repolymerize with itself, leading to creation of an elevated number of covalent C–C linkages.¹⁰⁶ The higher presence of these new bonds has the consequence of decreasing the linearity of the oligomers in favour of branched and cross-linked structures and increasing the average molecular weight of the extracted lignin, which in some cases can lead to reduced solubility. Most importantly, the formation of novel C–C linkages can also reduce possibilities for further functionalization. This is due to the fact that when condensation and repolymerization happen, the formation of new C–C bonds results either from radical reactions on the aromatic rings or from the disappearance of hydroxyl groups.¹⁰⁷ C–C bonds are also very difficult to break selectively, at least not without altering the other inter-unit linkages.¹⁰⁸ Moreover, when lignin repolymerizes, its oligomers tend to form a wide array of inter- and intra-molecular noncovalent bonds (e.g., hydrogen bonds, CH– π bonds, and π – π stacking). These interactions

have been hypothesized to hinder the solubility and/or miscibility of lignin with a great variety of solvents or polymers.^{109,110}

Incorporating lignin into materials is thus facilitated by undergoing as limited number of modifications as possible. This provides most of the original inter-unit bonds, hydroxyl groups, and aromatic ring positions, which can each be targeted for further chemical modification to meet the target application.

1.7 Strategies for incorporating lignin into novel materials and polymers

Although the physiochemical properties of lignin do not render it the best candidate for a simple blending with other polymers, the simplicity of this concept has led to several attempts to do so for various uses. Lignin has notably been mixed with polyolefins like polyethylene or polypropylene¹¹¹ and aromatic polymers such as polystyrene.¹¹² Other materials that have been explored include blends of lignin with polyethylene terephthalate¹¹³ and poly(butylendipate-co-terephthalate)¹¹⁴ for packaging applications. Lignin has been used as a filler in combination with polysiloxanes to increase the renewable portion of the final polymeric material¹¹⁵, or with polyacrylonitrile for the development of lignin-based carbon fibres.¹¹⁶ Blending lignin with polylactic acid has been explored for novel 3D printing materials¹¹⁷ and with polyamides for the development of flame retardants.¹¹⁸ Recent work by Romhányi and colleagues has shed some light on the properties, and on the consistency of these properties, of lignin-polymer blends.¹¹⁹ As reported by the authors, there have been many studies of these materials, but results have been inconsistent, as the same type of blends have led to differences in miscibility, physical, and mechanical properties. They notably prepared blends of lignosulfonates with several commercial polymers and showed that they could never detect perfect miscibility, but only incorporation of lignin in the form of microdroplets. The size of these microdroplets depended somewhat on the preparation of the blends, but mostly on thermodynamic factors, including intra- and inter-molecular interaction between lignin and the polymers. Finally, the mechanical properties of the blends were quite poor in terms of modulus and tensile strength, and they showed only one case where an application could be met for one of the prepared blends. They suggested that some of these challenges could be overcome by chemically modifying lignin to introduce new functional groups and make the non-covalent interactions more favourable during the blending process.

This approach has become more and more common in past years as our understanding of lignin structure has improved.

Several functional groups already present in the lignin make this biopolymer a good candidate for controlled chemical modification. Functionalization possibilities stem mainly from the reactivity of the aromatic rings of guaiacol and syringol units, as well as in the aliphatic hydroxyl groups present along the lignin backbone. In this chapter, we first touch upon the possibility of functionalization of the aromatic part of the phenylpropanoid units, followed by the combined reactions of phenols and hydroxyls, and finally on functionalization that can be performed at the α and γ position of the aliphatic part of the lignin backbone. A comprehensive scheme is provided in **Figure 1.8**.

1.7.1 Functionalization of the aromatic rings

One of the most common reactions that can be performed on the aromatic rings is the hydroxyalkylation of phenolic units using formaldehyde in the presence of a strong base such as NaOH (**Figure 1.8, b**). This reaction is analogous to the one that occurs during the formation of phenol formaldehyde resins (the targeted application). The goal is to have lignin perform the same function as phenol and substitute some of this petrol-based and toxic chemical to produce lignin-phenol-formaldehyde (LPF) resins to be used as adhesives in the preparation of plywood.¹²⁰ Another set of reactions performed on the phenolic units of lignin is the amination *via* the Mannich reaction, which introduces amino groups (**Figure 1.8, a**). This approach was performed by Du and colleagues who used Kraft lignin obtained from the Lignoboost process to synthesize and characterize a class of aminated lignin with potential use as polycationic polymers or surfactants.¹²¹ Nitration can also modify lignin by introducing electron withdrawing nitro groups onto the aromatic ring (**Figure 1.8, c**).¹²²

Finally, lignin is prone to electrophilic aromatic substitution in presence of formaldehyde and condensation with urea to form so-called lignin-urea-formaldehyde resins (**Figure 1.8, d**).¹²³ All pathways that covalently introduce non-native nitrogen atoms in lignin can allow for the synthesis of novel polyamines and polyamides, but have also been proposed as a way to create a new class of biocompatible and slow releasing fertilizers.¹²⁴

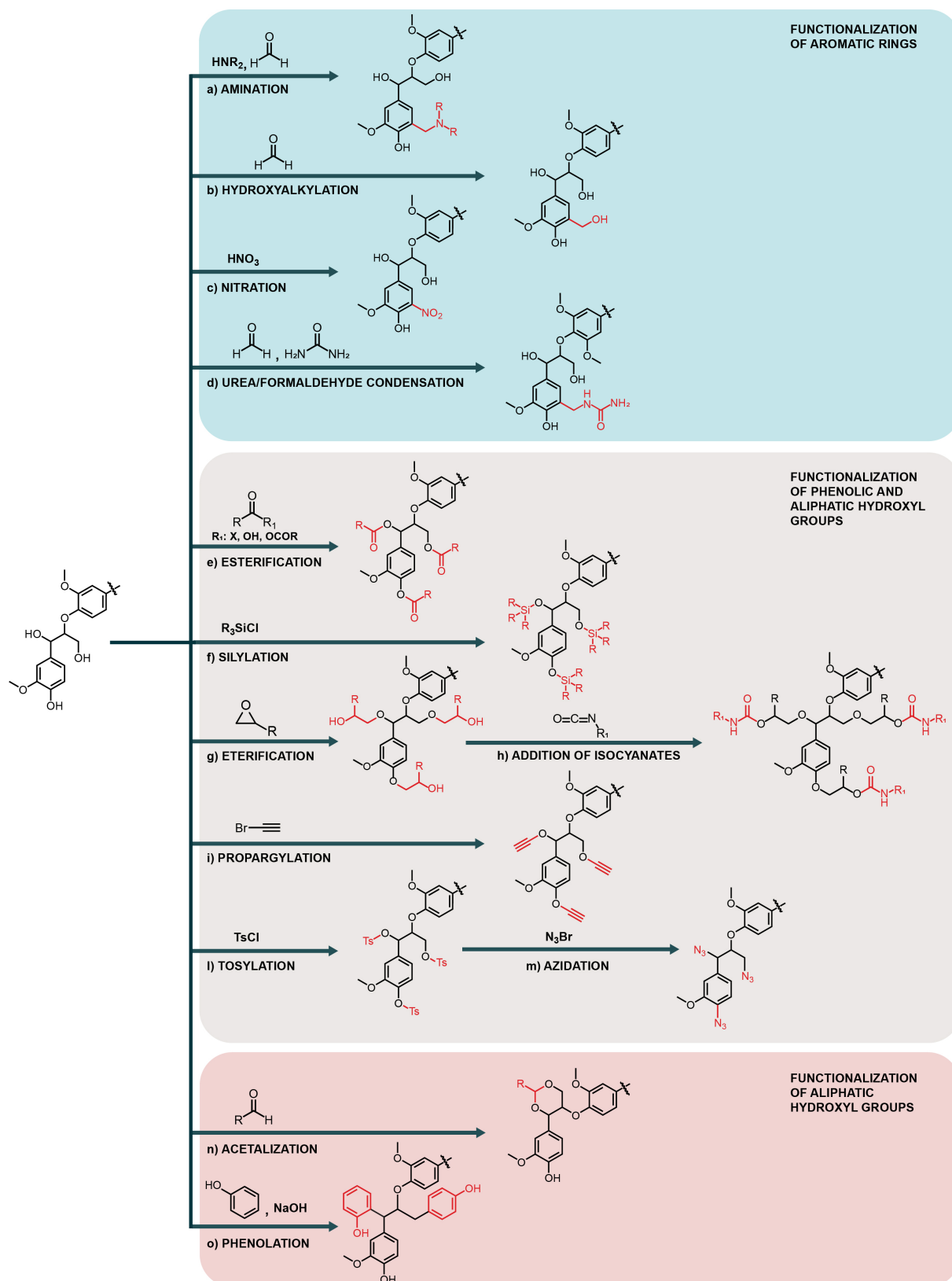


Figure 1.8. Possible chemical modifications of the lignin backbone. Functionalization of the aromatic rings are presented in the blue box, functionalization concerning both phenolic and aliphatic hydroxyl

groups are shown in the grey box, and finally functionalization reactions that occurs only on the hydroxyl groups of lignin are shown in the red box.

1.7.2 Reaction of phenolic and aliphatic hydroxyl groups

In addition to the targeting of lignin's aromatic rings, functionalization possibilities also exist for the phenolic and alkylic OH groups along the oligomer backbone. Esterifications are a category of common reactions for lignin functionalization and involve the reaction of lignin hydroxyl groups with acyl chlorides¹²⁵, anhydrides¹²⁶, lactones¹²⁷, lactides¹²⁸, and carboxylic acids (**Figure 1.8, e**).¹²⁹ Reactions with carboxylic acids have notably been used by Larrañeta and colleagues to incorporate up to 40% lignin in a new hydrogel that presented antibacterial properties and could be used to deliver hydrophobic drugs such as curcumin. This hydrogel was synthesized from the esterification reaction between lignin's hydroxyl groups and polyethylene glycol with the carboxylic acids present in poly(methylvinyl ether-co-maleic acid).¹³⁰ Esters are also the most commonly used groups to covalently attach lignin to multiple initiators for controlled polymerization such as atom transfer radical polymerization (ATRP)^{131,132} and reversible addition-fragmentation chain transfer (RAFT) polymerization.^{133,134}

Still within possible applications of esterification functionalizations, acetylations are commonly performed with acetic anhydride and pyridine to decrease the amount of intramolecular hydrogen bonds in lignin, in order to improve its miscibility with other polymers. Zhang and colleagues reported the production of carbon fibres from lignin, where even partial acetylation of the biopolymer increased processability during dry spinning. The remaining unreacted OH groups crosslinked during thermal treatment, leading to final fibres with high tensile strength compared to what had been previously reported in the literature¹³⁵. Acetylation can usually be performed at high yields and selectivity and thus has been used for several applications, including when there is a need to increase miscibility of lignin with non-polar materials, increase lignin solubility in organic solvents¹³⁶, or to decrease the glass transition temperature.¹³⁷ For this reason, acetylation is still the predominant reaction used for solubilizing lignin during sample preparation for gel-permeation chromatography. As reported by Buono and colleagues, silylation is a less common alternative reaction that provides similar and sometimes improved yields, thermal properties, and solubility enhancements.¹³⁸ Silylation, which is the addition of substituted silyl functionalities to lignin's hydroxyl groups,

can be used to quantitatively introduce other functional groups in the lignin backbone (**Figure 1.8, f**). Li and co-workers notably reported the synthesis of a vinyl-silylated lignin which was further copolymerized with polyacrylonitrile (PAN) to produce films. They compared the mechanical behaviour of this material with a copolymer of Kraft Lignin and PAN and reported that silylation and the introduction of vinyl groups significantly enhanced its properties by comparison to the unfunctionalized variants.¹³⁹

An important set of reactions also includes the etherification of hydroxyl groups to synthesize long chain polyethers, which can be carried out in several ways (**Figure 1.8, g**). Among these is the oxyalkylation reaction, normally carried out in presence of epoxides¹⁴⁰ or some of their reactive polymers such as poly(ethylene)-glycol diglycidyl ether (PEGDGE), that allow the linking of a polyether polymer to the lignin.¹⁴¹ However, epoxides and their derivatives are highly reactive, volatile, and toxic, and often require the use of high-pressure reactors.¹⁴² Due to their handling and associated environmental issues, substitute reactions have been proposed including the use of ethylene- and propylene carbonates, as reported by Liu¹⁴³ and Kühnel.¹⁴⁴ The addition of these long chain polyols on the lignin substrate has been mainly explored to produce novel lignin-epoxy resins¹⁴⁵ or bio-based polyurethanes, due to the possible addition of isocyanates to the hydroxyl groups (**Figure 1.8, h**).^{146,147}

Finally, another strategy for the introduction of various functional groups is to transform lignin's hydroxyls into good leaving groups for performing subsequent substitution reactions. This has been accomplished using the tosylation reaction (**Figure 1.8, l**).¹⁴⁸ The tosyl group is very versatile, as it allows for the introduction of other functional groups such as azides (**Figure 1.8, m**) that can be either easily reduced to primary amines or further reacted with alkyne group to form a 1,2,3-triazole through the Huisgen cycloaddition. Panovic and colleagues performed tosylation, azidation, and a final coupling reaction with an alkyne-functionalized fluorophore derived from vanillin, in order to produce a novel fluorescent lignin functionalized along the whole backbone.¹⁴⁹ Alternatively, alkyne groups can also be introduced on the phenylpropanoid units *via* the propargylation reaction (**Figure 1.8, i**).¹⁵⁰ This strategy was used by Sadeghifar and colleagues to produce a biodegradable film that displayed UV light absorbing properties, which was based on cellulose modified with azide groups and subsequently coupled with a propargylated lignin.¹⁵¹

1.7.3 Reaction of aliphatic hydroxyl groups

Phenolation reactions on the α and γ hydroxyl groups can effectively add phenolic groups by grafting them on the lignin side chain, which increases the number of aromatic reactive sites (**Figure 1.8, o**).¹⁵² This reaction has often been used to improve the synthesis of LPF resins, as the number of reactive sites in extracted lignin is often drastically lower than in native lignin due to repolymerization during extraction. Additional phenolic groups increase the quantity of reactive positions available on the aromatic rings, which maximises the number of electrophilic substitution reactions with formaldehyde. This results in increased crosslinking, which allows for a higher lignin content in these resins.¹⁵³

Importantly, most of the reactions described so far have been performed on lignins which were extracted according to the Kraft, Sulfite, or acid-catalyzed Organosolv procedures described above. These processes allow the recovery of lignins which have been significantly altered by condensation, repolymerization, and other side-reactions. In these conditions, although a sufficient number of chemical functionalities can be maintained for further chemical reactions, lignin has a high polydispersity in terms of molecular weight, and further steps of refining are needed to obtain homogeneous fractions for applications in materials.^{93,154} Therefore, even though most of these reactions have been shown to slightly improve the compatibility of lignin with other materials, successful applications are still severely limited.

Improving lignin incorporation into materials could potentially be achieved by maintaining a high number of functional groups in the lignin while avoiding its repolymerization during the extraction process. Functionalizing lignin with aldehydes involves their reaction with the α and γ hydroxyl groups of the β -O-4 linkage in the presence of an acid catalyst in order to form acetals (**Figure 1.8, n**), a process defined as Aldehyde-Assisted Fractionation (AAF). This reaction both avoids losing functionality by preventing repolymerization reaction, but also leads to extremely efficient functionalization. Analysis by 2D NMR showed that the degree of functionalization could exceed 90%.¹⁵⁵ Though this functionalization was first reported with formaldehyde, it was since then shown that this reaction works efficiently with a large array of aldehydes. It was also notably shown that by using a variety of multiple aldehydes, the solubility of the resulting lignins could be tuned making them soluble in vastly different solvents from water to toluene.^{155–157} This range of solubility could be further used to tailor lignin incorporation into several polymers.

1.8 Concluding remarks

To summarize, it is shown here that to mitigate the current climate crisis, the global reliance on fossil-based fuels and materials should be diminished in favour of feedstocks that prevent the accumulation of greenhouse gases, in particular CO₂, in the atmosphere. In line with this goal, lignocellulosic biomass (comprised of cellulose, hemicellulose, and lignin) is a promising candidate to replace the use of fossil fuels especially in material applications.

In particular, the principal aim of this chapter is to present the potential and the challenges associated with the direct use of lignin for the replacement of petrol-based polymers and materials. In addition to having a complicated chemical structure that varies across biomass species, lignin has a high reactivity due to the hydroxyl and aromatic functional groups present on its backbone. Most lignin isolation methods do not control this reactivity, which leads to irreversible condensation reactions. These reactions tend to increase the molecular weight, branching, functional complexity, and intrinsic tendency to form strong intra- and intermolecular bonds of lignin, making extracted lignin increasingly difficult to incorporate into polymers and materials¹⁵⁸. Therefore, chemical modifications of the lignin backbone are often required to introduce new functionalities that are compatible with the final materials. Aromatic rings, as well as phenolic and aliphatic OH, are the main functional groups that are chemical modification targets in lignin. When these modifications take place, some of the strong intra- and intermolecular bonds present in the original extracted lignin are broken, and thus lignin can be more easily incorporated in blends or covalently bound with other polymers for the development of more renewable or new functional materials. Even though lignin has several functional groups that can undergo chemical modifications, their total number is often severely reduced during lignin isolation, limiting the compatibility between lignin and polymers.

However, several recent developments could lead to rapid improvements in lignin use in materials. Improvements in analytical techniques, particularly NMR, have allowed us to gain a much clearer understanding of lignin's functional group distribution. In recent years, techniques have even emerged to quantify these functional groups in isolated lignin. This higher understanding of lignin's functionality has fostered the development of targeted chemical approaches that can both prevent condensation and quantitatively introduce new functionalities on the biopolymer. Altogether, these techniques could facilitate increased control of lignin's structure to approach the designed functionalities of fossil-based polymers.

Such improvements could greatly increase lignin incorporation into everyday materials, paving the way towards more sustainable chemicals and products.

Chapter 2 Objectives

In line with what was discussed in the previous chapter, the overall goal of my doctoral thesis is to overcome some of the major challenges related to the extraction, characterization and use of lignin for the integration of this biopolymer into existing materials, as well as for the development of new ones. Therefore, this thesis will be pursuing three main objectives.

2.1 Objective 1: Extraction and simultaneous chemical functionalization of lignin from lignocellulosic biomass

The first objective of my doctoral work is to develop a process for lignin valorization that consider this polymer as a main product of the process leading to the isolation of cellulose from biomass. As previously described, if no precautions are taken in designing a process that preserves the structure of lignin during biomass fractionation, lignin will inevitably undergo sever chemical modifications through condensation and repolymerization reactions. These uncontrolled side-reactions will consequently hinder lignin's further upgrading, also limiting the yields of additional chemical functionalization reactions performed on the remaining functionalities left on its backbone.

Moreover, the need to perform additional chemical functionalizations on lignin extracted with traditional methods inevitably means using more resources in terms of chemicals, solvents and purification steps, which translate in an overall diminished sustainability.

Keeping in mind these considerations, in the first objective of my thesis I aim to explore the possibility of using the Aldehyde Assisted Fractionation process, initially developed in our research group for the quantitative depolymerization of lignin to aromatic monomers, to extract lignin in high yields from lignocellulosic biomass and at the same time introduce on the biopolymer new chemical functionalities that were not present in its native structure. Although the AAF process has been demonstrated to be able to prevent lignin condensation by the formation of stable acetal between aldehydes and the β -ether units in lignin, this process has not yet been employed to specifically introduce on the lignin scaffold novel

functionalities. Multifunctional aldehydes (e.g., aldehydes that bear on the same molecule more than one functional group), are promising candidates to explore the extraction and simultaneous chemical functionalization of lignin from lignocellulose.

Therefore, the first goal of my work will be to perform AAF employing multifunctional aldehydes in order to evaluate their abilities to bind covalently to the lignin being extracted, while preventing condensation and repolymerization side-reactions.

2.2 Objective 2: Characterization of extracted lignins for their controlled chemical functionalization.

The second objective of this thesis is to use simple spectroscopic techniques to be able to quantify the newly introduced functionalities, in order to evaluate any correlation between the amount of multifunctional aldehydes used during the simultaneous extraction and the final amount of chemical functionalization introduced on the lignin oligomers.

Traditionally, as described in the Section 1.4, the characterization of lignin is a non-trivial task due to the complexity of its structure and the high number of different linkages and functionalities. In particular, spectroscopic techniques such as ^1H NMR are poorly employed in the characterization of lignin oligomers due to the overlapping of the polymer signals, which makes it an impractical and non-informative tool, even though it is a simple and fast technique. Therefore, the detection and quantification of chemical functionalities in lignin is often problematic and requires multidimensional NMR experiments, which are sometimes time consuming, require expensive instrumentation and are usually non quantitative.

In this work I hence aim at overcoming some of these issues by introducing on the lignin novel functionalities that can be easily monitored by monodimensional and fast spectroscopic techniques such as ^1H , ^{31}P NMR and FT-IR. The use of these fast and quantitative NMR techniques allows for precise control over lignin's overall chemical functionalization, demonstrating how complete control over the biopolymer structure and functionalization can be easily achieved during extraction.

2.3 Objective 3: Exploiting extracted multifunctionalized lignins in materials applications

The final goal of this doctoral work is to exploit extracted multifunctionalized lignins in materials applications and to compare material properties with those from lignin extracted by traditional methods, in order to observe if the targeted chemical functionalization achieved by multifunctional-AAF brings any benefit to the final application compared to other extracted lignins.

In the previous chapter it was discussed how in order to increase the compatibility between lignin extracted with traditional processes it was often necessary to perform additional functionalization reactions and introduce non-native functionalities. Even though these approaches increase the possibilities of using lignin in combination with polymers and other materials, the degree of functionalization is usually low as it is often directly correlated to the number of residual aliphatic and aromatic hydroxyl groups left on the lignin structure after extraction.

The final objective of my thesis is therefore to demonstrate that the functionalizations introduced onto the lignin through multifunctional AAF are pivotal to obtain desired properties in the final materials, and that the properties of these materials are either worse or not achievable via traditional technical lignins.

The overall goal of this thesis is to show how, in order to best valorize lignin without losing the other fractions of lignocellulosic biomass, it is beneficial to switch the approach towards this biopolymer. When extracted lignin is considered as a mere by product of the pulping process, its applications in materials remain limited. On the contrary, when the final application of lignin is taken into account before the biomass fractionation, it is possible to design versatile processes that allow us to obtain materials with unique properties, fully valorising all the fractions of lignocellulose.

Chapter 3 One-step extraction and controlled functionalization of lignin for phenolation reactions

This chapter was adapted from the following article with the permission of all co-authors and of the journal.

*Postprint version of the article: Stefania Bertella, Jeremy S. Luterbacher. “Simultaneous extraction and controlled chemical functionalization of hardwood lignin for improved phenolation”. *Green Chemistry*, **2021**, 23, 3459.*

My contribution: Designing and performing all the experimental work, drafting of the manuscript and figures.

3.1 Introduction

One of the most promising uses of lignin in the development of sustainable materials is the partial substitution of phenol and formaldehyde in PF resins, given the similarities between lignin's structure and that of phenolic resins.¹⁵⁹ However, this same lignin structure poses important challenges that ultimately hinder the use of this biopolymer in material applications. Specifically, the two main challenges of lignin are given by its irregularity, especially when isolated, which makes its consistent incorporation in these PF thermosets difficult, and the low reactivity of its phenolic groups, which limits crosslinking compared to pure phenol.^{160,161}

As discussed from Section 1.3.3, the heterogeneity of lignin arises not only from the different monolignol composition, but also from the variety of functional groups and chemical linkages that bind these subunits together (**Figure 3.1**, a). Amongst these linkages, the β -O-4

is the most abundant and, thus, the units containing them are most targeted for the chemical modification of lignin.¹⁶²

However, during traditional fractionation of lignocellulose, such as the case of Kraft (KL) or Organosolv (OSL) processes, lignin tends to condense, beginning with dehydration reactions that remove the α hydroxy groups in the β -ether units. This dehydration causes the formation of reactive carbocations that are prone to electrophilic substitution on the phenolic rings. These resulting repolymerization reactions lead to the formation of strong and new C–C linkages which are highly recalcitrant to further upgrading, i.e., they are difficult to break or selectively functionalize (**Figure 3.1, b**).¹⁰⁸ This recondensation, that occurs almost systematically with chemical lignin isolation, makes it very challenging to control the chemical structure of the final isolated lignin and ultimately the degree of functionalization that can be achieved on the polymer.

The structure of native lignin and to an even greater extent, that of isolated lignin, leads hence to low reactivity when used as a phenol substitute in PF resins.¹⁶³ This low reactivity mainly occurs because the positions on the phenolic ring are more occupied in isolated lignin and, to a lesser extent, native lignin, compared to simple phenol.¹⁶⁴ For this reason, functionalizing conventionally isolated lignins to increase their reactivity towards certain type of reactions is an approach that has been extensively used to valorize this sustainable biopolymer and make it more suitable to incorporation in materials.¹⁶⁵

In particular, to increase the compatibility and reactivity of lignin towards the synthesis of PF thermosets, while decreasing its recalcitrance, many researchers have attempted to maximize the number of reactive sites of the biopolymer.¹⁶⁶ A well-known reaction used to achieve this goal is phenolation (**Figure 3.1, d**). Generally, the preferred catalysts for phenolation are strong acids, due to the possibility of performing electrophilic aromatic substitution between phenol and the carbocations that forms on the α or γ position of the lignin, after dehydration at low pH (**Figure 3.1**). A drawback of this approach is that most of the PF resins are currently synthesized at high pH, which requires a neutralization and/or lignin isolation step after acid-catalyzed phenolation.^{167,168}

In this chapter, we sought an avenue to both prevent the condensation of lignin during isolation to provide a more regular structure and create an avenue for improved lignin functionalization. We aimed at achieving this goal by using multifunctional Aldehyde Assisted Fractionation with terephthalic aldehyde (TALD).

TALD could in fact stabilize the β -ether units in lignin via the formation of acetals, and at the same time introduce novel aldehyde groups on the lignin scaffold (**Figure 3.1, c**).¹⁶⁹

Amongst the main benefits of terephthalic aldehyde, the most important are that this molecule does not undergo aldol condensation due to the presence of the aromatic group and the absence of proton in α to the aldehyde.¹⁷⁰ TALD can also be sustainably sourced or be easily synthesized from renewable precursors. Indeed, Goulas et al. have recently reported that TALD could be produced via the heterogeneously catalysed oxidation of di-(hydroxymethyl) benzene, a molecule that can be synthesized from 5-hydroxymethyl furfural (5-HMF) derivatives and therefore from renewable carbohydrates.¹⁷⁰ Furthermore, Foyer et al. showed that it was possible to obtain thermoset resins of phenol with high thermal properties by substituting formaldehyde with TALD and conducting the reaction at high pH, demonstrating the reactivity of this dialdehyde towards phenolation reactions in basic conditions.¹⁷¹

In this work, we sought therefore to use TALD in the multifunctional AAF process to extract lignin at high yields while avoiding its condensation and precisely controlling the quantity of aldehydic functionalization on the scaffold of the biopolymer. We performed phenolation reactions in both acid and basic catalysis, comparing the result obtained on TALD-lignin with those from commercial Kraft Lignin (KL) and a mild Organosolv lignin (OSL).

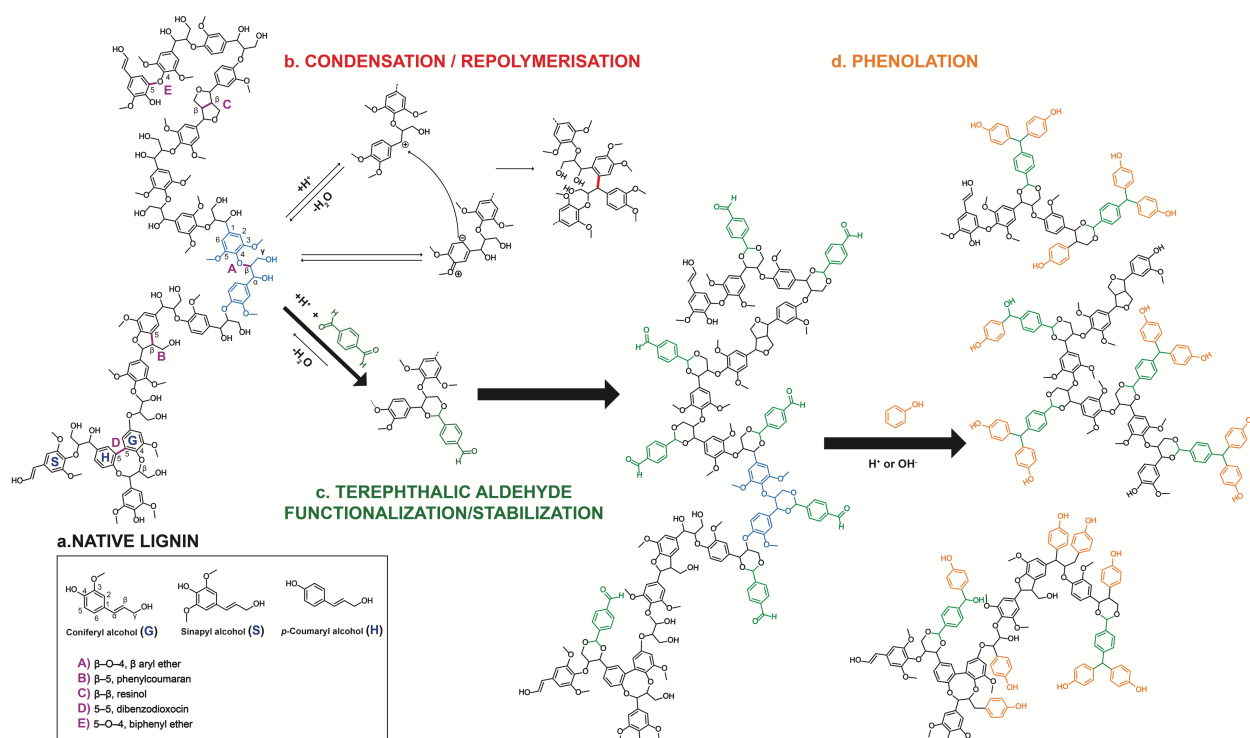
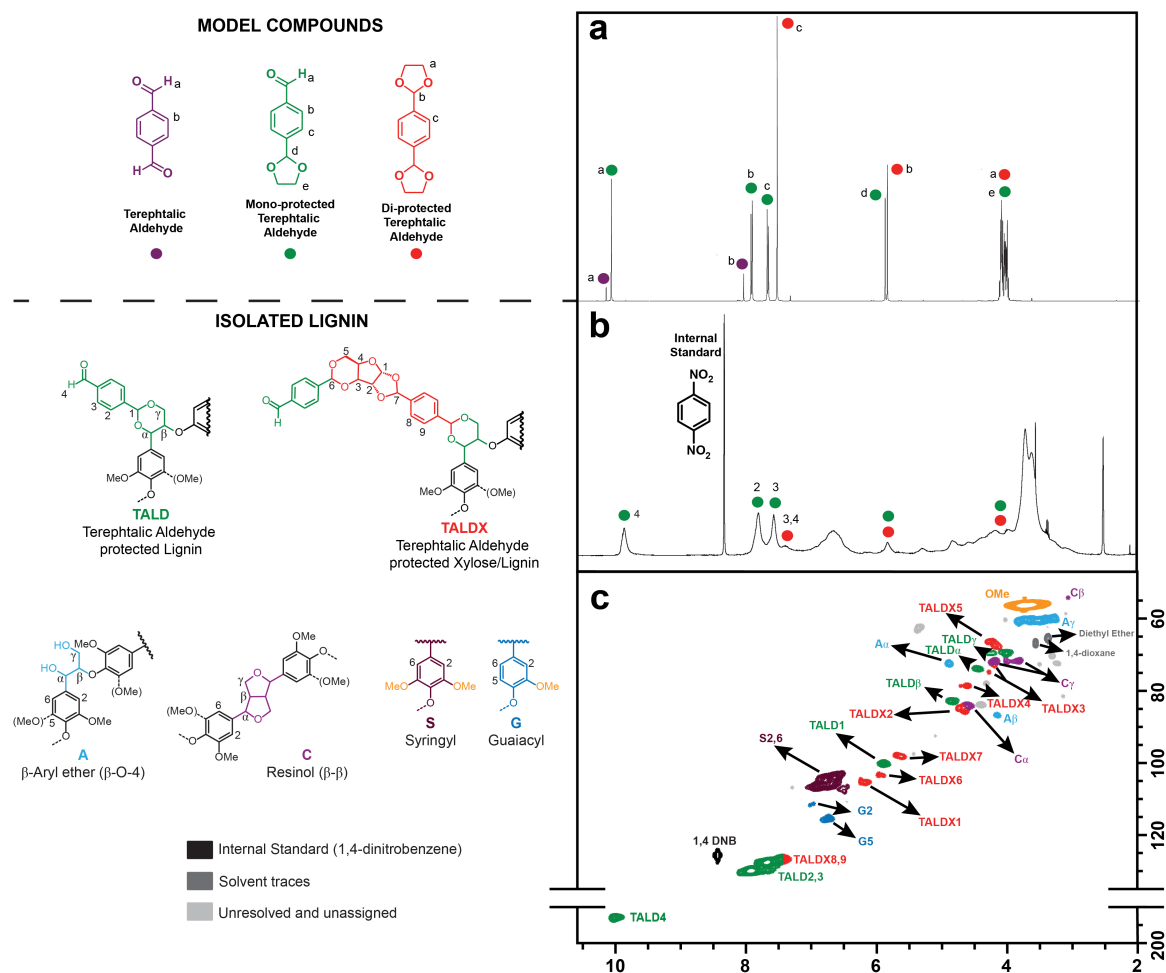


Figure 3.1. The structure of hardwood lignin and overview on the functionalization process of this chapter. (a) Proposed structure of native lignin in hardwood. (b) The mechanism of condensation and repolymerization reactions of lignin treated in strong acid conditions. (c) The TALD assisted fractionation mechanism and lignin structure described in this work. (d) The phenolation reactions of lignin performed in this work.

3.2 Lignin extraction and characterization

TALD functionalized lignins (TALD-lignins) were extracted from birch (*Betula pendula*) wood chips based on a modified procedure of our previously published aldehyde-assisted protocol.²⁴ In this process, lignocellulosic biomass was mixed with TALD at concentrations between 12.6 and 0.85 mmol/g dry biomass in an acid environment at 80 °C. These conditions favoured acetal formation and led to the stabilized lignin being solubilized into the organic solvent. Purified cellulose remained as an insoluble fraction, which was easily isolated by filtration. TALD-lignin could then be separated from the carbohydrates and the unreacted aldehyde by precipitation in diethyl ether. To perform control experiments, a OSL was also extracted in 80% ethanol in water for 5 h at reflux using HCl as a catalyst, following a protocol published by Zijlstra et al. (see Section A.2.3),¹⁷² whereas KL was obtained from a commercial source.

After the extraction, and without further treatments, isolated TALD-lignin, OSL and KL were all subjected to hydrogenolysis to evaluate the effectiveness of the lignin extraction as the resulting monophenolic molecules yield is an indirect indicator for the lack of condensation during extraction.^{173,174} The hydrogenolysis results, reported on the basis of the Klason lignin content in the original biomass, were then compared to those of the direct hydrogenolysis of native birch wood (Figure A.4 and Section A.3.2). Direct hydrogenolysis of untreated birch wood in THF produced 44.8 wt.% of aromatic monomers. In comparison, the hydrogenolysis of TALD, OSL and KL lignins led to the production of monomer yields of 39.4 wt.%, 7.2 wt.% and 1.7 wt.%, respectively. The monophenolic content is far superior when using TALD-lignin, despite both OSL and TALD-lignin having a high β -O-4 linkage content. However, OSL lignin, when extracted at such mild conditions, could only be obtained with a yield of 28 wt.%, whereas TALD lignins could be extracted with yields ranging from 81 to 100 wt.%. In comparison, KL were generally efficiently isolated from the biomass at high yields, but the condensed structures, with few ether linkages and a high content of uncleavable C–C bonds, resulted in a low yield of monophenolic molecules after hydrogenolysis.



to the spectrum obtained from isolated functionalized lignin (**Figure 3.2, b**), which revealed the close alignment between functionalized lignin peaks and their corresponding model compound structures. We also noted that the functionalized lignin's peaks broaden, as a result of the increase of the transverse relaxation time (T_2), which is typical of large molecules such as polymers and lignin oligomers. This broadening suggested that TALD was successfully bound to the biopolymer.

We also characterized the structure of the isolated lignin by Heteronuclear Single-Quantum Coherence NMR spectroscopy (HSQC-NMR). This technique allowed the identification of the signals assigned to the lignin scaffold characterized by the interunit linkages via the β -O-4 and β - β bonds, the C-H bonds of the syringyl and guaiacyl aromatic rings, and the signal assigned to the TALD functionalization (**Figure 3.2, c**).

Despite the extensive purification that included a Soxhlet extraction step and washing with diethyl ether, signals assigned to functionalized xylose (TALDX) were still found in the HSQC spectra. As the presence of such a significant amount of impurities present on the lignin after purification was unlikely, we hypothesized that the TALD could also partly act as a cross-linking agent between xylose and the lignin β -ether units. To confirm this hypothesis, we performed Diffusion Ordered Spectroscopy-NMR (DOSY-NMR). This technique allows the resolution of molecules present in a system based on their capacity for diffusion in solution, which reflects their difference in molecular weight. The spectra obtained for the TALD-lignin in DMSO- d_6 (**Figure A.3**) suggested that all these aforementioned signals present in the sample, in the region of interest, are thus likely part of the same molecular system. This result indicated that TALD functionalized xylose was likely directly bound to the lignin. The exact amount of this carbohydrate impurity however could not be quantified by standard or quantitative HSQC-NMR due to the variable differences in relaxation time and intensity of the signals. In fact, some of the carbohydrate signals were barely detectable after using a longer relaxation time during spectra acquisition. In such samples, the signal to noise ratio was low enough to cause substantial errors, which prevented reliable quantification. GPC measurement and DOSY NMR measurements also indicated that cross-linking between different lignin oligomers was unlikely to occur. We did not observe significant differences in measured molecular weights or diffusion behaviours in lignin samples, regardless of the

amount of TALD used during the extraction or even when using a lignin extracted with propionaldehyde, an aldehyde that cannot facilitate crosslinking (Table A.3).

We further characterized the structure of TALD-lignin via Diffuse Reflectance Infrared Fourier Transform (DRIFT) spectroscopy (**Figure 3.3**). Infrared techniques are a useful tool for the characterization of functional groups, and particularly for the detection of carbonyls, being that these functional groups have generally a strong transmittance signal at around 1700 cm^{-1} . We therefore compared the spectra of TALD-lignin extracted with a high (12.6 mmol/g dry biomass) or low (0.85 mmol/g dry biomass) amount of TALD with the spectrum of a lignin extracted in the presence of formaldehyde. The spectra of TALD-lignin showed a strong signal at 1702.5 cm^{-1} corresponding the carbonyl stretch. This signal, as expected, was not present in formaldehyde-stabilized lignin, since its carbonyl group disappears in the formation of the acetal. Noticeably, the relative intensity of the carbonyl stretch compared to the hydroxyl stretch at 3447.5 cm^{-1} was higher for the lignin that was extracted at a higher concentration of TALD than that for the lignin isolated with a lower concentration of the same aldehyde. This suggested a strong correlation between the concentration of TALD introduced during the extraction process and the amount of functionalization achieved on the lignin.

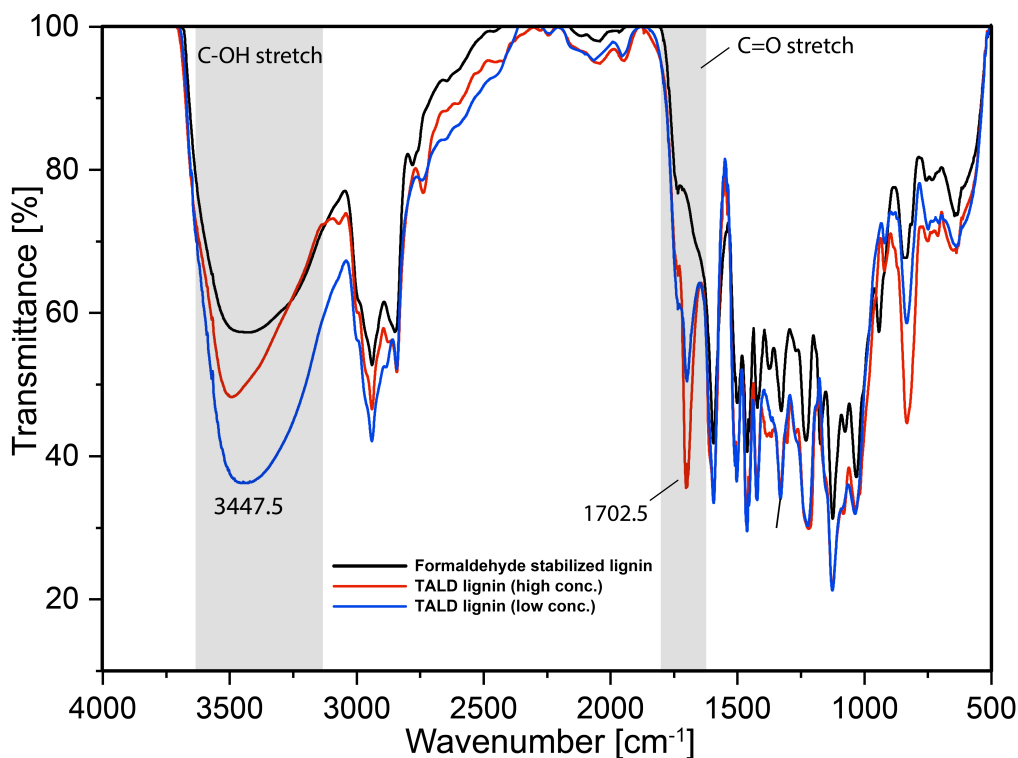


Figure 3.3. DRIFT spectra of formaldehyde and lignin functionalized with terephthalic aldehyde (TALD-lignin).

3.3 Controlling and quantifying the degree of TALD functionalization on isolated lignin

The structure of isolated lignins doesn't usually allow for quantitative or even qualitative determination of functional groups via ^1H NMR due to overlapping of the proton signals. However, in the ^1H NMR and HSQC-NMR spectra of TALD-lignin, the signals of bound TALD's free aldehyde group ($\delta_{\text{H}}/\delta_{\text{C}}$ 10.01/193.4 ppm) did not overlap with any other peak, which could allow its straightforward quantification by ^1H NMR. To do so, we used 1,4-dinitrobenzene (1,4-DNB) as an internal standard, because it did not react with lignin under analysis conditions and its ^1H NMR signal is a single peak at 8.42 ppm that did not overlap with other peaks associated with TALD-lignin (**Figure 3.2**, b). We then performed Inversion Recovery experiments on the signals of the free aldehyde at 10.01 ppm and of the internal standard at 8.42 ppm, in order to measure their longitudinal relaxation time constant (T_1) and assure full recovery of the peaks in between spectra acquisitions. The results (**Figure A.2**)

showed that the T_1 values were 2.33 s for the free aldehyde and 2.62 s for 1,4-dinitrobenzene. From these values we then decided to acquire spectra with a minimum delay time of 14 s. This method was then used to quantify the degree of functionalization of a series of lignins isolated using increasing concentration of TALD (**Figure 3.4** and Section A.3.1).

The concentration of TALD added to the reaction correlated with the quantity of residual free aldehyde groups on the corresponding extracted lignin, increasing from a minimum of 0.47 mmol/g of aldehyde groups to a plateau at 1.85 mmol of aldehyde functionalities per gram of isolated lignin. This correlation demonstrates that the concentration of TALD used during the isolation process can be tuned to precisely control the degree of functionalization of lignin.

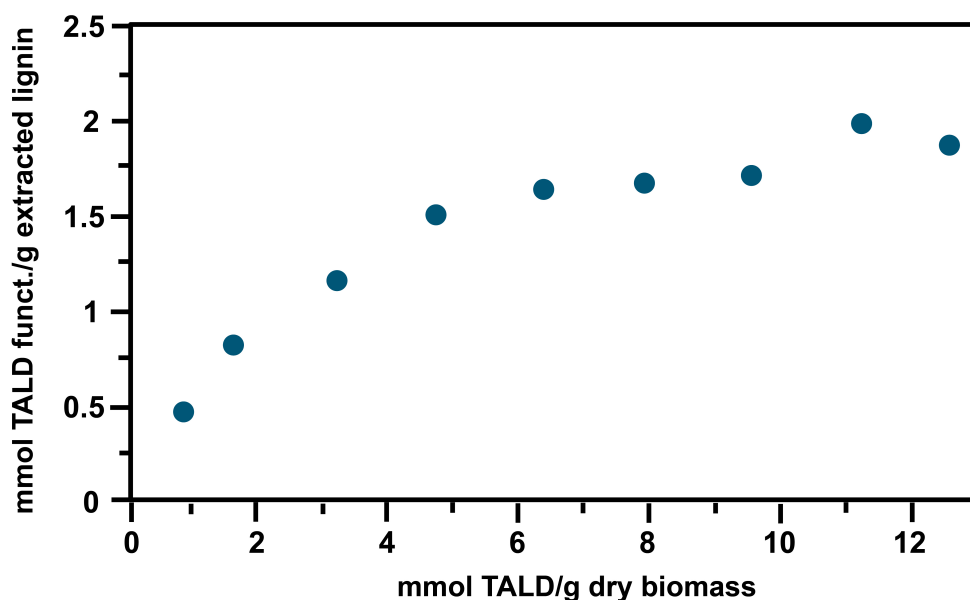


Figure 3.4. Effect of initial TALD concentration over final functionalization.

3.4 Phenolation of TALD-lignin

Exploiting the versatility of the aldehyde functionality and their reactivity with phenol in both acid and base conditions, we conducted phenolation reactions in both of these environments on TALD-lignin with an aldehyde content of 1.89 mmol/g (**Figure 3.5, a**).^{175,176} We compared the results to those obtained with a commercial KL and a OSL under the same conditions. The phenol was used as both the reagent and solvent during phenolation. Acidic phenolation (APH) of lignin was conducted following a procedure previously reported by Podshun et al.¹⁵², with some modification. Basic phenolation (BPH) was performed with the same ratio of lignin to phenol but catalysed by an aqueous solution of NaOH (Section A.2.4).

After isolation, lignins were structurally characterized by HSQC-NMR to confirm the success of the reactions. We observed increases in peak volumes within the aromatic region of the HSQC spectrum after acid (TALD-APH lignin) and basic (TALD-BPH lignin) phenolation (**Figure 3.5**, b, c and d). After reaction of TALD-lignin with phenol, the signal of the aromatic proton in the *ortho* and *meta* position of TALD shifted from $\delta_{\text{H}}/\delta_{\text{C}}$ 7.66/127.44 and $\delta_{\text{H}}/\delta_{\text{C}}$ 7.91/129.95 ppm to higher fields at $\delta_{\text{H}}/\delta_{\text{C}}$ 6.96/129.44 ppm. Furthermore, a new signal corresponding the phenol units bound to the lignin appeared at $\delta_{\text{H}}/\delta_{\text{C}}$ 6.68/115.35 ppm, indicating the success of the reaction in both catalytic conditions. The DRIFT spectra of these lignins further confirmed phenolation due to the signal of carbonyl stretch disappearing in both APH- and BPH-TALD-lignins, while the relative intensity of the hydroxyl stretch increased in both cases (**Figure 3.5**, e). This change suggested that a higher quantity of phenolic groups was successfully bound to the lignin and that the aldehyde was consumed as hypothesized in the mechanism (**Figure 3.5**, a).

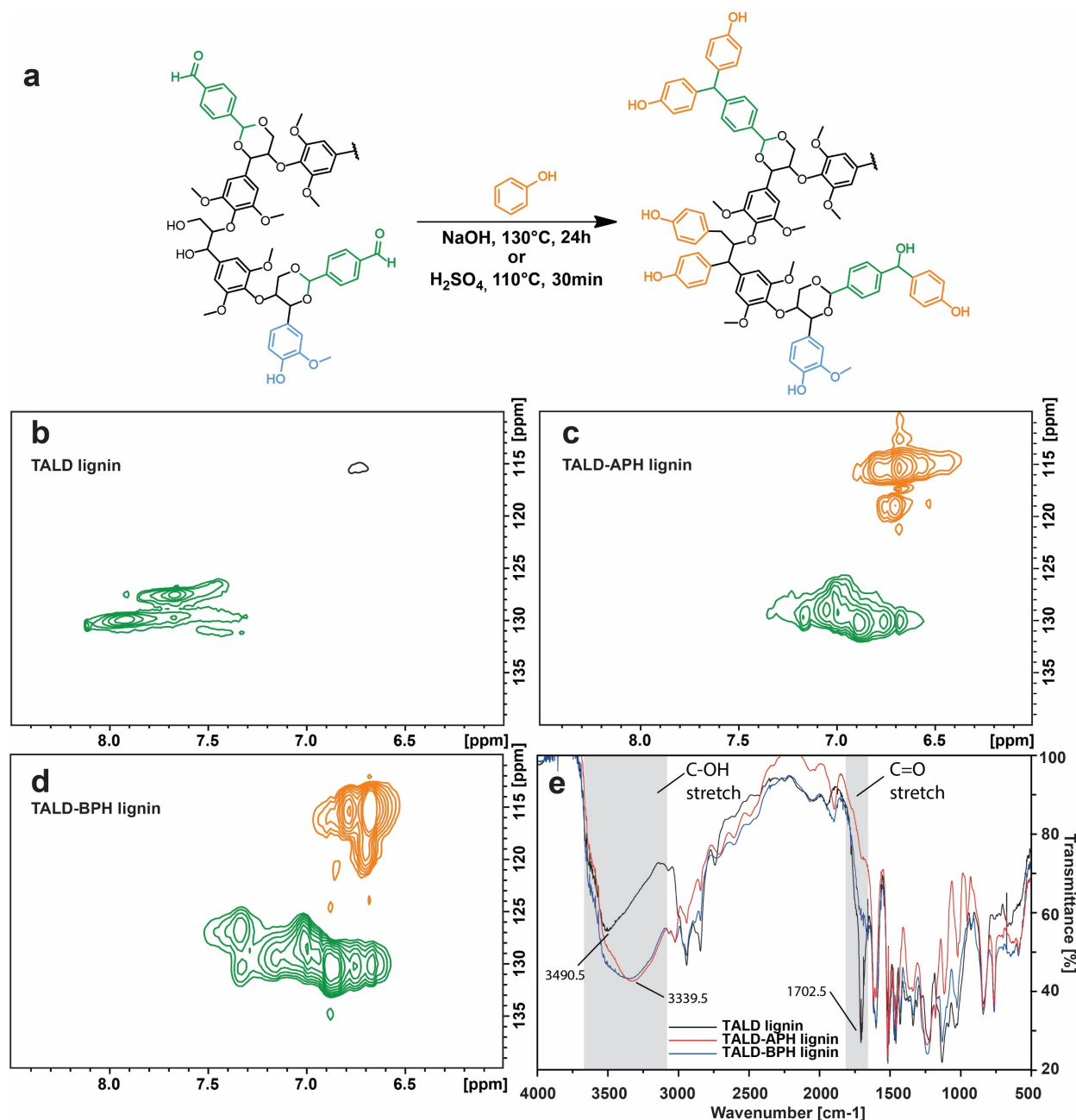


Figure 3.5. Acid and basic phenolation of lignin functionalized with terephthalic aldehyde (TALD-lignin). (a) Presumed reaction mechanism. Peak growth in the aromatic region of the HSQC spectra before (b) and after phenolation in acid (c) and basic (d) conditions. Peak colours in panels (b-d) correspond to functionalities depicted in (a). (e) DRIFT spectra of TALD-lignin before and after phenolation.

We then used ^{31}P NMR to quantify the quantity of aliphatic and aromatic hydroxy groups, and thus quantitatively compare the added phenol in both acid and basic conditions⁸⁶. When comparing spectra before and after reaction, we observed a clear decrease in the signal

assigned to aliphatic hydroxy groups and a corresponding increase of the signal assigned to phenolic units (**Figure 3.6**, a). The quantitative comparison of phenolic groups per effective extracted lignin (where “effective” indicates that the weight of the TALD functionalization was subtracted from the weight of TALD-lignin in order to have comparable results between the three lignins) shows that both TALD-lignin and Mild-Acidolysis Organosolv lignin have a higher and similar content of aliphatic hydroxy groups (respectively 3.21 mmol/g and 3.10 mmol/g) compared to KL (**Figure 3.6**, b). The similar content of aliphatic units in TALD and OSL lignin could be explained by the fact that for the first lignin a certain degree of β -ether units will be non-functionalized by the acetal formation with TALD, but still sterically protected by adjacent functionalized β -ether units, which will prevent condensation. A confirmation of this could be seen in HSQC spectra of TALD-Lignin (**Figure 3.2**, c) where it is possible to clearly see the signals of unfunctionalized α and β hydroxy groups (δ_H/δ_C 4.87/74.2 ppm for OH_α , δ_H/δ_C 4.12/86.9 ppm for OH_β). On the other hand, OSL will see less functionalisation but likely undergo a certain degree of condensation even at mild conditions of extraction, as shown by the lower overall yields, which would result in a decrease of hydroxy groups compared to the native lignin. In the case of KL, the aliphatic content is 1.55 mmol/g, which indicates a more condensed structure, which was expected due to harsh extraction conditions. Isolated KL had a higher amount of guaiacyl units (1.84 mmol/g) than the other two lignins because the commercial KL used in this study was derived from softwood, which contains only guaiacyl units, while birch contains a higher fraction of syringyl units. Second, the high temperature and basicity used during Kraft pulping favoured condensation reactions, but also a partial depolymerization of the lignin, which consequently could have led to an elevated number of phenolic end groups.⁹³

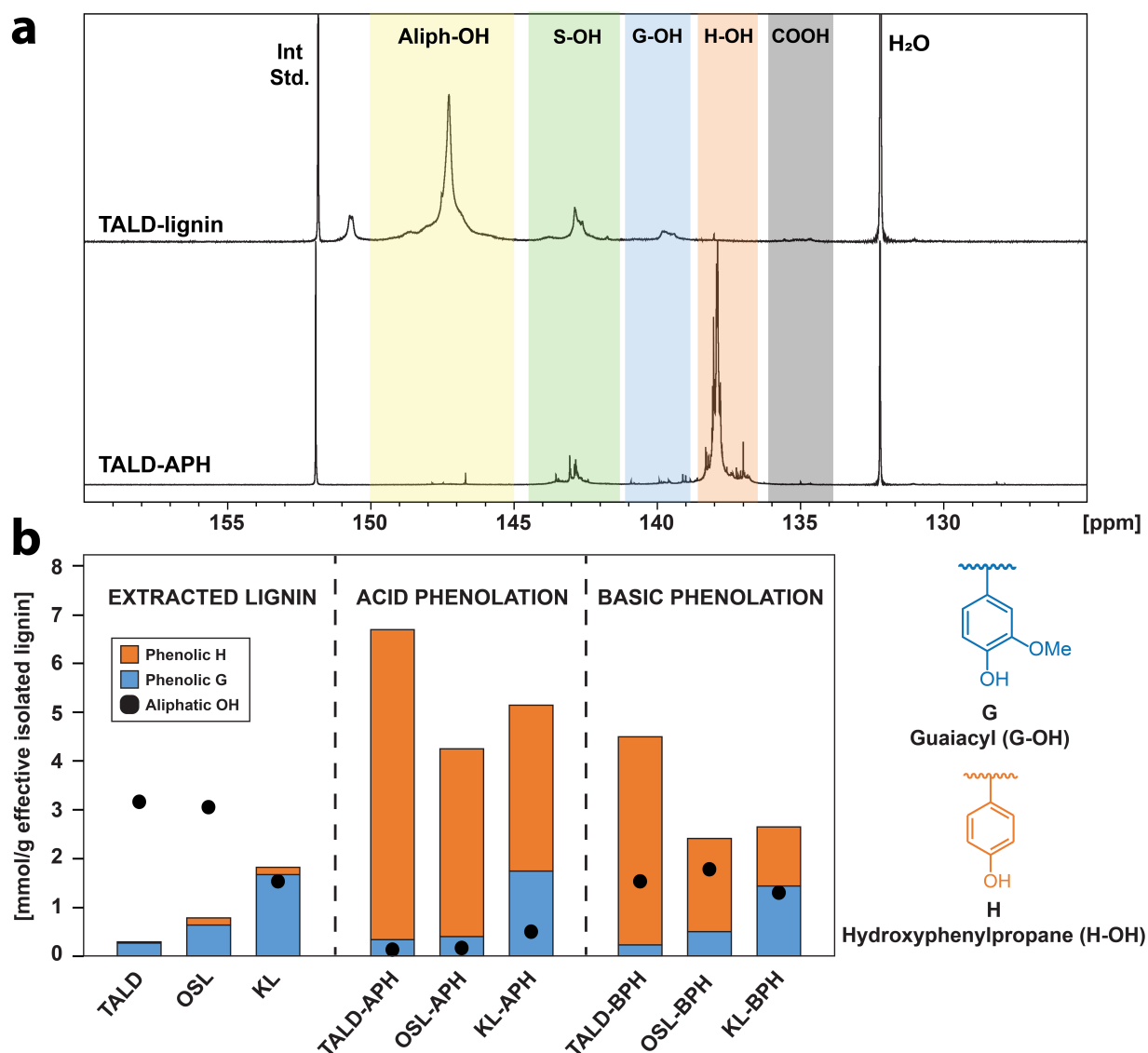


Figure 3.6. Characterization of phenolated lignins. (a) ^{31}P NMR spectra of lignin functionalized with terephthalic aldehyde (TALD-lignin) before and after acid phenolation using TMDP as phosphorylating agent. (b) Yields of phenolation for different lignins in acid and basic conditions.

After acid and basic phenolation, all lignin presented an increase of phenolic units and a decrease in aliphatic hydroxy groups regardless of the catalyst used (**Figure 3.6, b**). Phenolation conducted in presence of concentrated sulfuric acid was the most effective in introducing new hydroxyphenyl units in the lignin. Mild organosolv and KL showed a 5.47- and 2.83-fold increase in their respective quantity of total phenolic units, with a final phenolic content of 4.31 mmol/g and 5.22 mmol/g of lignin, respectively, which was in line with previously reported results.¹⁵² In comparison, the functionalization of TALD-lignin increased the aromatic hydroxyl content 23.4-fold with a total phenolic amount of 6.79 mmol/g of

effective isolated lignin, which, to the best of our knowledge, is the highest phenolation value reported in literature. Furthermore, in the case of TALD-lignin and OSL, two lignins with a higher content of β -ether units, the phenolation in acid conditions also favoured partial depolymerization of the biopolymer (Table A.4), which was not the case for KL, which lacked β -ether units even before phenolation as evidenced by the low yields obtained after hydrogenolysis.

The aldehyde functionality also proved to be beneficial during phenolation in presence of NaOH. When functionalized in basic conditions, TALD-lignin showed a 15-fold increase of total phenolic units, with a final content of 4.57 mmol/g. Both mild organosolv and KL showed an increase in hydroxyphenyl units after phenolation under basic conditions with a respective total phenolic content of 2.44 mmol/g and 2.69 mmol/g, even though aldehyde groups were not present in the original scaffold of these two aromatic polymers. This increase could be explained by these lignins forming intermediates and reactive species that react with phenol to form covalent bonds at harsh basic conditions. Alternatively, this phenol may not have been covalently bound to the lignin but, and instead been physically attached with the biopolymer through non-covalent interactions. However, DOSY-NMR of the lignins (Figure A.3) showed that in DMSO-d₆, a solvent that forms strong hydrogen bonds with phenolic molecules and thus disfavours intermolecular interactions between lignin and phenol,¹⁷⁷ all phenolated lignins showed a unique diffusion behaviour in solution, suggesting that phenol was covalently bound to the polymeric scaffold and not just interacting with it physically.

3.5 Concluding Remarks

We demonstrated that the aldehyde stabilization process previously used to maximize the production of monomers from lignin is also an effective tool for the controlled and simultaneous extraction and chemical modification of lignin. Furthermore, this process allows us to introduce functional groups on the lignin scaffold that were not originally present on the biopolymer and that could then be further modified. We notably demonstrated that this method offers the unique possibility to functionalize lignin with free aldehyde groups. This aldehyde functionalization could be used to strongly increase the reactivity of lignin towards phenolation in both acid and base-catalysed systems. The use of any fossil-based phenol as a solvent for phenolation reactions creates health and sustainability drawbacks. However,

efforts are being made in order to minimize the impact of phenol by either sourcing the molecule from biobased feedstocks¹⁷⁸ or by developing resins where the phenolic part of said polymers are substituted by more sustainable and bio-based alternatives.^{179–181} The increased reactivity of TALD-lignin in phenolation resins suggests that this kind of functionalization could be beneficial for the subsequent integration of a higher fraction of lignin into phenolic resins, which would not eliminate the use of fossil-based phenol but at least contribute to reducing its use. Because aldehydes are versatile chemical functionalities that can react under mild conditions to obtain a variety of other important functional groups such as amines, carboxylic acids and hydroxy groups, we believe that this work could expand lignin functionalization possibilities, and ultimately enable substituting fossil-based materials with renewable alternatives.

Chapter 4 Extraction and Surfactant Properties of Glyoxylic Acid Functionalized Lignin

This chapter was adapted from the following article with the permission of all co-authors and of the journal.

Postprint version of the article: Stefania Bertella, Monique Bernardes Figueirêdo, Gaia De Angelis, Malcolm Mourez, Claire Bourmaud, Esther Amstad, Jeremy S. Luterbacher. "Extraction and Surfactant Properties of Glyoxylic Acid Functionalized Lignin". ChemSusChem, 2022, accepted.

My contribution: Design of the experimental work, lignin extraction and characterization, partial characterization of emulsions, drafting of the manuscript and figures.

4.1 Introduction

The radical coupling of sinapyl, coniferyl and *p*-coumaryl alcohols for the formation of lignin give rise to a heterogeneous polymer which is not only composed of different monomers, but also involves an array of chemical interunit linkages (**Figure 4.1, a**)¹⁸², as explained in more details in Chapter 1.

The amphiphilic chemical structure of native lignin that arises from its biosynthesis, composed of a hydrophobic aromatic core and hydrophilic hydroxy groups, makes this biopolymer a promising alternative for the development of bio-based surface-active compounds.^{183–185}

However, the severe conditions traditionally needed during biomass fractionation make lignin prone to condensation and cause it to lose hydrophilic hydroxyl groups in favour of the formation of C–C bonds (**Figure 4.1, b**)¹⁰⁸, ultimately decreasing lignin's abilities to lower surface tension of water/oil mixtures.

Despite this, examples of extracted lignins used for the development of bio-based surfactants have been reported. Soares et al. for example recently described the use of Kraft lignin extracted from the black liquor of an industrial pulp and paper plant to prepare a sustainable biocide via the stabilization of an aqueous solution of thymol.¹⁸⁶ In addition, lignosulfonates, a by-product of the sulfite pulping process, have been reported to lower the surface tension of water and oil mixtures, given their aromatic core structure and the presence the sulfonate anionic groups which are introduced during extraction.^{187,188}

To increase the properties of lignin as surfactant, chemical modification is however consequently often necessary to introduce better hydrophilic groups along the polymer chains.¹⁸⁹ For instance, reactions of sulfethylation¹⁹⁰, esterification¹⁹¹, etherification¹⁹² as well as grafting through Reversible Addition–Fragmentation Chain-Transfer (RAFT) polymerization¹⁹³ have been carried out on lignin oligomers to explore their further use as surfactants. However, in addition to the increased number of synthetic steps needed to reach the final products, most of these reactions also rely on the use of fossil-based or toxic reagents, which could decrease the environmental benefit of using lignin as the surface active ingredient.¹⁹⁴

In the previous chapter I have shown that a great degree of control over the extracted lignin chemical structure could be obtained by introducing aldehydes during the biomass fractionation process. This process, defined as Aldehyde-Assisted Fractionation (AAF), avoids the condensation and repolymerization reactions on the lignin scaffold by the formation of stable acetals in the β -ether units and the aldehydes introduced during the biomass fractionation (**Figure 4.1, c**).¹⁹⁵ Moreover, when multifunctional aldehydes are used, it is consequently possible to introduce chemical functionalities on the lignin backbone that were not present in its original structure, tuning therefore the final properties of the isolated material.^{196,197}

In this chapter, we took advantage of the AAF process to extract lignin in presence of glyoxylic acid (GA), in order to produce a lignin (GA-lignin) containing a controlled amount of carboxylic acids on its polymeric chains, in a single step from lignocellulosic biomass (**Figure 4.1, d**). We then investigated the surface activity properties of GA-lignin in several water/oil systems and evaluated the stability of water/mineral oil emulsion using GA-lignin as a surfactant at different pH values over time. After this, we used GA-lignin as an active component in the preparation of a cosmetic formulation of hand-cream and finally we

benchmarked the surface activity of GA-lignin against other lignin-based as well as non bio-based industrial surfactants.

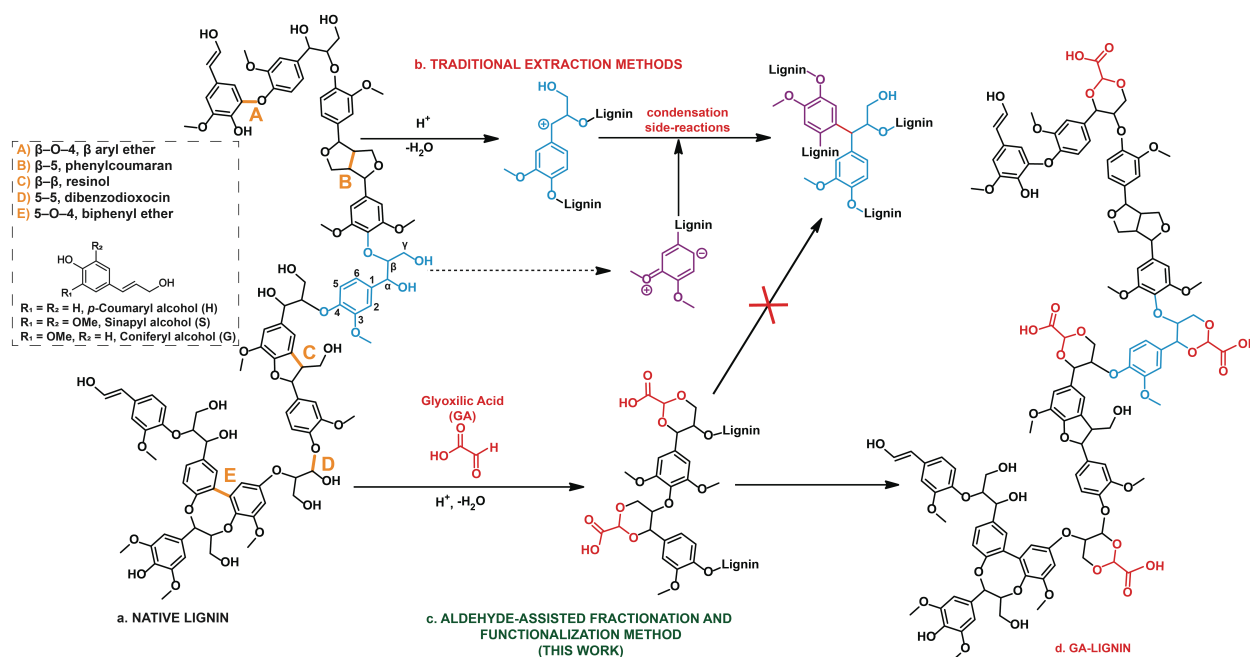


Figure 4.1. Overview of the lignin extraction and functionalization presented in this chapter. (a) The structure of native lignin in lignocellulosic biomass. (b) the reactions of condensation and repolymerization in traditional lignin fractionation. (c) The aldehyde-assisted fractionation with glyoxylic acid. (d) The structure of extracted GA-lignin that is used as a surfactant.

4.2 Extraction and Characterization of Glyoxylic acid functionalized lignin

We extracted Glyoxylic Acid functionalized lignin (GA-lignin) from birch wood (*Betula pendula*), following a previously published procedure for Aldehyde Assisted Fractionation with some modifications (see detailed procedure in Section B.2.1).¹⁵⁷ Briefly, 5 g of wood chips, glyoxylic acid monohydrate, 0.8 mL of HCl 37 wt.% in water (acting as the acid catalyst) and 25 mL dioxane as solvent were inserted in a reagent bottle equipped with a cap and a magnetic stirrer. The reaction was run at 85 °C for 3 h under vigorous stirring to favour both the full fractionation of the biomass components and to maximize the formation of acetals between glyoxylic acid and the lignin. After filtration of the reaction mixture, the cellulose-rich fraction was isolated as a solid via filtration. The organic filtrate was first concentrated and then precipitated in 850 mL of distilled water to obtain the insoluble GA-lignin as a fine powder, which was then filtrated and dried at 45 °C under vacuum before characterization.

We characterized the resulting lignin via Heteronuclear Single-Quantum Coherence (HSQC) NMR spectroscopy (**Figure 4.2, a**) for which it was possible to assign all the signals relative to the different linkages present in the hardwood lignin after extraction. The extracted GA-lignin spectrum presented all the characteristic signals of AAF-functionalized lignin. In particular, the peak corresponding to the newly formed acetals at $\delta_{\text{H}}/\delta_{\text{C}}$ 4.86/96.2 ppm confirmed that glyoxylic acid had successfully reacted with the lignin. However, the HSQC spectrum also contained evidence that the aldehyde incorporation was incomplete, as the signals corresponding to the native β -O-4 bonds were still visible. In addition, the signals at $\delta_{\text{H}}/\delta_{\text{C}}$ 4.92/62.1 ppm and at $\delta_{\text{H}}/\delta_{\text{C}}$ 4.08/83.5 ppm were attributed to the incorporation of a chlorine atom in the alpha position of the β -ether unit, in a competing mechanism to the acetalization reaction, as also reported by Zijlstra et al.¹⁹⁸ This side-reaction has generally not been previously observed as one of the main side-reactions when lignin was extracted in presence of other aldehydes such as formaldehyde or propionaldehyde¹⁵⁵, suggesting that GA was slightly less effective than other aldehydes at forming acetals with the lignin polymer. However, as traditional HSQC-NMR experiments only provide qualitative structural information, we decided to quantify the amount of GA present on the lignin by using the ^{31}P NMR protocol for lignin hydroxy groups determination developed by Meng et al.⁸⁶ From the ^{31}P -NMR spectrum (**Figure 4.2, b**), we could identify the signals relative to the aliphatic groups as well as that of the free phenols of the syringyl, guaiacyl and p-hydroxyphenyl units. As expected, the ^{31}P NMR spectrum of GA-lignin also presented strong signals centred at 135 ppm relative to the newly introduced carboxylic acid groups (highlighted in red on **Figure 4.2, b**), that could be quantified by using a known amount of *N*-hydroxy-5-norbornene-2,3-dicarboximide (NHND) as an internal standard. We then decided to verify if just by varying the amount of GA introduced in the reactor during the biomass fractionation we could control the final chemical functionalization of the lignin, as we previously shown possible with terephthalic aldehyde (TALD).¹⁹⁶ Such control also proved to be successful for GA (**Figure 4.2, c**). The correlation between the amount of GA used during the fractionation reaction versus the mmol of carboxylic acids quantified on the extracted lignin by ^{31}P NMR was close to linear before reaching a plateau at around 6.5 mmol of GA/g of dry biomass, similarly to what observed in the case of TALD-lignin¹⁹⁶, confirming the potential of controlling the chemical functionalities of lignin during the extraction process.

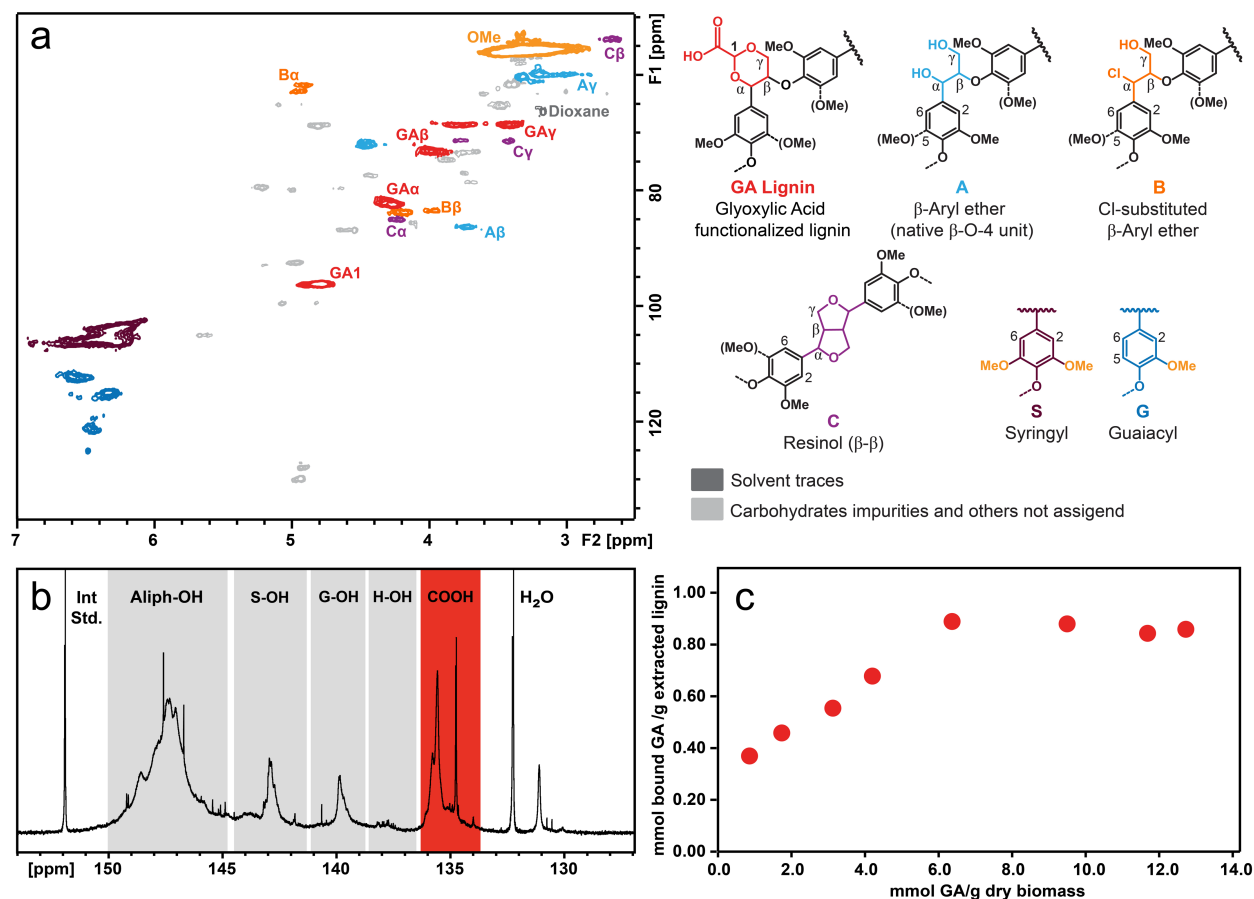


Figure 4.2. Characterization of GA-lignin. a) HSQC-NMR with peaks assignment. b) Example of a ³¹P NMR spectrum with area assigned to the P-functionalized carboxylic acids signal highlighted in red. c) Effect of initial GA concentration over the final GA-functionalization of the extracted lignin measured by ³¹P NMR.

4.3 Surface Tension Measurements

Given the hydrophobic aromatic backbone of GA-lignin and the newly introduced hydrophilic carboxylates through Aldehyde Assisted Fractionation, we exploited these features for use of GA-lignin as a new bio-based surfactant. Specifically, we measured if and how the presence of GA-lignin, extracted with 14 mmol GA/g dry biomass, could lower the interfacial/surface tension of different water/air or water/oil systems in acid, basic or neutral pH, compared to the same systems without the presence of lignin. GA-lignin showed the ability to lower the interfacial tension of all these systems regardless of the pH at which the measurements were taken (**Figure 4.3**). In particular, we observed that for the water/air system GA-lignin could lower the surface tension up to 57% at a concentration of 10 mg/mL (**Figure 4.3, a**). At the

same concentrations, GA-lignin lowered the interfacial tension of water/cyclohexane (**Figure 4.3, c**) and water/toluene systems (**Figure 4.3, d**) up to 92% and 91%, respectively. Finally, in the water/mineral oil system (**Figure 4.3, b**), the presence of GA-lignin was able to lower the surface tension up to 96%, from the starting value of 40 mN/m to the final value of 2 mN/m.

Generally, we observed that a higher solution pH led to lower values of interfacial tension. This could be explained by the different degree of protonation that the chemical features of GA-lignin present at pH 14, 7 and 1. In particular, at pH 14 both carboxylates and phenolics are in a deprotonated form, at pH 7 only the carboxylates are deprotonated, whereas at pH 1 both phenolics and carboxylic acid are fully protonated. Therefore, at high values of pH the amphiphilic characteristics of fully deprotonated GA-lignin are enhanced compared to its protonated form in a strong acidic environment.

To verify the hypothesis that carboxylates had an active role in lowering the values of interfacial tension, we also performed a control experiment by repeating the same measurements but using instead a lignin extracted in presence of propionaldehyde (PA-lignin), which did not have any added carboxylate functionalities (See Section B.2.4). The addition of PA-lignin to the water system at pH 7 had a minimal effect on the values of measured interfacial tension, which was only lowered by 15% at 10 mg/mL (**Figure 4.3, a**, grey line), confirming the hypothesis that carboxylate groups are pivotal to provide a system with good amphiphilic properties.

As the sample preparation (see Section B.4.1) involved a first complete dissolution of the GA-lignin in 1 M NaOH, followed by adjustment with 0.1 M HCl to reach the desired pH values, NaCl was generated. The presence of the additional salt could potentially influence the measured interfacial tension values and therefore we also performed an additional control measurement on a sample that was prepared by first dissolving GA-lignin in 1 M NaOH at pH 14, and then by adding the same amount of NaCl that a sample prepared with pH adjustment to 7 would contain (see Section B.4.1).

From the surface tension measurements (**Figure 4.3, a**, yellow dot), we did not observe any strong salt influence on the value of interfacial tension, as the difference between samples at pH 14 with or without NaCl was only 3 mN/m.

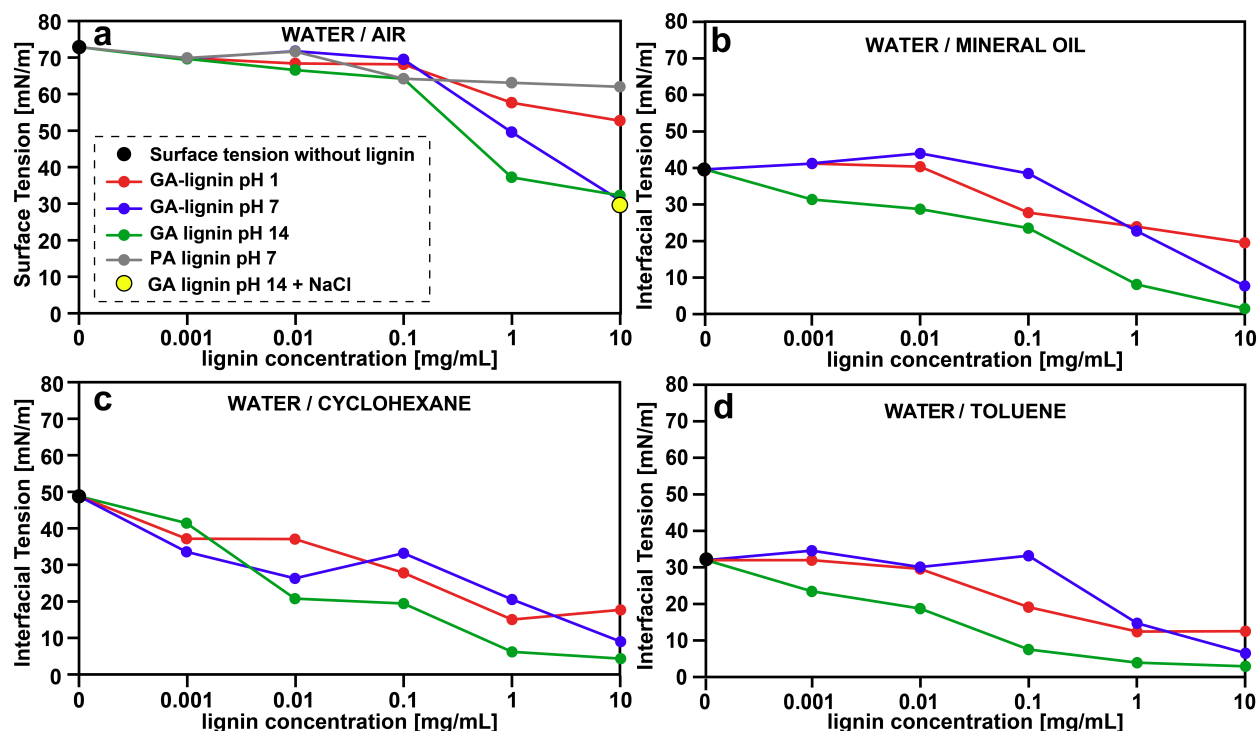


Figure 4.3. Concentration-dependent surface tension measurements of water containing GA-lignin at different pH values (pH 1 red lines, pH 7 blue lines, pH 14 green lines) and different oil phases (a. air, b. mineral oil, c. cyclohexane and d. toluene). Black dots correspond to the initial interfacial tension values (without lignin), the grey line corresponds to propionaldehyde-functionalized lignin (PA-lignin), and the yellow dot corresponds to a GA-lignin sample at pH 14 with additional NaCl.

4.4 Microscopy Imaging of water-Mineral Oil emulsions over time

We investigated the stability of the emulsions formed by adding 1 mL of water containing GA-lignin at a concentration of 10 mg/mL and at different pH values (1, 7, 14), or without lignin at pH 7 for the control experiment, to 0.5 mL of mineral oil, which is a common ingredient in the preparation of creams and lotions for skin care and cosmetic applications. Since the surfactant was in the continuous aqueous phase, which was in excess compared to the oil phase, the produced emulsions were expected to be oil in water. This hypothesis was confirmed by fluorescence microscopy, where it was possible to see that the fluorescent lignin was only visible in the continuous aqueous phase and not in the organic inner phase (see Figure B.3).

We also monitored the emulsions over the course of 30 days by both inspection with the naked-eye and with optical microscopy (**Figure 4.4**). Unsurprisingly, the control

water/mineral oil emulsion that did not contain any GA-lignin had very poor stability and started to coalesce shortly after preparation, with complete phase-separation already at day 7. The emulsions that contained GA-lignin as the surfactant had instead a higher stability, although this stability decreased with increasing values of pH. The system prepared at pH 14 formed emulsions that were stable for two weeks and started to coalesce thereafter reaching full phase-separation at day 30. This could be explained by the fact that at high pH the GA-lignin is fully deprotonated and therefore the different lignin oligomers electrostatically repel each other, preventing the molecules from tightly packing at the interface, which could decrease emulsion stability. In comparison, the emulsions at pH 7 and pH 1 both showed higher stability. Even though some coalescence was visible for the system prepared at pH 7, the presence of emulsions was still confirmed at day 30 with the optical microscope images. At pH 1, the system appeared completely stable over the course of the 30 days and the photographs of the prepared emulsions in the vial as well as the microscopy images did not change in appearance. However, from the microscope images, we clearly observed that this system was behaving differently, as some aggregates could be observed. We propose that at pH 1 GA-lignin was not only in the aqueous solution, but started also to form a colloid of aggregates, which generated a Pickering emulsion as previously reported in literature^{199,200}. We confirmed the presence of aggregates by performing dynamic light scattering (DLS) experiments on the aqueous phases at different pH values containing GA-lignin (see Section B.4.4). Even though DLS does not give information about their concentration, the sample at pH 1 showed the presence of bigger particles compared to the solutions at lower pH, which was consistent with the formation of Pickering emulsions, the different behaviour and higher stability of emulsion prepared at low pH. In conclusion, the systems at neutral and acid pH showed high stability (up to one month), most likely because we formed Pickering emulsions. This high stability opens up the possibility of using this type of lignin for cosmetic application, for example in the preparation of creams and lotions.

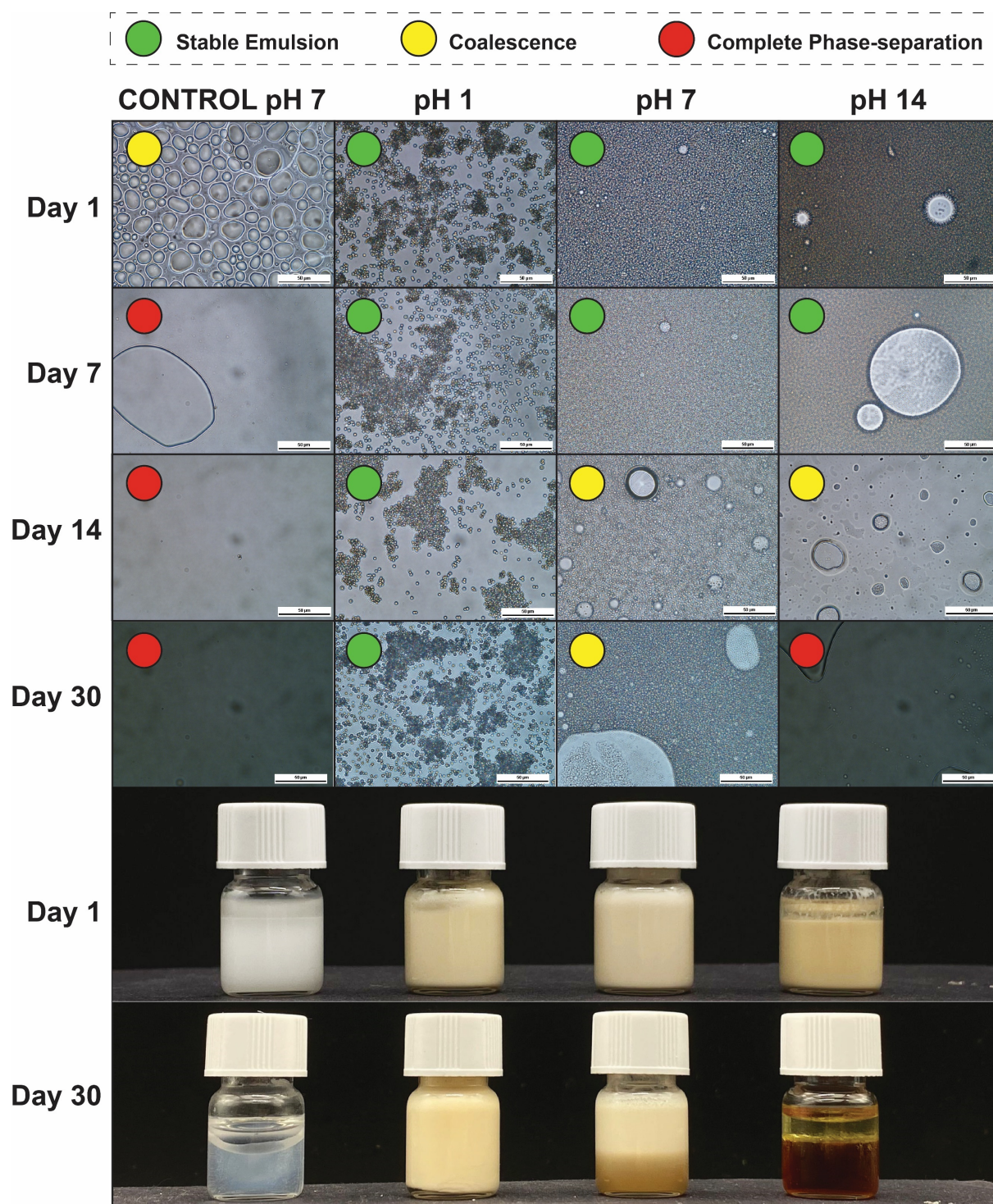


Figure 4.4. Images of different water/mineral oil emulsions at different pH taken over the course of 30 days: (Top) taken with optimal microscopy with a scale bar of 50 μm and coloured dots to mark the stability of the emulsions; and (Bottom) taken with traditional photography of the full vials containing the emulsions at day 1 and day 30 (Bottom).

4.5 Preparation of a hand-cream formulation using GA-lignin as surfactant.

Based on the results obtained on the surfactant stability at neutral and acid pH, we then explored the use of GA-lignin as surfactant in the preparation of cosmetics. Specifically, we simulated the preparation of a simple hand-cream made of ingredients commonly used in the cosmetic industry (**Figure 4.5**) by mixing water at pH 4 containing 1 wt.% of GA-lignin as the surfactant, and mineral oil as the moisturizer containing 1 wt.% of citral (3,7-dimethyl-2,6-octadienal) as a scent. The ratio of the mixed water and oil phases was 2:1. Xanthan gum was added as thickener.

For this experiment we also prepared two controls, one that had the same composition but did not contain any lignin (**Figure 4.5**, a) and one where the GA-lignin was substituted by industrial Kraft Lignin (**Figure 4.5**, b).

From the microscopy images taken just after the cream preparation, we noticed that the emulsions formed in the control experiment without any surfactant formed bigger and heterogeneous droplets (**Figure 4.5**, a), confirming again the need of for a surfactant to make a homogeneous and stable preparation. The creams that contained Kraft or GA-lignins had a better texture and generally formed more homogeneous emulsions. However, we could easily observe how the control cream containing industrial Kraft lignin (**Figure 4.5**, b) had an altered colour given by the presence of the dark lignin. Moreover, sample B had the very distinctive smell of Kraft lignin, which is usually associated with smoked wood and sulphur containing compounds, which completely covered the smell of citral. In contrast with this, the hand cream preparation made with GA-lignin (**Figure 4.5**, c) yielded a cream where the color was minimally altered and the citral scent was not noticeably altered by the presence of lignin. In addition, this emulsion was extremely robust and stable over long periods of time (no change in appearance for over 4 months).

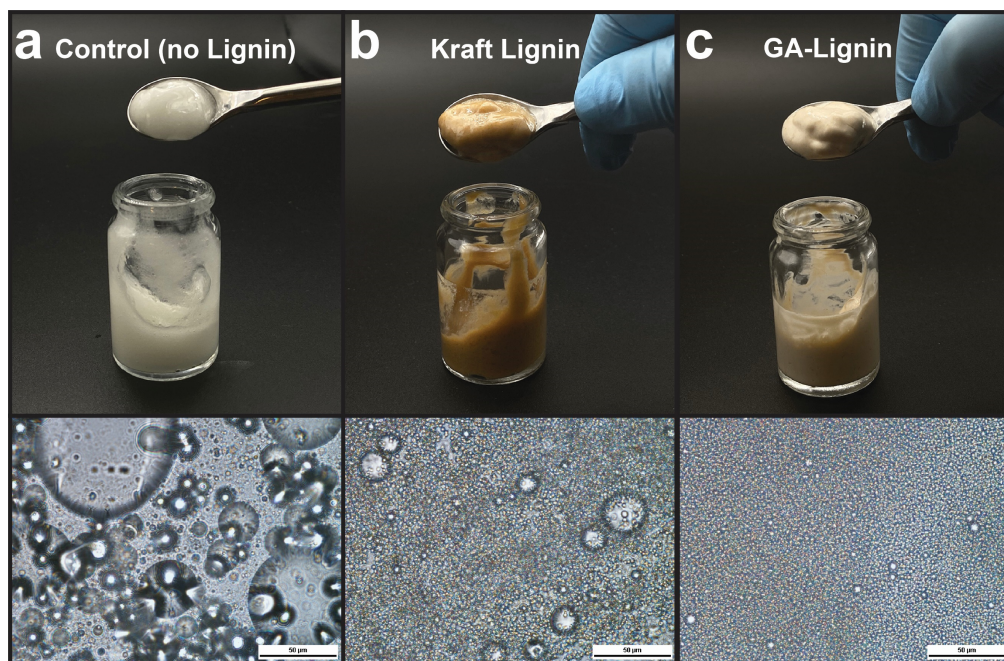


Figure 4.5. Photographs (top) and microscopy images with a scale bar of 50 μm (bottom) of creams prepared by using water, mineral oil, lignin, xanthan gum and citral. Sample a is a control cream prepared without lignin, Sample b contains Kraft lignin as surfactant and Sample c contains GA-lignin as surfactant.

4.6 Surface tension comparison of GA-lignin with other lignin-based and industrial surfactants

After demonstrating the ability of GA-lignin to lower the water/air surface tension and to be a valuable ingredient in the formation of stable formulations of cosmetics, we decided to benchmark the ability of GA-lignin to lower the surface tension of the water/air system compared to other lignin-based surfactants commercially available or previously reported in literature, and to common non-biobased industrial surfactants. As previously shown, GA-lignin (**Figure 4.3 a** and **Figure 4.6**, red bars) was able to lower the surface tension of the water/air from 72.8 mN/m (**Figure 4.6**, green bar) to 31 mN/m regardless of the pH of the aqueous phase. Specifically, GA-lignin at pH 7 and 14 lowered the surface tension as well or better than all the other lignins, such as the industrial Kraft lignin and lignosulfonates, or literature reported lignins that underwent further chemical modification to impart them with surfactant properties. These include sulfomethylated lignin²⁰¹, dodecyl succinic acid²⁰²,

polyethylene glycol- (PEG)²⁰³ or polyacrylamide- (PAM)²⁰⁴ grafted lignins (**Figure 4.6**, blue bars).

Average GA-lignin at pH 7 and 14 also led to similar values of surface tension when compared to widely used non-biobased industrial surfactants at the concentrations of 10 mg/mL, such as sodium dodecylsulfate (SDS), sodium dodecylbenzene sulfonate (SDBS) and sodium dioctyl sulfosuccinate (DOSS) (**Figure 4.6**, grey bars). Although GA-lignin at pH 1 appears to generally perform poorly, the measured value of surface tension of the water/air system is not entirely indicative of its real performance. As previously discussed, at low values of pH the emulsification mechanism of GA-lignin is different than at higher pHs, with the formation of aggregates and therefore of Pickering emulsions (**Figure 4.4**), the stability or formation of which is only partly correlated to the interfacial tension.²⁰⁵

Overall, the advantages of GA-lignin compared to other options come from the fact that in order to extract this type of material it is not necessary to use sulfur-containing molecules, as in the case of Kraft or lignosulfonates, which limits the associated drawbacks related to smell.²⁰⁶ Moreover, GA-lignin is directly functionalized during its extraction, which avoids the need to perform further time and energy consuming chemical modifications to enhance its properties. Finally, in comparison to fossil-based surfactants, GA-lignin could be entirely bio-sourced, as glyoxylic acid can be produced by reduction of CO₂ derived oxalic acid²⁰⁷ or from the oxidation of bio-based ethylene glycol²⁰⁸, confirming how this type of material could facilitate in the transition from fossil to bio-based materials.

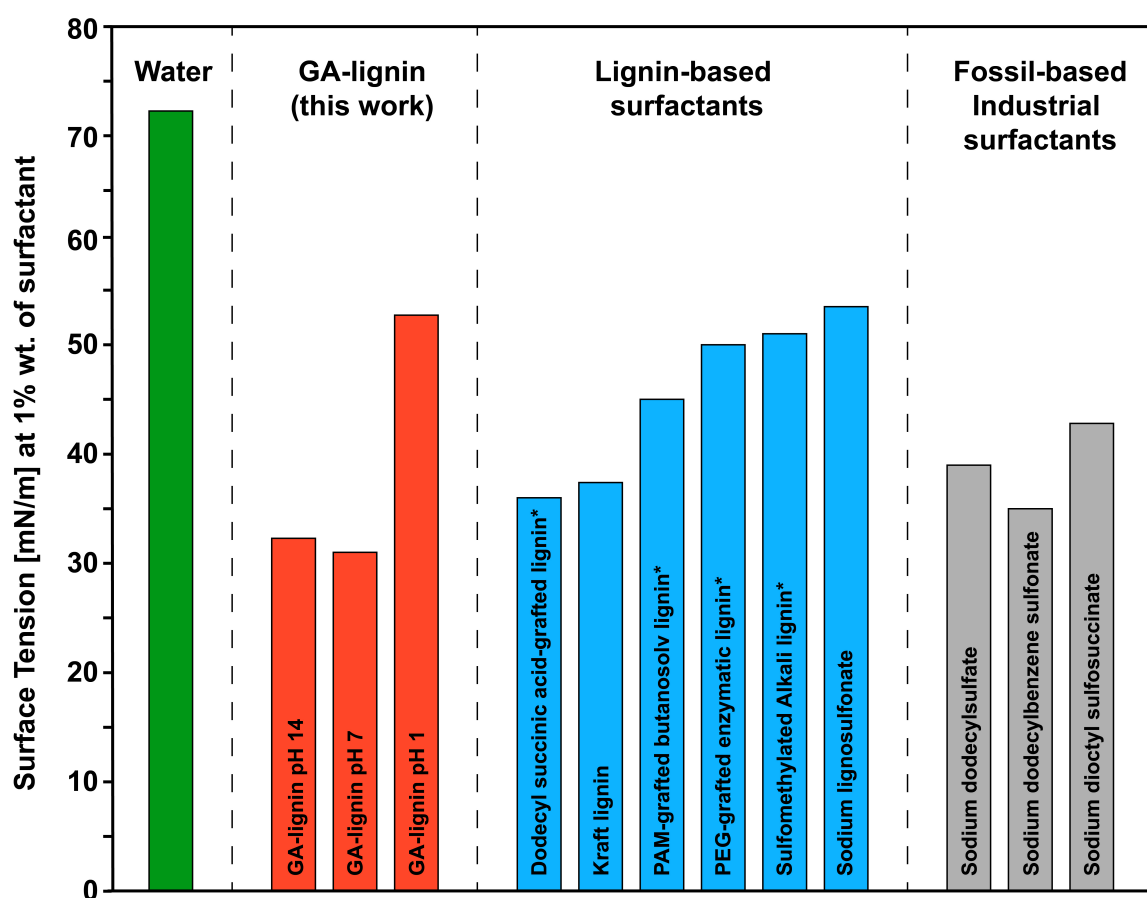


Figure 4.6. Comparison of the water/air surface tension using various surfactants. Green bars: water/air surface tension without added surfactants. Red bars: water/air surface tension with GA-lignin at different pH values. Light-blue bars: water/air surface tension with industrial or chemically modified lignin. Grey Bars: water/air surface tension with industrial fossil-based surfactants. All measurements are done at a surfactant concentration of 10 mg/mL and at pH 7 if not indicated otherwise. An asterisk (*) indicates that the values were taken from literature. Dodecyl succinic acid-grafted lignin is taken from Delgado et al.²⁰², PAM-grafted butanosolv lignin is taken from Migliore et al.²⁰⁴, PEG-grafted enzymatic lignin is taken from Shi et al.²⁰³, Sulfomethylated alkali lignin is taken from Ouyang et al.²⁰¹

4.7 Concluding Remarks

In this chapter we showed that GA-lignin could be extracted in a single step from lignocellulosic biomass and that the final degree of functionalization on the lignin could be tuned and controlled by varying the amount of reagents during the fractionation process. GA-lignin was then successfully used as a surfactant without further modification; showing an

ability to lower the water/air surface tension that was similar or better compared to other chemically modified lignins and fossil-based surfactants. Imaging of emulsions with mineral oil, cyclohexane or toluene showed that these types of emulsions could be stable more than 30 days, and that the pH had an influence on the formation of traditional or Pickering emulsion. GA-lignin was then used as a surface-active compound in the preparation of a simple hand-cream by mixing ingredients widely exploited in the cosmetic industry. The resulting hand cream formed a stable emulsion where, in contrast to the use of sulfur-containing Kraft lignin, both colour and smell were not affected by the presence of GA-lignin.

These lignins have the added benefit that they can be produced in concert with highly digestible cellulose and glyoxylic acid-stabilized xylose, which has been directly used for the production of sustainable bioplastics.²⁰⁹ Overall, the chemistry shown in this work could allow both the tailoring of lignin properties, and the straightforward valorization of all major biomass fractions, which could ultimately make biorefineries more profitable and sustainable.

Chapter 5 Extraction of bi-functionalized lignin for controlling properties of gelatin-based hydrogels

5.1 Introduction

In the previous chapters of this thesis we have described and shown how the lack of control in lignin chemical's structure due to condensation and repolymerization reactions is what traditionally makes the incorporation of isolated lignin with other materials particularly difficult, either due to its reduced miscibility with other materials including organic solvents or aqueous systems or its limited reactivity.¹⁰⁹ To partially overcome these issues, we have described how a common strategy to increase lignin compatibility with other materials is its functionalization through the residual hydroxyl groups or aromatic rings to introduce novel functionalities that were originally not present in the isolated lignin.²¹⁰ However, these strategies also present several drawbacks, such as the limited number of sites on condensed lignin that are available for further functionalization and the frequent trade-off between lignin solubility and its reactivity. Furthermore, the need to perform several synthetic and purification steps often decreases the overall sustainability of the final functionalized lignins and limits their use in high-end applications.²¹¹ In the previous chapters we have demonstrated that by extracting lignin in presence of aldehydes, the condensation and repolymerization reactions could be avoided by the formation of stable acetals on the β -ether units, in a process known as Aldehyde-Assisted Fractionation (AAF) (**Figure 5.1, a**).¹⁰⁵ Furthermore, we showed that multifunctional aldehydes could be employed to simultaneously extract and functionalize lignin at high yields and with a high control over the final chemical structure, overcoming some of the previously mentioned challenges such as the reduced reactivity of lignin or its limited solubility in aqueous solutions.^{196,197}

For multiple high-end material applications including soft-tissue engineering, the materials designed must not only be biocompatible, but they must present well-defined rheological, adhesive and mechanical properties in order to mimic the surrounding environment in which they are employed, and to ultimately trigger the desired biological responses. Moreover, when designing these types of materials, it is important to keep in mind that the different components present must have the right compatibility in terms of miscibility and needed chemical reactivity.^{212–214} A case where all these factors weigh in is the engineering of gelatin-based hydrogels.²¹⁵ Gelatin is a collagen-derived protein that due to its nature possesses excellent biocompatibility and bioactivity.²¹⁶ Once dissolved in hot water and cooled down to room temperature or below, gelatin can form a hydrogel. Such hydrogel networks are physically held together and fabricated through molecular entanglements and Van der Waals interactions including ionic, hydrogen-bonding, hydrophobic forces, etc.²¹⁷ Due to the non-covalent nature of these interactions, hydrogels composed of only gelatin often exhibit poor mechanical properties.²¹⁸ In particular, the temperature-sensitive gelation mechanism and the mechanically poor hydrogel network are the primary drawbacks of using gelatin-based hydrogels in high-end soft-tissue engineering applications since they are not stable at body temperature. Because of this, several studies have tried to introduce chemical crosslinking within the gelatin network to improve the mechanical and/or rheological properties of the resulting hydrogels.^{219,220} These strategies however often result in the need to perform chemical modifications on the gelatin or introduce molecules in the hydrogel network that end up influencing the biological properties of the resulting materials.^{221,222}

Lignin would be an interesting biobased material to strengthen hydrogels. However, its condensed structure and lack of appropriate functionalities prevents good incorporation into these biomaterials. In particular, good incorporation and crosslinking in a hydrogel depends on both solubility in water and reactive groups that can react with the hydrogel. However, imparting dual functionality on lignin in a controlled way has never been done before. Here, we demonstrated that the AAF process can be used to simultaneously extract lignin and introduce two different non-native functional groups, namely aldehydes and carboxylic acids, by using simple mixtures of terephthalic aldehyde (TALD) and glyoxylic acid (GA) (**Figure 5.1, a**). Moreover, the different quantities of the functional groups can be precisely controlled and monitored by NMR spectroscopy. This uniquely functionalized lignin was both soluble in water at physiological pH and could crosslink with gelatin without further modifications. The introduction of lignin in the gelatin network resulted in the formation of new hydrogels with

unique and controlled rheological, mechanical, adhesive, and self-healing properties. None of these improvements occurred in cases where one of the functionalities was missing, which demonstrates the importance of precisely engineering lignin for the development of advanced material applications. In addition, the resulting material was not cytotoxic, which is important in the context of tissue engineering applications.

This work is a proof of concept that aims at showing how engineered lignins can be easily obtained from lignocellulosic biomass according to their final application, enabling therefore a more substantial use of this aromatic biopolymer in high-end applications.

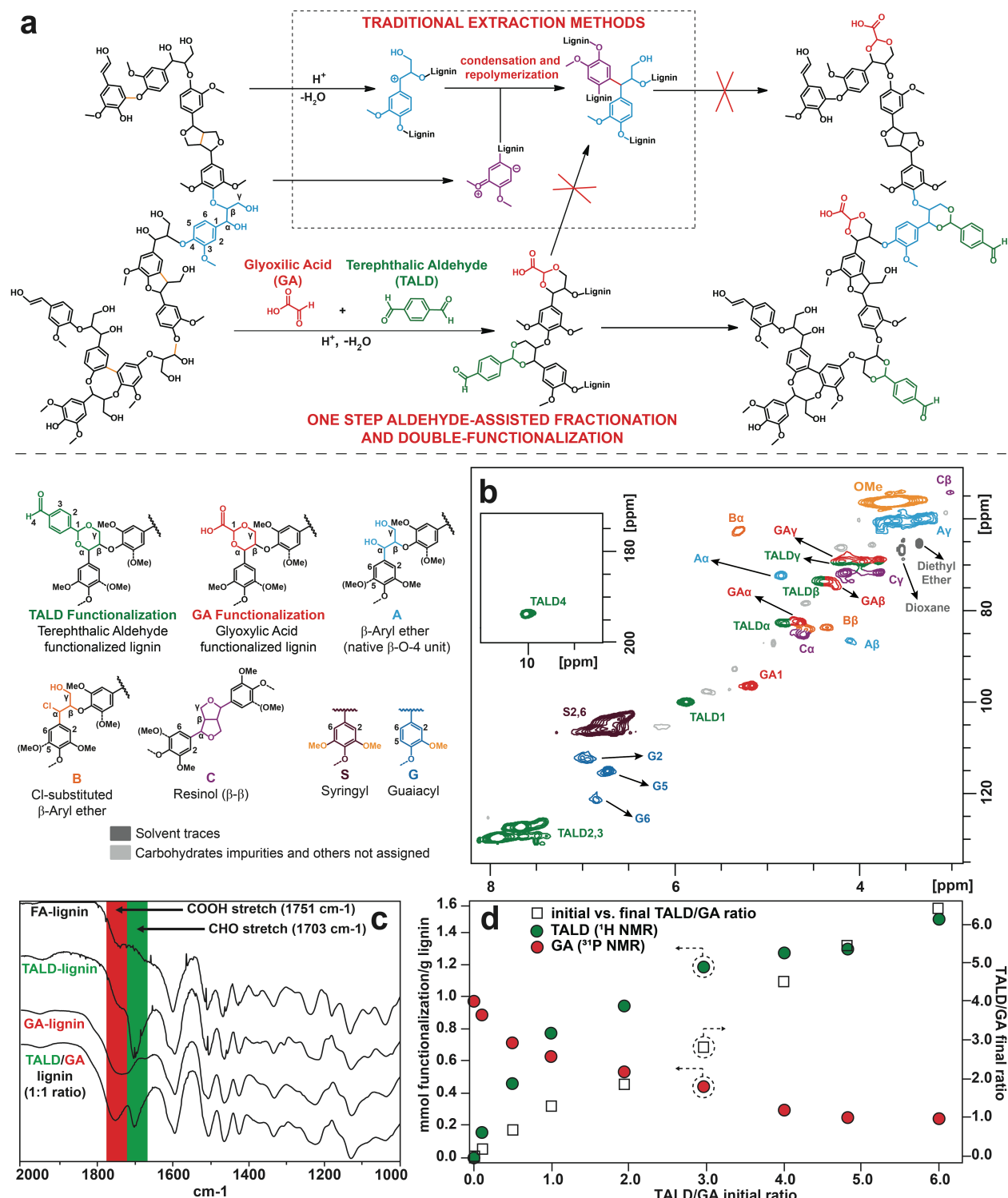


Figure 5.1. Extraction and characterization of TALD/GA-lignin. a) Overview of the extraction and simultaneous functionalization of lignin with TALD and GA. b) HSQC-NMR spectrum of TALD/GA lignin extracted with an initial TALD/GA ratio of 1. c) DRIFT spectra of formaldehyde functionalized lignin (FA-lignin), mono-functionalized GA and TALD-lignins and bi-functionalized TALD/GA lignin extracted with an initial TALD/GA ratio of 1. The peak associated with the stretch of COOH

groups is highlighted in red while the peak associated with the stretch of the aldehyde carbonyl group is highlighted in green. d) Quantification of TALD and GA via ^1H NMR and ^{31}P NMR respectively in the TALD/GA-lignin samples extracted with different TALD/GA initial ratios. The resulting TALD/GA ratios on the extracted lignin as a function of the initial ratio of aldehydes and carboxylic acids in the reaction is also shown.

5.2 Lignin Extraction and Characterization

The extraction and simultaneous chemical functionalization with two functional groups of lignin was achieved by following the AAF procedure previously developed in our research group, using in this case a total of 11.5 mmol of glyoxylic acid (GA) and terephthalic aldehyde (TALD) at different ratios (see Section C.3.1).^{157,196} We performed 8 extractions with TALD/GA ratios ranging from 0.10 to 6.01. Two additional control experiment were performed where lignin was extracted only in the presence of 11.5 mmol of GA or TALD.

We then characterized the extracted lignins by NMR. The structure of the extracted TALD/GA-lignins was first confirmed by Heteronuclear Single-Quantum Coherence (HSQC) NMR experiments, which we used to assign all the signals relative to the lignin core structure and the units characterized by the main interunit linkages, such as the β -O-4, β - β , guaiacyl and syringyl aromatics⁸⁷ (**Figure 5.1**, b). This technique notably allowed us to confirm the success of the simultaneous double functionalization of the lignin with the multifunctional aldehydes, as the signals at $\delta_{\text{H}}/\delta_{\text{C}}$ 5.88/100.03 ppm and $\delta_{\text{H}}/\delta_{\text{C}}$ 5.17/96.5 ppm were assigned to TALD and GA bound with the lignin hydroxyl groups through the formation of acetals.

The double functionalization of TALD/GA-lignins was also confirmed by Diffuse Reflectance Infrared Fourier Transform (DRIFT) spectroscopy, a technique that allows for qualitative determination of functional groups such as carbonyls and carboxylic acids, which lead to absorbance bands around 1700 and 1750 cm^{-1} respectively. We compared the spectrum obtained from a lignin extracted in presence of formaldehyde (FA-lignin) with the spectra obtained from the mono functionalized TALD-lignin, GA-lignin, and the double functionalized TALD/GA-lignin (**Figure 5.1**, c). As expected, FA-lignin did not present any carbonyl functionalization signal and only a very small peak in the range assigned to COOH groups, presumably due to those groups already present in the hardwood native lignin²²³. The

DRIFT spectrum of mono-functionalized GA-lignin on the contrary showed a stronger signal at 1751 cm^{-1} , compatible with the COOH stretch deriving from the GA functionalization, while the spectrum of TALD-lignin showed instead a strong signal corresponding to the stretch of carbonyl groups at 1703 cm^{-1} , confirming the presence of the newly introduced aldehyde functionalization. Finally, the spectrum of the double functionalized TALD/GA-lignin extracted with equimolar amount of TALD and GA showed two peaks of similar intensity corresponding to the stretch of both COOH and CHO groups, confirming double functionalization of the aromatic polymer during its extraction.

Quantification of the TALD and GA bound on the nine extracted lignins was determined by mono dimensional quantitative NMR experiments, using ^1H NMR for aldehydes and ^{31}P NMR for carboxylic acids groups, following the procedures reported in our previous work (see Section C.4.2).

The results obtained from the quantitative NMR measurements showed that with a higher TALD/GA ratio used during extraction, the amount of TALD covalently bound to the lignin consistently increased, while the contrary happened for GA. Moreover, we found that the ratio of TALD/GA introduced in the reactor prior to extraction led to a linear correlation with the TALD/GA ratio measured on the lignin after extraction (**Figure 5.1, d**). These results demonstrated that simply varying the aldehyde quantities introduced during AAF allowed precise control of the type and degree of lignin functionalization, even when several functionalities were targeted.

5.3 Hydrogel preparation and rheological studies

We then took advantage of the multiple functionalities of TALD/GA-lignin to prepare gelatin-lignin based hydrogel with controlled rheological properties.

We first performed solubility tests in aqueous solution at pH 14 (see Section C.5). The resulting solubility of the lignin samples appeared to decrease with increasing TALD/GA ratio, indicating the importance of the carboxylic acid functionalization in providing sufficient solubility in aqueous solutions. A solubility limit was reached for the lignin extracted with equimolar amounts of TALD and GA (see Figure C.4), and moreover the recovered Na^+ salts of this lignin containing a TALD/GA ratio of 1 were found to be soluble in phosphate-

buffered saline (PBS) at physiological pH (7.4). Therefore, we used this soluble lignin with the highest TALD/GA ratio to prepare the gelatin-based hydrogels.

We started by preparing hydrogels that contained an arbitrary total content of 8 wt.% of solids (gelatin+lignin) and 92 wt.% of PBS.

To obtain the hydrogels we first prepared separate aqueous solutions of gelatin and TALD/GA-lignin, which were then mixed and cooled at 4 °C for 15 h to obtain the final materials (see detailed procedure in Section C.6).

As a result, we prepared a total of five hydrogels (**TALDGA-Gel**) with a TALD/GA lignin content ranging from 1 wt.% to 5 wt%, and a gelatin content ranging from 7 wt.% to 3 wt%., in order to have a constant total content of solids of 8 wt.%.

As a control, we also prepared gelatin-based hydrogels where TALD/GA lignin was replaced by purely GA functionalized-lignin (**GA-Gel**), in order to evaluate how the presence or absence of aldehyde groups affected the properties of the final materials. Finally, an 8 wt.% hydrogel comprised of only gelatin (**N-Gel**) was also obtained to study if the presence or absence of lignin had an overall impact on the properties of the hydrogels.

Oscillatory rheology was used to probe the mechanical properties of all hydrogels. The oscillatory amplitude sweeps were run at 1 rad/s frequency to define the linear viscoelastic region (LVER) for each hydrogel. The storage oscillatory shear moduli (G') of all hydrogels was systematically greater than loss shear moduli (G''), confirming the viscoelastic behavior (Figure C.7). All hydrogels displayed a wide linear viscoelastic window, signifying that these hydrogels have a broad processing region. However, at higher strain amplitude (>10%), a deviation from linear viscoelasticity was observed in TALDGA-Gel and GA-Gel hydrogels, indicating the breakdown of the hydrogel structure.

We further examined the frequency-dependent rheological behavior of all hydrogels in LVER by performing frequency sweep tests (Figure C.8), and to better examine the differences between all the various hydrogels, we plotted the values of G' and G'' oscillatory shear moduli at 1% shear strain and 11.9 rad/s angular frequency (**Figure 5.2**, a-b).

By comparing the G' and G'' values between various TALDGA-Gel and the control GA-Gel hydrogels, we noticed a consistent difference in storage and loss moduli, which broadened upon increasing the amount of lignin into the hydrogels. The storage moduli of TALDGA-Gel were between 45 and 319% higher than the G' values recorded for the control GA-Gel

(**Figure 5.2, a**), and a similar trend, but with a more marked difference, was observed for the G'' value of TALDGA-Gel and GA-Gel hydrogels (**Figure 5.2, b**), in which the loss moduli of TALDGA-Gel hydrogels were up to 694% higher than the controls.

These data could be explained by looking at the chemical bonds and interactions that TALD/GA or GA lignins are able to promote or hinder in the gelatin-based hydrogels (**Figure 5.2, c-e**). As previously explained, gelatin-based hydrogels are held together by non-covalent interactions such as hydrogen and Van der Waals bonds (**Figure 5.2, c**). When TALD/GA lignin is introduced in the network, the presence of aldehyde groups promotes the formation of Schiff bases between gelatin and lignin (**Figure 5.2, e**), creating a cross-linked network able to store a higher amount of energy, as demonstrated by the rheological measurement. *Vice versa*, when aldehyde groups are missing in the lignin scaffold, such as is the case for GA-lignin (**Figure 5.2, d**), the presence of unbound lignin can be detrimental for the overall rheological properties of the formed hydrogels. The absence of aldehyde groups in the lignin not only hinders the formation of a cross-linked structure, but additionally the aromatic and hydrophobic core structure of lignin can also partially block the formation of non-covalent interaction between gelatin, resulting in generally worse storage and loss moduli. These hypotheses were also in line with what was observed during kinetic study of gelation for the different produced hydrogels (see Section C.7.1), where the presence of TALD/GA lignin shortened the gelation time to min due to the fast formation of imines, while the same hydrogels produced in presence of GA lignin had a gelation time of hours (**Figure C.5**).

The proportion of lignin introduced into the gelatin also plays an important role in the final rheological properties of the produced materials.

As seen from the frequency sweep measurement (**Figure C.8**) and from **Figure 5.2 a-b**, the storage moduli of TALDGA-Gel containing 1%, 2% and 3% of lignin were respectively increased by 37%, 17% and 9% in comparison to *N*-Gel, whereas further substitution of gelatin with TALD/GA lignin led to decreased values of G' when compared to *N*-Gel.

This demonstrates that when between 12.5-37.5% of the total gelatin weight is substituted with TALD/GA lignin both chemical and physical crosslinks density dictate the shear modulus of TALDGA-Gel hydrogels.

This behavior can be explained by the concentration of functional groups in the two polymers involved in the formation of the hydrogels. As reported by Sisso et al.²²⁴ and Kale et al.²²⁵, the concentration of free amino groups in gelatin is between 0.28-0.29 mmol/g, while as quantified by ^1H NMR experiments (**Figure 5.1**, Section C.4.2.2), the concentration of

aldehyde groups in the TALD/GA lignin used for the preparation of hydrogel is 0.78 mmol/g. This means that when gelatin and lignin are in a ratio of 3:1, the concentration of the two reactive functional groups in the final hydrogel is approximately stoichiometric, and therefore saturation of cross-linking points is achieved. This also suggests that further addition of TALD/GA lignin will not increase the covalent crosslink density in TALDGA-Gels. On the contrary, a higher concentration of TALD/GA lignin would start to eliminate the physical and/or any non-covalent interactions that are inherited by gelatin, similarly to the case of GA-Gels, resulting in decreased storage moduli.

For these reasons, we used hydrogels comprised of 6 wt.% of gelatin and 2 wt.% of lignin to perform all the further material characterization.

SEM was used to investigate the topology of freeze-dried hydrogel samples. As presented in **Figure 5.2 f**, *N*-Gel showed a dense randomly packed porous structure. The porous network is irregular, and no pattern was observed in the framework. On the contrary, the surfaces of GA-Gel (**Figure 5.2, g**) and TALDGA-Gel (**Figure 5.2, h**) exhibited a pattern and regularity of wrinkled wall structures. This suggests that both lignins (GA and TALD/GA) were homogeneously distributed inside the hydrogel and increased the roughness of gelatin framework after establishing a network. When scanned thoroughly, we observed that TALDGA-Gel had higher regularity in the pattern than GA-Gel, confirming that TALD/GA lignin interacts better with gelatin than GA lignin due to having aldehydes that covalently crosslinks TALDGA-Gel hydrogel with the amines present in gelatin.

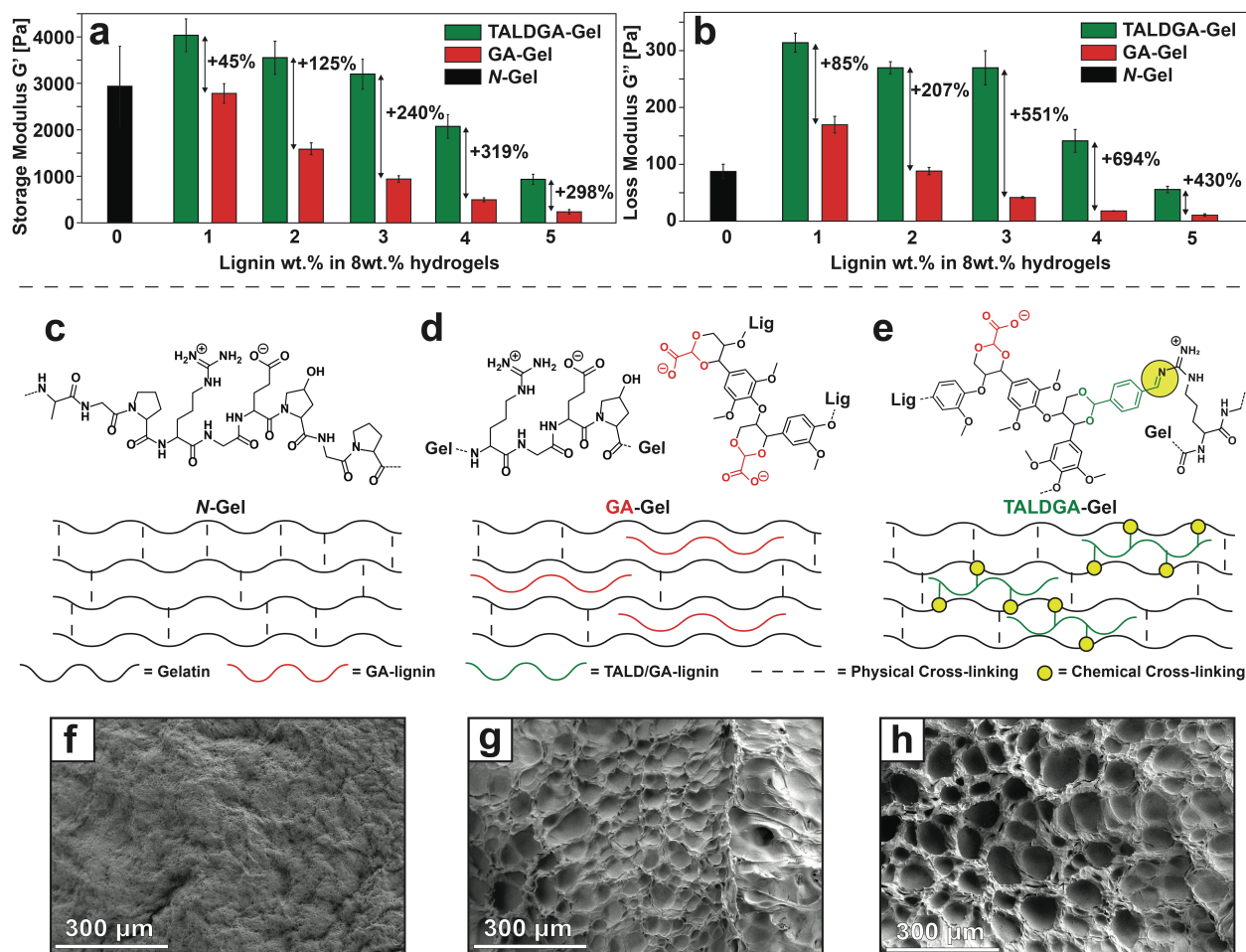


Figure 5.2. Chemical interactions between gelatin and lignin of different produced hydrogels and their rheological properties. a) Storage Moduli of TALDGA-Gel (green), GA-Gel (red) and N-Gel (black) hydrogels reported at 1% shear strain and 11.9 rad/s angular frequency. b) Loss Moduli of TALDGA-Gel (green), GA-Gel (red) and N-Gel (black) hydrogels reported at 1% shear strain and 11.9 rad/s angular frequency. c-e) Formation and chemical interaction of gelatin based hydrogels described in this work (N-Gel, GA-Gel and TALDGA-Gel). f-h) SEM images of N-Gel, GA-Gel and TALDGA-Gel.

5.4 Mechanical, adhesive, and self-healing properties of prepared hydrogels.

We then evaluated the adhesion performances of the TALDGA-Gel, GA-Gel, and N-Gel by using a lap-shear adhesion setup (see Section C.7.5).²²⁶ **Figure 5.3**, a shows the shear adhesion strength obtained for three different hydrogels, including TALDGA-Gel (26.7 ± 5.8 kPa), GA-Gel (23.6 ± 5.5 kPa), and N-Gel (7.8 ± 0.8 kPa). The results obtained show that

through lignin incorporation in the gelatin-based hydrogels, the adhesion capability of the hydrogel system was conspicuously enhanced. The results demonstrate that in the case of TALDGA-Gel and GA-Gel the adhesive contact between the hydrogel and the gelatin coated glass substrate increased respectively by 196% and 169%, compared to *N*-Gel.

The mechanical properties of the three different hydrogels were then determined through compression tests (**Figure 5.3, b**). The compression curves showed that although the three samples exhibited similar mechanical behaviour at lower deformations (less than 50% strain), TALDGA-Gel showed both higher strain-to-failure and compressive strength, while for GA-Gel the compressive strength was about 2.5 times higher than *N*-Gel.

Moreover, with GA-Gel we achieved a strain-to-failure of 80%, while the *N*-Gel presented no more than 65% strain. In contrast, TALDGA-Gel demonstrated much higher compressive performances (>80% strain-to-failure), indicating the increased toughness of this hydrogel. Comparatively, the compressive moduli of the hydrogels (obtained by linear interpolation of the stress-strain curve in linear region) were not significantly different, showing that the presence of lignin did not substantially alter the stiffness of the gelatin-based hydrogels.

The result obtained from the compression tests could also be visually reproduced by compressing by hand *N*-Gel, GA-Gel and TALDGA-Gel between two hard surfaces (**Figure 5.3, c-e**). We observed that upon compression of the samples, *N*-Gel was very prone to breaking at lower compression strength, while GA-Gel required more energy to break (**Figure 5.3, d**). Upon releasing the compression force between the two hard surfaces (**Figure 5.3, e**), the two control samples showed cracks and loss of their original shape, while TALDGA-Gel remained intact.

Our results revealed therefore that by addition of TALD/GA lignin, the mechanical properties of the final obtained hydrogel could be finely tuned, similarly to what observed for their rheological properties. In fact, in addition to stronger interfacial interactions, the enhanced toughening mechanism in lignin-incorporated hydrogels improved the resistance to crack initiation and consequently their adhesion strength, compared to *N*-Gel.

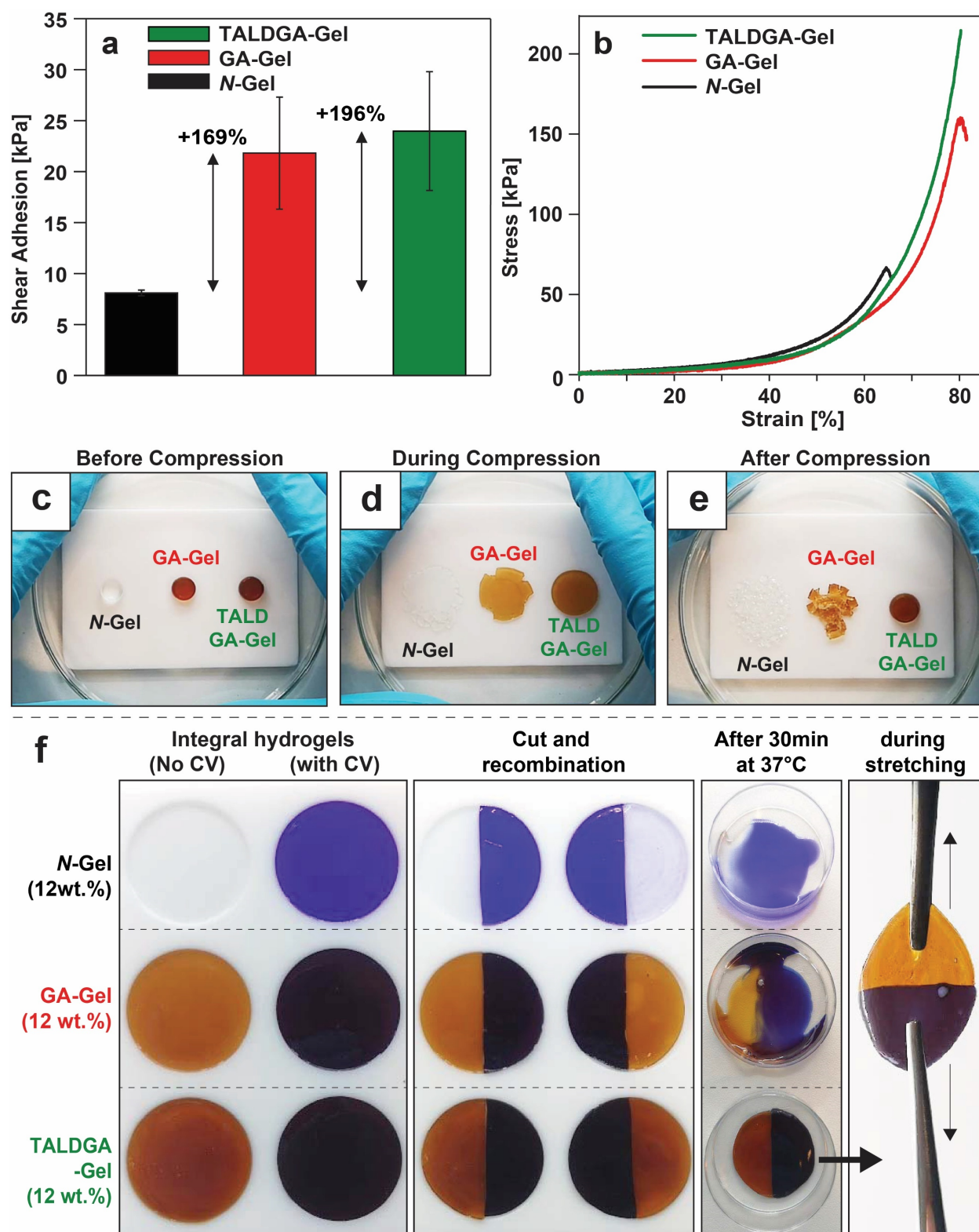


Figure 5.3. Representative shear adhesion performance (a) and stress-strain curves (b) of TALDGA-Gel, GA-Gel, and N-Gel hydrogels. Pictures of TALDGA-Gel, GA-Gel, and N-Gel hydrogels before, during and after compression (c-e). Self-healing properties of N-Gel, GA-Gel and TALDGA-Gel with a total solid content of 12 wt.% (f).

We then studied the stability of hydrogels at 37 °C, and we initially observed that, even though TALDGA-Gel appeared to be more resistant towards degradation and liquefaction compared to its control hydrogels, the total concentration of 8 wt.% was not sufficient to preserve the structure of the hydrogels for over 30 min at 37° C. We thus progressively increased the total solid content of TALDGA-Gel, keeping a 3:1 ratio between the gelatin and the lignin fractions, and after incubating the materials obtained at 37 °C for 30 min, we observed that 12 wt.% TALDGA-Gel was enough to maintain the hydrogel macromolecular structure for a prolonged period of time.

Following this, we performed self-healing experiments. We prepared two set of hydrogels for the TALDGA-Gel, GA-Gel and *N*-Gel hydrogels, staining one of each set with a drop of Crystal Violet (CV) (**Figure 5.3**, f). The hydrogels from the stained and unstained sets were then cut in half and recombined, and placed in petri dishes inside an incubator set at 37 °C. After 30 min we observed that both the GA-Gel and *N*-Gel hydrogels had completely lost their initial shape and appeared liquefied (**Figure 5.3**, f). In contrast, the TALDGA-Gel had preserved its initial shape, suggesting again that the presence of TALD/GA and chemical crosslinking could affect the stability of the prepared material. Moreover, after cooling the sample back to room temperature, we observed that the two halves of the stained and unstained TALDGA-Gel hydrogels were attached and did not separate upon stretching of the material (**Figure 5.3**, f). These observations demonstrated that the stability of the macromolecular structure of the prepared hydrogel at 37 °C could be reconducted to the presence of the bi-functional TALD/GA lignin. Moreover, the possibility of reversibly forming the chemical interactions within the hydrogel structure suggested that this type of material could be employed in soft-tissue engineering applications, where self-healing is often a desirable property.

In summary we observed that even though the monofunctional GA-lignin was generally able to partially increase the adhesion response and the resistance to compression of the hydrogels, an enhanced adhesiveness and compressive strength, as well as self-healing properties and resistance to increased temperature were solely induced by the presence of TALD/GA lignin, demonstrating once again the benefit of engineering lignin with multiple and controlled functionalities.

5.5 Cytotoxicity and bacterial toxicity

The possibility to modulate rheological properties of TALD/GA lignin-gelatin hydrogels as well as their observed increased adhesive and mechanical strength suggest that this type of material could find potential applications in soft-tissue engineering²²⁷. One of the most crucial properties in such a field, especially in the case of biological settings, is compatibility between the hydrogel material and the living cells. Therefore, we studied the cytotoxicity of TALDGA-Gel, GA-Gel, and N-Gel hydrogels against mammalian Vero cells by performing MTS assays (see Section C.7.7). As presented in **Figure 5.4 a**, all prepared hydrogels were harmless for mammalian cells, proving biocompatibility of this lignin-based material. In addition, due to the reported antibacterial properties of lignin²²⁸, we also performed bacteria toxicity tests on two bacterial strains (see Section C.7.8), but as shown in **Figure 5.4 b-c** we couldn't observe any decrease in *E. coli* or *S. aureus* concentration, probably due to the overall low loading of lignin in the TALDGA-Gel hydrogel.

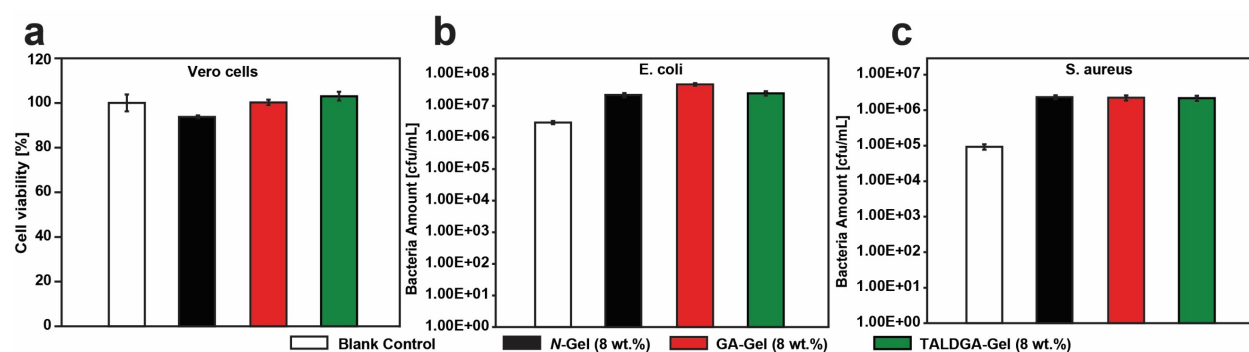


Figure 5.4. Cytotoxicity on mammalian Vero cells (a) and bacteria toxicity of *E. coli* (b) and *S. aureus* (c) of N-Gel, GA-Gel and TALDGA-Gel.

5.6 Concluding remarks

In the work here described, we have presented a new strategy based on Aldehyde Assisted Fractionation for the extraction and simultaneous functionalization of lignin with multiple non-native functional groups. In particular we extracted and functionalized lignin with non-native aldehydes and carboxylic acids in a single step by using mixtures terephthalic aldehyde (TALD) and glyoxylic acid (GA), showing how the amount of each functional group could be precisely controlled and monitored by means of mono dimensional NMR experiments. We also showed that different ratios of functional groups influenced the properties of the

extracted TALD/GA lignins with regard to solubility and reactivity. Specifically, we employed these lignins in the development of chemical cross-linked lignin/gelatin based hydrogels, showing how the presence of bifunctional TALD/GA lignin in the hydrogels was critical to: improve the rheological, mechanical, and adhesive properties; introduce the ability to self-heal; and promote resistance to high temperatures. Finally, we showed that the developed hydrogels didn't show any cytotoxicity with regard to mammalian cells, suggesting that these types of material could be safely used in biological and soft tissue engineering applications. In addition, we proved how the absence of one of these functional groups would negate most of these benefits, indicating the importance of being able to precisely target multi-functional lignins in material applications. Given the versatility of the process, this concept could be expanded to introduce many other functional groups on lignin for a variety of diverse application in material development. Furthermore, there is no particular reason this technique cannot be extended to the introduction of more than two functional groups. The importance of carefully controlled lignin functionalization, as presented this work, could facilitate the development of lignin-based materials for high-value applications. These applications could help overcome the longstanding view of lignin as a low-value waste stream in biorefineries.

Chapter 6 Conclusion

6.1 Summary of the work

In this doctoral thesis I have shown that the Aldehyde Assisted Fractionation process, initially developed for the quantitative depolymerization of lignin into aromatic monomers, could be modified by the use of multifunctional aldehydes in order to extract functionalized lignins that could be used as such in material applications.

In the strategy presented in this work, the multifunctional aldehyde introduced during the isolation of lignin serves two goals: protecting the lignin from condensation side-reactions and leaving on the biopolymer scaffold new functional groups. In fact, by the formation of stable acetals between lignin and the aldehyde, the core structure of lignin composed of mainly β -ether units is preserved, while through the same acetal bonds residual functionalities present on the aldehyde can be covalently bound to the lignin.

I have also demonstrated that the degree of lignin's functionalization could be quantified by monodimensional spectroscopic techniques such as ^1H and ^{31}P NMR, allowing for the controlled chemical modification of lignin directly during its extraction.

By having a full control over their chemical structure, we were therefore able to isolate lignins that were specifically designed for their final application and that consequently showed enhanced properties compared to lignins isolated by traditional methods.

Particularly, in Chapter 3 I showed that the lignin extracted in presence of terephthalic aldehyde (TALD), bearing novel aldehydic functionalities on its scaffold, showed an increased reactivity towards phenolation reactions compared to organosolv or industrial Kraft lignin, regardless of the acidic or basic catalytic conditions used.

Chapter 4 presented the strategy to alternatively obtain lignin modified with carboxylic acids, which could be achieved by performing AAF in presence of glyoxylic acid (GA). This newly extracted lignin was used for the development of new bio-based surfactants, which showed

increased surface-active properties compared to Kraft lignin, lignosulfonates, or other industrially relevant fossil-based surfactants.

Finally, in Chapter 5 I expanded the concept previously introduced to demonstrate that more engineered lignins could be obtained by employing a mixture of TALD and GA during AAF, showing that even in this case a high degree of control could be obtained, and that the amount of each functionality introduced on the lignin could be precisely controlled. I showed how having a lignin functionalized with both aldehydes and carboxylic acid was pivotal in increasing the rheological, mechanical and self-healing properties of gelatin-based hydrogels, ultimately highlighting how the process presented in this work could be a steppingstone to obtain engineered lignins for high-end applications.

6.2 Outlook

The work presented in this doctoral thesis led to new opportunities for lignin valorization in material applications, and in a broader sense to provide a new avenue for the transition from fossil-based materials towards more sustainable alternatives.

The versatility of the strategy described in this thesis was demonstrated to work similarly well for different aldehydes, used either singularly or in a mixture. This suggests that the same concept could be expanded and applied to a plethora of other multifunctional aldehydes, ultimately leading to the extraction from lignocellulosic biomass of “custom-made” lignins with optimized functionalization for their target application.

In order to obtain the same degree of control in lignin functionalization, it will, however, be necessary to improve existing analytical techniques, or to develop new ones, that will allow for a prompt quantification of introduced functional groups. Although aldehydes and carboxylic acids that we covalently bound to the lignin by using terephthalic aldehyde and glyoxylic acid were easily determined by monodimensional NMR spectroscopy as described in this thesis, there are many other relevant functional groups for lignin modification for which the quantification via NMR is not trivial, due to signal-overlap with the lignin. This is the case for example for alkene, alkyne, azide or acrylate groups that are relevant groups for performing polymerization and click-chemistry reactions, but whose NMR signals fall in the same regions as the lignin peaks.

A possibility to tackle these challenges is the use of quantitative HSQC-NMR experiments. Although they have been used to quantify key signals in the lignin scaffold, they still need optimization for the simultaneous quantification of the different functional groups of lignin.

Finally, in the hope of fully valorize the biomass undergoing multifunctional AAF, it will be necessary to fully characterize the other two components of lignocellulose involved in the process, namely cellulose and hemicellulose. In particular, the C5 and C6 sugars composing hemicellulose have a similar fate to lignin during biomass fractionation, as they have also been shown to react with aldehyde in the formation of stable diacetals. The multifunctional AAF will be hence a promising tool for the simultaneous extraction of functionalized fractions of biomass which could have interesting properties, for example, in the development of polymers and other materials.

However, it will be necessary, especially when multiple aldehydes are used, to put a particular focus on the purification of obtained products and recovery of solvents and unreacted reagents, in order to make the process economically feasible and ultimately possible on a large scale.

Appendix A Appendix for Chapter 3

A.1 Chemicals and materials

All commercial chemicals were of analytical grade and were used without further purification. 2-Chloro-4,4,5,5-tetramethyl-1,3,2-dioxaphospholane 95% (TMDP), Terephthalic aldehyde 99% (TALD), 5% ruthenium on carbon, dichloromethane >99%, dimethylsulfoxide >99% (DMSO), ethylene glycol >99%, ethyl acetate >99.5%, potassium bromide, *p*-Toluenesulfonic acid monohydrate >98.5% (*p*-TsOH) and sodium hydroxide were purchased from Sigma Aldrich. 1,4-Dioxane and sodium hydrogen carbonate were purchased from Carl Roth. Chromium (III) acetylacetonate, 97%, pyridine 99.5% were purchased from Acros Organics. Chloroform- d_3 99.8% ($CDCl_3$) and dimethylsulfoxide- d_6 (DMSO- d_6) were purchased from Cambridge Isotope Laboratories. Hydrochloric acid 37% w/w (HCl) and tetrahydrofuran (THF) stabilized with 0.025% w/w of BHT were purchased from Fisher Chemical. Diethyl ether was purchased from Carlo Erba. Decane was purchased from TCI Europe NV. Toluene was purchased from VWR. Phenol 99%, *N*-Hydroxy-5-norbornene-2,3-dicarboximide, 97% were purchased from Alfa Aesar.

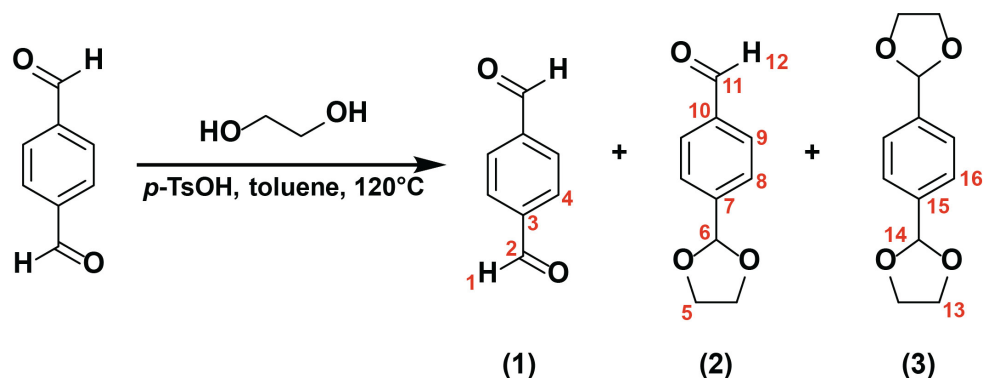
The Kraft Lignin (KL) used in this work as a benchmark for the phenolation reactions was UPM's BioPiva™ 100, currently used as replacement for phenol in plywood production. The Kraft lignin was dried in a vacuum oven at 45 °C for 24 h prior to its use.

Birch wood (*Betula Pendula*) was procured by Prof. Michael Studer from the Bern University of Applied Sciences. The tree was harvested in May of 2018 in Solothurn, Switzerland. It was first debarked, the trunk was cut in wood chips and dried at 40 °C for 24 h. The wood chips were subsequently transported to EPFL and cleaned from residual leaves and bark. The wood chips were then milled with a 6 mm screen and sieved with a 0.45 mm mesh.

A.2 Experimental Methods

A.2.1 Synthesis of Model compounds

Synthesis of a mixture of Terephthalic Aldehyde, 4-(1,3-Dioxolan-2-yl)benzaldehyde, and 1,4-bis(1,3-dioxolan-2-yl)benzene



Terephthalic aldehyde (2.04 g, 15.2 mmol) and *p*-toluenesulfonic acid (0.7 g, 4.08 mmol) were dissolved in 40 mL of toluene in a 100 mL round bottom flask. Ethylene glycol (1.5 g, 24.1 mmol) was then added to this solution. The reaction was equipped with a Dean-Stark apparatus and was first heated at 120 °C for 3 h, then cooled to room temperature. Following cool down, the solvents were evaporated in vacuo. The residue was then redissolved in 50 mL of dichloromethane and extracted with a saturated aqueous solution of NaHCO₃ (2x50 mL) and brine (1x50 mL). The organic phase was dried over anhydrous Na₂SO₄, filtered and dried in a rotary evaporator to obtain a yellow syrup (2.8 g, 2.8% w/w compound 1, 64.5% w/w compound 2, 32.7 % w/w compound 3 calculated by ¹H NMR) which was used without further purification. ¹H NMR (CDCl₃): δ_H 4.00-4.12 (m, H₅, H₁₃), 5.81 (s, H₁₄), 5.85 (s, H₆), 7.47 (s, H₁₆), 7.62 (d, J=8.2 Hz, H₈), (d, 7.85, J=8.2 Hz, H₉), 8.02 (s, H₄), 10.01 (s, H₁₂), 10.11 (s, H₁). ¹³C NMR (CDCl₃): δ_C 65.2 (C₁₃), 65.4 (C₅), 102.8 (C₆), 103.4 (C₁₄), 126.5 (C₁₆), 127.1 (C₈), 129.8 (C₉), 130.1 (C₄), 136.9 (C₁₀), 139.0 (C₁₅), 139.9(C₃), 144.4 (C₇), 191.5 (C₂), 191.9 (C₁₁)

A.2.2 Extraction of terephthalic aldehyde protected lignin

5 g of birch wood chips, terephthalic aldehyde (see ratios in **Table A.1**) and 25 mL of dioxane were introduced into a 100mL round bottom flask with a magnetic stirrer and stirred until the aldehyde was fully dissolved. When the aldehyde was fully dissolved, 0.8 mL of hydrochloric acid 37% w/w were added to the mixture. The round bottom flask was equipped with a condenser and a gas bubbler to create an air lock. The mixture was then heated at 85 °C for 3h under vigorous stirring. The system was then cooled to room temperature, following which 1.15 g of NaHCO₃ were slowly added to the mixture and stirred for 45 min. The reaction mixture was then filtered and the retentate was washed with dioxane. The filtrate was evaporated in a rotary evaporator. The solid residue was inserted in a 100 mL round bottom flask and washed with distilled water for one hour, filtered again and dried overnight in a vacuum oven at 45 °C to obtain a cellulose-rich solid.

The evaporated dioxane-filtrate was redissolved in 15 mL of fresh dioxane, precipitated in 400 mL of diethyl ether and stirred for 1 h to dissolve most of the carbohydrates and unreacted terephthalic aldehyde. The mixture was then filtered and purified overnight with a Soxhlet extractor using diethyl ether as a solvent to remove all impurities. The washed solid was then dried overnight in a vacuum oven at 45 °C to obtain terephthalic aldehyde protected lignin.

Table A.1. Biomass/terephthalic aldehyde ratios used during of lignin extractions

Sample	Dry birch wood chips [g]	Terephthalic Aldehyde [g]	mmol TALD/g dry biomass
1	4.729	8.004	12.62
2	4.714	7.125	11.27
3	4.751	6.102	9.58
4	4.716	5.018	7.93
5	4.701	4.023	6.38
6	4.760	3.017	4.73
7	4.722	2.030	3.20
8	4.754	1.029	1.61
9	4.722	0.538	0.85

A.2.2.1 Mass Balance of terephthalic aldehyde protected lignins

The yields of cellulose rich solids, lignin and carbohydrate derivatives shown in **Table A.2** are calculated based on the composition of birch biomass previously published by Amiri et al. shown in **Figure A.1**.¹⁵⁷

The yield of effective lignin is calculated according to the following equations:

$$\text{Effective isolated lignin} = g_{\text{isolated lignin}} - n_{\text{bound TALD}} \times 118.04 \text{g/mol} - n_{\text{residual TALD}} \times 134.13 \text{g/mol}$$

Equation A.1. Effective isolated lignin

$$\text{Lignin Extraction Yield}_{\text{Klason}} [\text{wt. \%}] = \frac{\text{Effective isolated lignin}}{\text{Original Klason Lignin Content}} \times 100$$

Equation A.2. Lignin Extraction Yield_{Klason}

Where in the equations:

$g_{\text{isolated lignin}}$: mass of isolated lignin

$n_{\text{bound TALD}}$: mmol of TALD covalently bound to the isolated lignin (measured by ¹H NMR according to Section A.3.1)

118.04 g/mol: Molecular weight of a TALD molecule when covalently bound to the lignin

$n_{\text{residual TALD}}$: mmol of residual TALD impurities in the isolated lignin (Calculated by ¹H NMR according to Section A.3.1)

134.13g/mol: Molecular weight of residual free terephthalic aldehyde.

Table A.2. Yields of cellulose rich solids, isolated lignin and carbohydrate derivatives after pretreatment.

Sample	Cellulose rich solid [%]^a	Lignin [%]^b	Furfural [%]^c	HMF [%]^c	TALDX [%]^c
1	53.08%	90.62%	0.21%	1.10%	4.29%
2	52.16%	103.32%	0.38%	1.20%	5.43%
3	59.88%	84.38%	0.15%	0.98%	4.13%
4	56.62%	99.44%	0.19%	1.05%	4.93%
5	60.02%	87.83%	0.15%	0.92%	4.76%
6	57.42%	99.66%	0.21%	1.18%	4.67%
7	63.95%	85.08%	0.14%	0.85%	3.74%
8	58.22%	87.96%	0.12%	1.98%	3.55%
9	60.30%	80.59%	0.10%	1.12%	2.51%

^a calculated based on the initial weight of dry biomass, ^b based on the initial Klason Lignin content, ^c based on the initial xylan content.

A graphical representation for Sample 1 is presented as an example in **Figure A.1**.

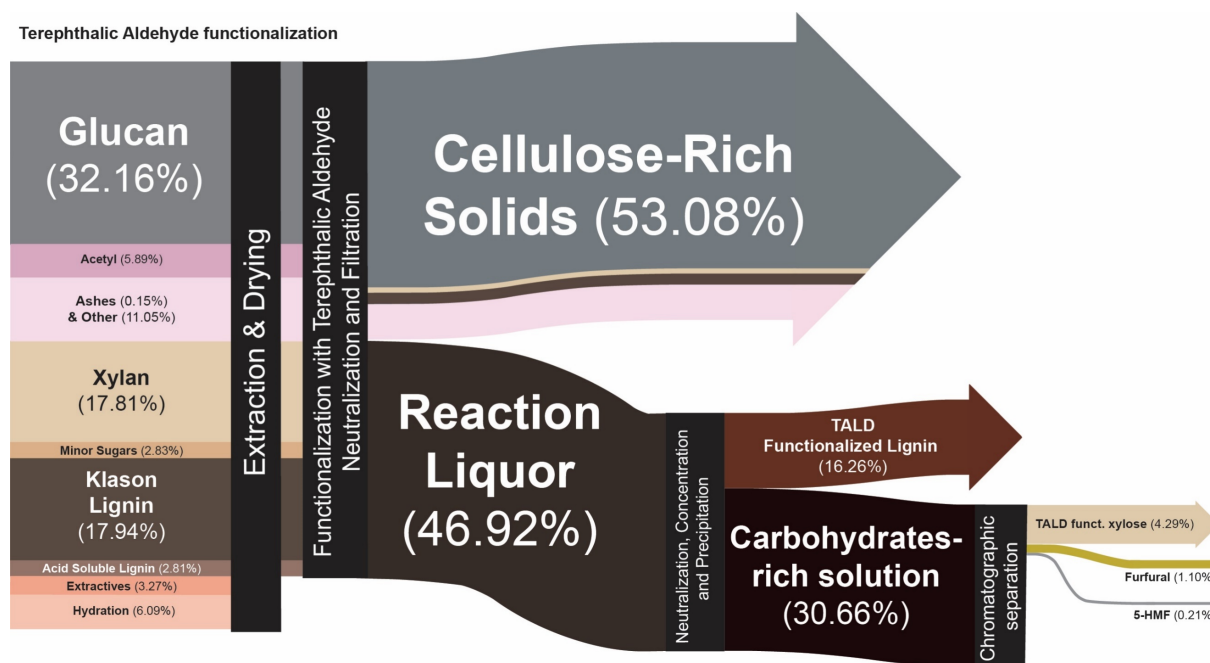


Figure A.1. Mass balance of the terephthalic aldehyde-facilitated fractionation of lignocellulosic biomass for sample 1.

A.2.3 Extraction of Mild Organosolv Lignin (OSL)

10g of birch wood was introduced in a 250 mL round bottom flask with 80 mL of an 80:20 Ethanol:H₂O solution. 1.6 mL of HCl 37% in H₂O w/w were then added to this solution. The extraction was refluxed under vigorous stirring for 5 h. The solid residue was filtered, washed with ethanol and dried under reduced pressure. 15 mL of acetone were subsequently added to dissolve the lignin, which was then precipitated in 300 mL of deionized water. This lignin was filtered and dried. For a further purification lignin was then dissolved in dioxane and precipitated in diethyl ether. The precipitate was then filtered and dried overnight in a vacuum oven at 45 °C. OSL was obtained with a yield of 28 wt.% on an initial Klason lignin content basis.

A.2.4 Phenolation of lignins

A.2.4.1 Acid catalysed phenolation

Phenol was put in a 10 mL Reacti-Vial™ equipped with a magnetic stir bar. The reagent was melted and 0.5 g of lignin were added. Then, 0.108 mL of concentrated H₂SO₄ were added dropwise and the reaction was run for 30 min at 110 °C. The reaction was then cooled to room temperature and 5 mL of DMSO were added to the vial. The resulting solution was added dropwise to 300 mL of deionized water previously adjusted to pH 1 with H₂SO₄. After the precipitation, the phenolated lignin was filtered and washed with water until the filtrate's pH was measured as neutral with pH indicator strips. The collected lignin was then dried overnight in a vacuum oven at 45 °C.

A.2.4.2 Basic catalysed phenolation

Phenol was put in a 10mL Reacti-Vial™ equipped with a magnetic stir bar. The reagent was melted and then 0.5 g of lignin were added. Then, 0.2 mL of a 30% w/w NaOH solution in water were added dropwise and the reaction was run for 24 h at 130 °C. The reaction was then cooled to room temperature and 5 mL of DMSO were added to the vial. The resulting solution was added dropwise to 300 mL of deionized water previously adjusted to pH 1 with H₂SO₄. After precipitation, the lignin was filtered and washed with water until the filtrate's pH was measured as neutral with pH indicator strips. The collected lignin was then dried overnight in a vacuum oven at 45 °C.

A.2.5 Hydrogenolysis of lignin into aromatic monomers

100 mg of isolated lignin were added to a 50 ml high-pressure Parr reactor equipped with a magnetic stirrer together with 100 mg of 5 wt.% Ru/C and 20 mL of tetrahydrofuran. The reactor was then closed and was first purged with N₂, then twice with H₂ and finally pressurized with 40 bar of H₂ before starting the reaction. The reactor was heated with high-temperature heating tape (Omega) connected to a variable power supply which was controlled by a PID temperature controller (Omega). The reaction was stirred at 600 rpm for 3 h at 250 °C. Afterward, the reactor was cooled down to room temperature with a flow of compressed air and H₂ was evacuated from the reactor.

A.2.6 Characterization of lignins

A.2.6.1 Diffuse Reflectance Infrared Fourier Transform (DRIFT) spectroscopy

DRIFT spectroscopy was performed on a PerkinElmer Frontier IR instrument. Samples were prepared by mixing approximately 15 mg of lignin and 0.5 g of KBr in a mortar until obtaining a homogeneous solid powder. Spectra were collected at room temperature from 500 to 4000 cm^{-1} with a scan number of 32. The background was recorded using solid KBr finely ground in a mortar.

A.2.6.2 Gel-permeation Chromatography (GPC)

The number average (M_n) and weight average (M_w) molecular weight of lignin samples, as well as their polydispersity index (PD) were determined by gel-permeation chromatography (GPC) using an Agilent 1260 15 infinity equipped with a refractive index detector and 2x Agilent PL-Gel Mixed C+ guard column set. GPC analyses were conducted in tetrahydrofuran (1 ml/min @40 °C) and the calibration was performed with polystyrene standards (Table A.3).

Table A.3. Molecular weight of isolated TALD lignin and propionaldehyde stabilized lignin determined by GPC.

Sample	M_n [g/mol]	M_w [g/mol]	PD
1	2500	5700	2.3
2	2400	6300	2.6
3	2600	6800	2.6
4	2500	6500	2.6
5	2500	6400	2.6
6	2400	6300	2.6
7	2500	5800	2.4
8	2400	5700	2.4
9	2500	5400	2.2
Propionaldehyde-stabilized lignin	3100	7400	2.4

Table A.4. Molecular weight of various isolated lignins determined by GPC.

Sample	Mn [g/mol]	Mw [g/mol]	PD
TALD	2600	6900	2.6
TALD-APH	600	900	1.5
TALD-BPH	2900	3900	1.4
OSL	2800	9000	3.2
OSL-APH	500	800	1.5
OSL-BPH	1100	2300	2.1
Kraft	900	1800	2.0
Kraft-APH	1100	1700	1.5
Kraft-BPH	1000	2100	2.1

A.2.6.3 Nuclear Magnetic Resonance (NMR)

The NMR characterization of the model compounds was performed on a Bruker Avance III 400 MHz spectrometer equipped with a BBFO-Plus probe. The ^1H and ^{13}C spectra of the model compounds were recorded using the standard pulse sequences from Bruker. The NMR characterization of lignin samples were performed on Bruker Avance 600 or 800 MHz spectrometers equipped with a 5 mm BBO and TCI cryoprobe respectively. The spectra were processed using the software Bruker TopSpin 3.6.1.

Quantitative ^1H , ^{13}C and HSQC (Heteronuclear Single-Quantum Coherence) spectra of functionalized lignins were recorded using standard pulse sequences with some modifications: D1=10s, NS=8, P1=8us, TD=65536, O1P (F2, F1)=6.175ppm, 125ppm, SW (F2, F1)=13.0186ppm, 150ppm.

The central peak of the solvent peaks was systematically used as reference (CDCl_3 : $\delta_{\text{H}}/\delta_{\text{C}}$ 7.24/77.23, DMSO-d_6 $\delta_{\text{H}}/\delta_{\text{C}}$ 2.50/39.50). Inversion Recovery experiments were performed to determine the relaxation time of the signals relative to the terephthalic aldehyde functionalization and the internal standard (**Figure A.2**).

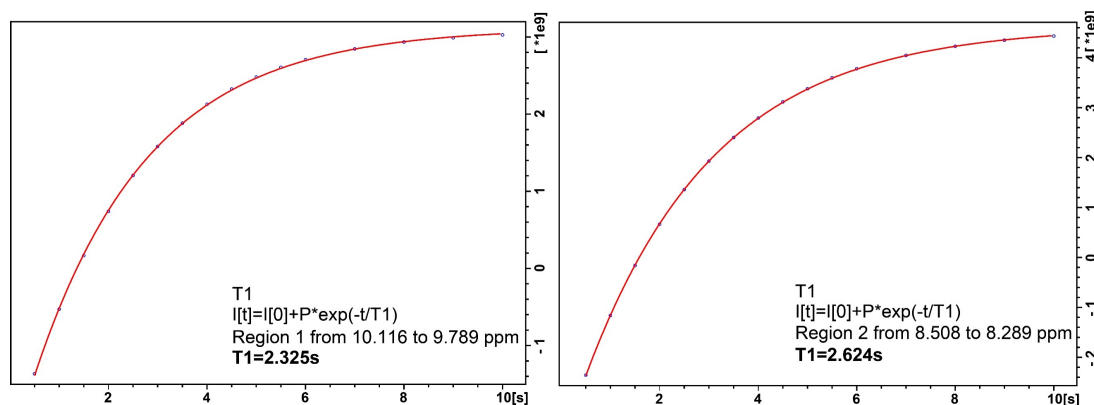


Figure A.2. T1 relaxation time estimates for the NMRs of TALD-functionalized lignin and the internal standard (1,4 DNB).

The Bruker DOSY (Diffusion Ordered SpectroscopY) pulse sequence (ledbpgp2s) was used to investigate the diffusion of molecular systems in solution. The DOSY diffusion time interval (d20) and gradient pulse length (p30) were set at 0.1 s and 2000 ms, respectively, with a recycle delay (d1) of 2 s. Each 1D free induction decay had 4K complex points with 8 scans averaged. The diffusion gradients were ramped from 2% to 98% at linear increments to generate 16 increments in the diffusion dimension. All experiments were performed at a temperature of 298 K. DOSY spectra for TALD lignin (sample 1), KL-BPH and OSL-BPH are shown in **Figure A.3**.

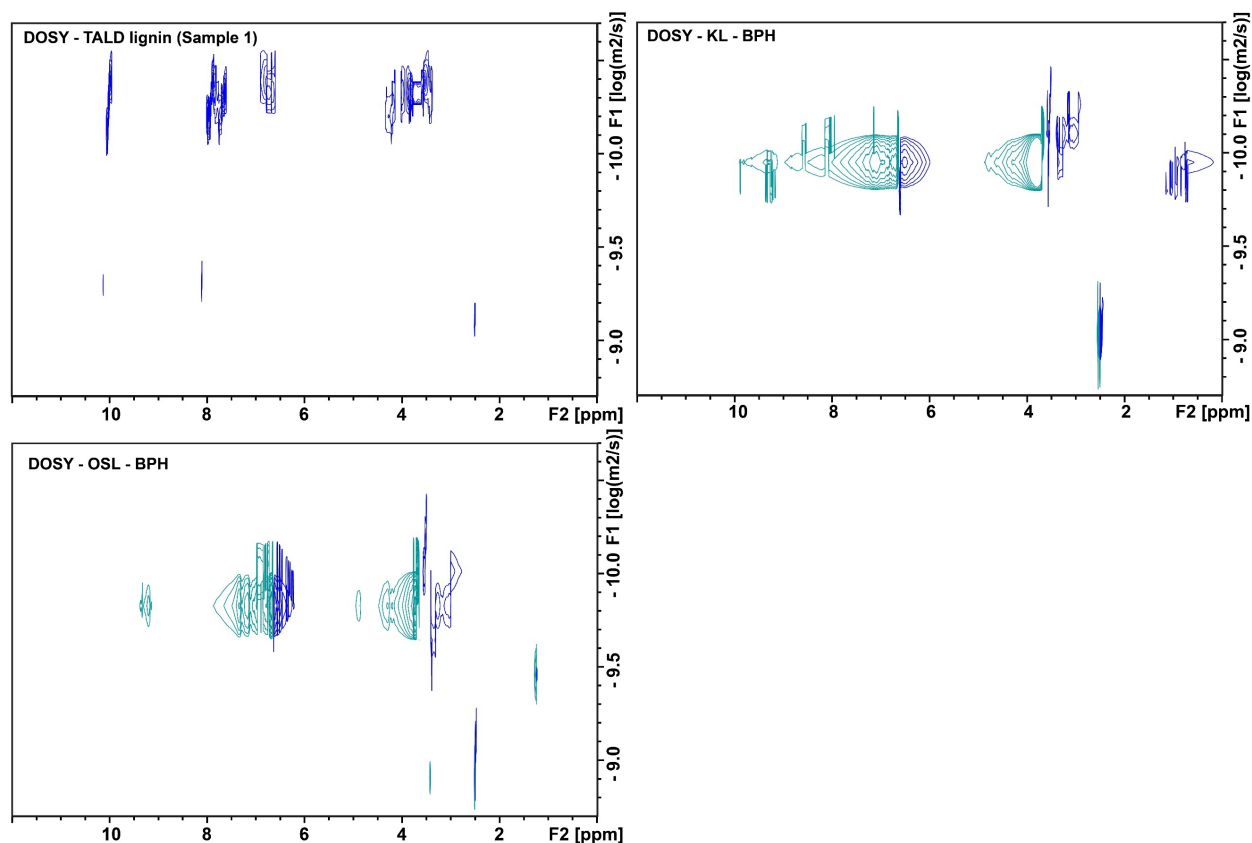


Figure A.3. DOSY spectra of TALD lignin (sample 1), KL-BPH and OSL-BPH.

^{31}P NMR and hydroxyl group quantification was performed following a protocol published by Meng et al. by working under inert atmosphere (**Table A.5**).⁸⁶ Lignin samples were dried overnight at 45 °C under vacuum. Approximately 30 mg of lignin were massed in a glass vial, to which was added 0.1 ml of a solution of deuterated pyridine and chloroform (1.6:1, v/v) containing chromium (III) acetylacetonate solution (~5.0 mg/mL,) and *N*-Hydroxy-5-norbornene-2,3-dicarboximide (NHND) as an internal standard (~18.0 mg/mL). Subsequently, 0.5mL of a solution of deuterated pyridine and chloroform (1.6:1, v/v) was added and stirred until full dissolution of the lignin. Once the solution was clear, 0.1mL of 2-chloro-4,4,5,5-tetramethyl-1,3,2-dioxaphospholane (TMDP) were carefully added to the solution. The mixture was stirred for 1h and then transferred to an NMR tube and analysed within 3h. The NMR spectra were recorded on a Bruker Avance 600 MHz spectrometer equipped with a 5 mm BBO cryoprobe. The experimental NMR parameters used were: Pulse program= Inverse gated decoupling pulse (zgig), SW=100 ppm, O1P=140 ppm, AQ=0.8 s, D1=10 s, NS=128.

Table A.5. Quantification of aliphatic, phenolic, and carboxylic hydroxyl groups on various lignins via ^{31}P NMR. The results are reported in mmol/g of effective lignin. Aliph-OH refers to the aliphatic hydroxyl groups, 5-Subst.-OH refers to phenolic groups on aromatic rings substituted at the position 5 (such as Syringol units), G-OH refers to phenolic groups of Guaiacol units, H-OH refers to phenolic groups of Hydroxyphenylpropane units and COOH refers to carboxylic acid groups.

Sample	Aliph-OH [mmol/g]	5-Subst.-OH [mmol/g]	G-OH [mmol/g]	H-OH [mmol/g]	COOH [mmol/g]
TALD	3.21	0.70	0.27	0.02	0.07
TALD-APH	0.13	0.10	0.34	6.45	0.04
TALD-BPH	1.55	0.62	0.23	4.34	0.20
OSL	3.10	0.56	0.64	0.14	0.06
OSL-APH	0.16	1.09	0.40	3.91	0.09
OSL-BPH	1.80	0.75	0.50	1.94	0.27
Kraft	1.55	1.37	1.69	0.15	0.39
Kraft-APH	0.50	1.90	1.77	3.45	0.33
Kraft-BPH	1.32	1.36	1.45	1.23	0.43

A.3 Analytical Methods

A.3.1 Quantification of free aldehyde in terephthalic aldehyde protected lignin by ^1H NMR

40-60 mg of Terephthalic aldehyde protected lignin were massed in an NMR tube. 50 μL of a solution of 1,4-dinitrobenzene (1,4-DNB) in DMSO-d_6 (89.7g/L) were then introduced in the NMR tube, to which, 500 μL of additional DMSO-d_6 were added. If needed, the sample was briefly sonicated until full dissolution of the lignin sample. The exact quantities used in this preparation are shown in **Table A.6**. ^1H NMR spectra were recorded with a long D1 (at least 10 s) to allow for the lignin signals and internal standard to fully recover.

The spectrum was then processed, phased and the baseline was corrected by using the command ABS in the Bruker TopSpin software. The spectrum was then integrated. The peak

of 1,4-dinitrobenzene (1,4-DNB, the internal standard) at 8.43 ppm was calibrated to 4 protons. The integral of the peak assigned to the free terephthalic aldehyde group (TALD) bound to the lignin at 10.01 ppm and the integral the peak assigned to the unbound terephthalic aldehyde at 10.14 ppm were then estimated.

The quantification of bound and residual terephthalic aldehyde were then calculated using the equations detailed below.

The integrals of the peaks assigned to 1,4-dinitrobenzene and bound terephthalic aldehyde were normalized by the number of protons generating the signals according to **Equation A.3** and **Equation A.4**.

$$\text{Normalized 1,4DNB integral} = (\text{measured I. S. integral})/4$$

Equation A.3. Normalized 1,4-DNB integral.

$$\text{Normalized aldehyde integral} = (\text{measured aldehyde integral})/1$$

Equation A.4. Normalized aldehyde integral.

The number of moles of 1,4-dinitrobenzene generating the integral could then be calculated with **Equation A.5** by knowing the quantity and purity of the internal standard introduced into the NMR tube.

$$\text{mmol 1,4DNB in NMR sample}$$

$$= (\text{mg 1,4DNB in NMR tube} * 0.98)/(168.11 \text{ mg / mmol})$$

Equation A.5. mmol 1,4-DNB in NMR sample.

Where 168.11 mg/mmol is the molecular weight of 1,4-dinitrobenzene and 0.98 is the purity of the internal standard used for these analyses.

The number of moles of free aldehyde generating the signal of TALD bound to the lignin was then calculated with **Equation A.6**.

$$\text{mmol aldehyde in NMR sample}$$

$$= (\text{Normalized aldehyde integral})/(\text{Normalized 1,4DNB integral}) \\ * (\text{mmol 1,4DNB in NMR sample})$$

Equation A.6. mmol aldehyde in NMR sample

Finally, the number of moles of free aldehyde bound to the lignin per gram of isolated lignin could be calculated according to the **Equation A.7**.

mmol of free aldehyde in 1g of lignin

$$= (\text{mmol aldehyde in NMR sample})/(\text{mg of lignin in NMR tube}) * 1000$$

Equation A.7. mmol of free aldehyde in 1g of lignin.

Table A.6. Detailed quantities used for ¹H NMR quantification of the functionalized lignins and quantification results.

Sample	mg lignin	mL I.S solution	mL DMSO-d ₆	mmol bound TALD/g lignin	mmol residual TALD/g lignin
1	52.7	0.05	0.5	1.88	0.060
2	50.5	0.05	0.5	1.99	0.053
3	45.4	0.05	0.5	1.72	0.049
4	54.9	0.05	0.5	1.68	0.037
5	50.4	0.05	0.5	1.64	0.040
6	49.0	0.05	0.5	1.51	0.022
7	45.8	0.05	0.5	1.16	0.036
8	50.5	0.05	0.5	0.83	0.003
9	49.2	0.05	0.5	0.47	0.002

A.3.2 Quantification of aromatic monomers from hydrogenolysis of isolated lignin by GC (Gas Chromatography)

After the hydrogenolysis reaction was complete and cooled to room temperature, the reactor was brought to atmospheric pressure by purging the H₂ and then opened. 0.5 mL of internal standard solution (decane in 1,4-dioxane 10 g/Kg) were added to the reaction mixture and stirred with a spatula until homogeneous. The mixture was then transferred with a Pasteur pipette to a syringe equipped with a Chromafil Xtra H-PTFE 20/25 syringe filter and filtered. 1 mL of the filtrate was transferred to a GC vial and analysed with a GC (Agilent 7890B series) equipped with an HP5-column and a flame ionization detector (FID). The injection temperature was 300 °C. The column temperature program was: 40 °C (3 min), 30 °C/min to 100 °C, 40 °C/min to 300 °C and 300 °C (5 min). The detection temperature was 300 °C. The monomer yield on Klason lignin basis was calculated according to recent published guidelines

which are based on the area of the monomer and the area of decane in the GC chromatogram.¹⁷⁴ The detailed calculation is presented here below:

$$n_{\text{decane}} = \frac{W_{\text{decane in sample}}}{MW_{\text{decane}}}$$

Equation A.8. n_{decane}

$$n_{\text{monomer}} = \frac{A_{\text{monomer in sample}}}{A_{\text{decane in sample}}} \times n_{\text{decane}} \times \frac{ECN_{\text{decane}}}{ECN_{\text{monomer}}}$$

Equation A.9. n_{monomer}

To compare the results between samples with different monomeric composition and products with different degrees of hydrodeoxygenation and side truncation, the monomer yield was calculated by using the native molecular weight (**Table A.7**) of guaiacyl or syringyl β -O-4 units generating the different monomers after hydrogenolysis (**Figure A.5**).

$$\text{Monomer yield [wt\%]} = \frac{\sum(n_{\text{monomer}} MW_{\text{native}})}{\text{Effective isolated lignin}} \times \text{Lignin extraction yield}_{\text{klason}}$$

Equation A.10. Monomer Yield [wt.%]

The monomer yields of the isolated yields are shown in **Figure A.4**.

In the equations,

$W_{\text{decane in sample}}$ (mg): the mass of decane used as an internal standard in each analysed sample;

MW_{decane} (mg mmol⁻¹): the molecular weight of decane (142 mg mmol⁻¹);

n_{decane} (mmol): the molar amount of decane in each analysed sample;

n_{monomer} (mmol): the molar amount of monomer in each analysed sample;

$A_{\text{monomer in sample}}$: the peak area of monomer in the GC-FID chromatogram;

$A_{\text{decane in sample}}$: the peak area of decane in the GC-FID chromatogram;

ECN_{decane} : the effective carbon number (10) of decane;

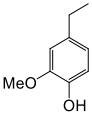
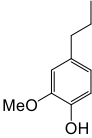
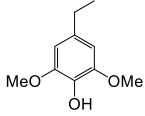
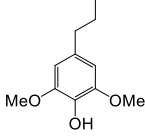
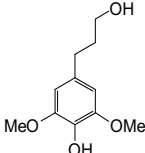
ECN_{monomer} : the effective carbon number of the lignin monomer molecule (**Table A.7**);

MW_{native repeating unit} (mg mmol⁻¹): the molecular weight of native guaiacyl and syringyl β-O-4 units (see **Figure A.5**).

Lignin extraction yield_{klason}: Extraction yield based on Klason lignin content as defined in **Equation A.2**.

Effective Isolated lignin: Mass of lignin corrected per amount of covalently bound TALD as defined in **Equation A.1** and **A.3.1**.

Table A.7. Structure, name and effective carbon number used (ECN) of lignin monomers obtained using THF as the GC solvent.²²⁹

Lignin monomer structure	Name	Effective carbon number in THF (ECN _{monomer})	MW monomer after hydrogenolysis [g/mol]	MW of native repeating unit [g/mol]
	4-Ethyl-guaiacol	7	152.19	196.20
	4-Propyl-guaiacol	8	166.22	196.20
	4-Ethyl-syringol	7	182.22	226.23
	4-Propyl-syringol	8	192.25	226.23
	4-Propanol-syringol	7.4	212.25	226.23

The monomer yields of isolated lignins based on these calculations are represented in **Figure A.4**.

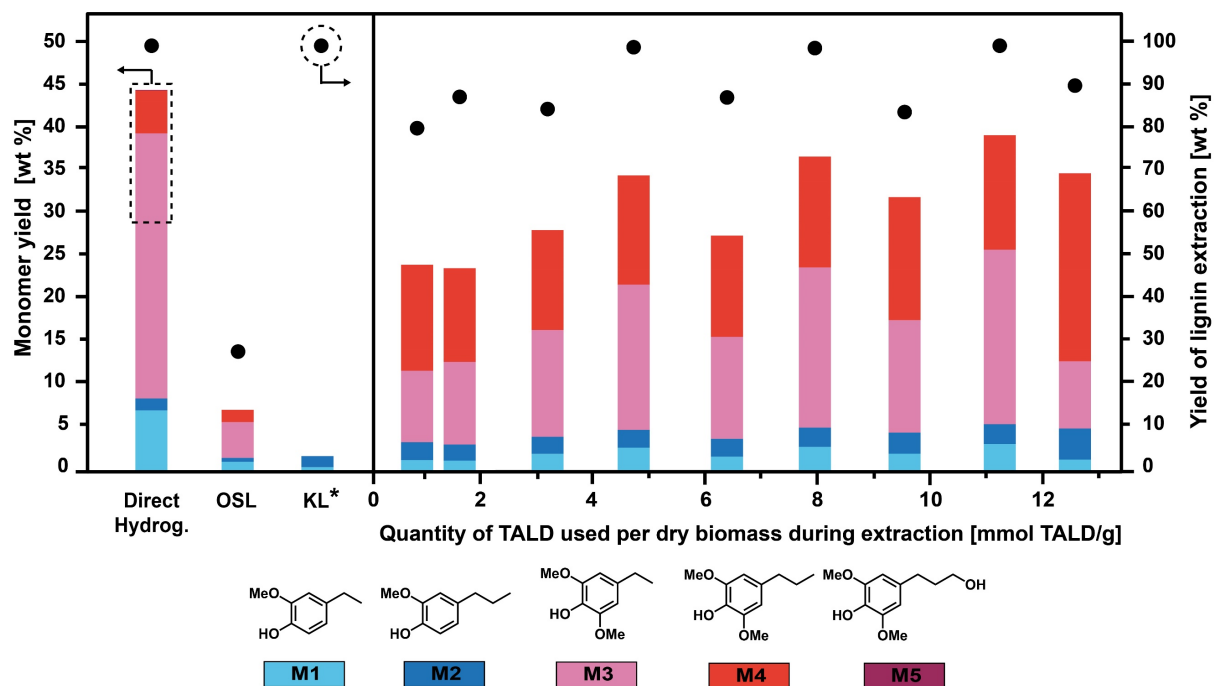


Figure A.4. Depolymerization and extraction yields of TALD-functionalized lignins, OSL and KL.

*For Kraft Lignin, we assumed (1) that the Klason lignin of the original biomass used to produce Kraft lignin (which we did not have access to) was the same as that of the biomass used for the other experiments and (2) that the lignin extraction yield (which was unknown) to produce this Kraft lignin was 100%. In this way, we likely overestimate yields from Klason lignin but avoid any unfair comparison with our results.

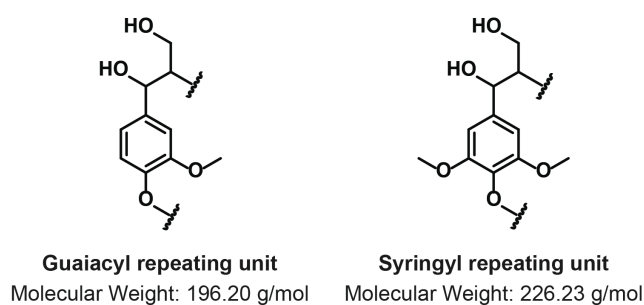


Figure A.5. Structure of the native guaiacyl and syringyl repeating units and their molecular weight.

Appendix B Appendix for Chapter 4

B.1 Chemicals and materials

All commercial chemicals were of analytical grade and were used without further purification. 2-Chloro-4,4,5,5-tetramethyl-1,3,2-dioxaphospholane 95% (TMDP), Mineral Oil, sodium hydroxide, sodium bicarbonate, Sudan Black B certified by Biological Stain Commission were purchased from Sigma Aldrich. 1,4-Dioxane, sodium lignosulfonate 93% (pulverized) and calcium lignosulfonate 93% (pulverized) were purchased from Carl Roth. Chromium (III) acetylacetonate 97%, pyridine 99.5%, glyoxylic acid monohydrate 98% (GA), propionaldehyde 99+% (PA), and cyclohexane 99.5% were purchased from Acros Organics. Chloroform-d₃ 99,8% (CDCl₃) and dimethylsulfoxide-d₆ (DMSO-d₆) were purchased from Cambridge Isotope Laboratories. Hydrochloric acid 37% w/w (HCl) and tetrahydrofuran (THF) stabilized with 0.025% w/w of BHT were purchased from Fisher Chemical. The kraft Lignin in this work was UPM's BioPiva™ 100, which was dried in a vacuum oven at 45 °C for 24h before its use. Birch (*Betula Pendula*) wood chips were supplied by Prof. Michael Studer from the Bern University of Applied Sciences. The tree was harvested in May 2018 in Solothurn, Switzerland. Beech (*Fagus sylvatica*) wood was provided by a Swiss woodcutter, Jimmy Rochat.

B.2 Experimental Methods

B.2.1 Biomass preparation

The Birch tree trunk was debarked, cut into wood chips and dried at 40 °C for 24 h. Afterwards, the wood chips were transported to EPFL (Lausanne, Switzerland) where they were separated from residual leaves and bark, milled with a 6mm screen and sieved with a 0.45 mm mesh. The Beech tree trunk was debarked and then chipped to form particles approximately 5 cm wide. These wood chips were then spread on a tarp for two weeks to dry before being reduced using a Retsch cutting mill (6mm grid).

B.2.2 Glyoxylic Acid (GA)-lignin extraction

Approximately 5 g of birch wood chips (6.09% hydration), glyoxylic acid monohydrate (see ratios in **Table B.1**), 0.8 mL of HCl 37 wt% in water, and 25 mL of dioxane were introduced in a 100 mL flat-bottomed flask along with a 30 mm-long magnetic stirrer. The cap was firmly screwed, and the flask was heated at 85 °C in an oil bath. The stirring was gradually increased from an initial rate of 500 rpm to 700 rpm over the course of an hour. After three hours of reaction, the flask was removed from the oil bath and allowed to cool to room temperature. The reaction mixture was then filtered with filter paper (Macherey-Nagel, MN640d) to remove the cellulose-rich solids. The retentate was washed three times with dioxane to remove all soluble compounds. The filtrate, containing the lignin, hemicellulose and residual unreacted GA, was then concentrated on a rotary evaporator at 45 °C and a pressure of 90 mbar. For the isolation of GA-lignin, a 1 L flat-bottomed flask was filled with approximately 850 mL of deionized water. The water was stirred with a 50mm bar stirrer at 400 rpm, and the concentrated solution was introduced dropwise, causing the lignin to precipitate as a fine powder. The water solution was then left to stir for 45 min. Finally, the solution was filtered on a 0.8 µm Nylon filter to separate the GA-lignin from the water-soluble hemicellulose fraction. The lignin was dried for at least 24 h in a vacuum oven at 45 °C before use.

B.2.3 Calculation of Effective Extracted lignin

The yields of effective extracted lignin shown in **Table B.1** are calculated based on the composition of the same birch wood used in the work previously published by Talebi Amiri et al.¹⁵⁷ and according to the following equations:

$$\text{Effective isolated lignin} = g_{\text{isolated lignin}} - n_{\text{bound GA}} \times 58.01 \text{ g/mol}$$

Equation B.1. Effective Isolated lignin

$$\text{Lignin Extraction Yield}_{\text{Klason}} [\text{wt. \%}] = \frac{\text{Effective isolated lignin}}{\text{Original Klason Lignin Content}} \times 100$$

Equation B.2. Lignin extraction yield on Klason lignin bases.

Where in the equations:

$g_{\text{isolated lignin}}$: mass of isolated lignin

$n_{\text{bound GA}}$: mmol of GA covalently bound to the isolated lignin (measured by ^{31}P NMR according to Section B.3.2)

The value 58.01 g/mol corresponds to the molecular weight of a GA molecule when covalently bound to the lignin.

Table B.1. Experimental data and corresponding yields for the GA-lignin samples

Sample	Dry biomass in reactor [g]	GA monohydrate in reactor [g]	GA/dry biomass [mmol/g]	Lignin extraction yield (on Klason Lignin basis) [%]
1	4.699	0.372	0.859	78%
2	4.709	0.752	1.735	55%
3	4.715	1.356	3.124	65%
4	4.701	1.818	4.200	77%
5	4.731	2.773	6.366	71%
6	4.781	4.179	9.497	77%
7	4.717	5.073	11.684	61%
8	9.391	11.001	12.725	74%

B.2.4 Propionaldehyde (PA)-lignin extraction

The extraction of PA-lignin was performed following a procedure published by Lan et al.¹⁵⁵ Briefly, 20 g of beech wood chips were added into a 500 mL round bottomed flask along with 180 mL of dioxane, 19 mL of propionaldehyde (15.2 g, 261 mmol), 8.4 mL of HCl 37 wt.% (100 mmol) and a magnetic stirrer. The reaction mixture was heated to 85 °C in an oil bath and stirred for 3 h. Afterwards, the solution was cooled to room temperature and neutralized with 8.4 g of NaHCO_3 (100 mmol). The reaction mixture was left to stir for an additional 30 min and was then filtered on a Büchner to separate the insoluble cellulose-rich fraction from the soluble lignin and hemicellulose fractions. The filtrate was concentrated with a rotary evaporator at 45 °C and 50 mbar for approximately 20 min until its viscosity had noticeably increased. This mixture was then precipitated dropwise in 200 mL of diethyl ether to yield the

propionaldehyde-stabilized lignin. The lignin was finally filtered on a Buchner, washed with fresh diethyl ether, and dried at 45 °C in a vacuum oven overnight.

B.3 Characterization of lignin samples

B.3.1 Heteronuclear Single-Quantum Coherence (HSQC-NMR)

The NMR samples were made by dissolving 50 mg of lignin in 0.5 mL of deuterated DMSO- d_6 . A Bruker AV- Neo (AV-III) spectrometer equipped with a 5 mm BBO probe-head capable of producing magnetic field pulse gradients in the z-direction of 54G/cm was used to record all NMR spectra. Frequencies were 400.03 MHz for ^1H NMR and 100.58 MHz for ^{13}C NMR. The HSQC (Heteronuclear Single-Quantum Coherence) spectrum of the GA-lignin was also recorded using the standard pulse sequences from Bruker, except that 32 scans were used. All the spectra were then processed using the software Bruker TopSpin 3.6.1.

A typical HSQC spectrum of Propionaldehyde functionalized lignin (PA-lignin) is shown in **Figure B.1**.

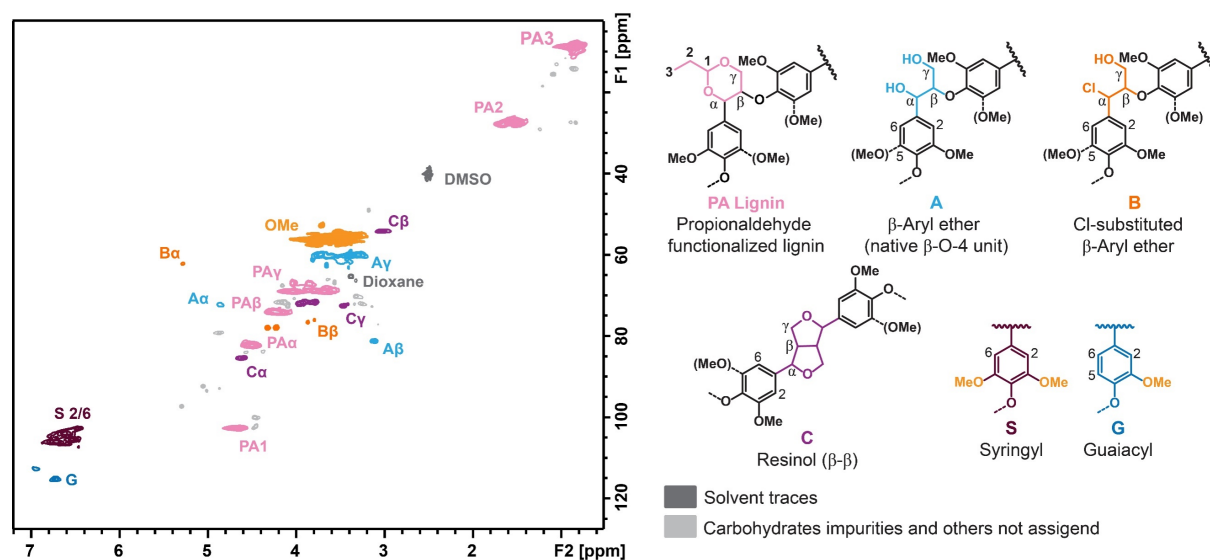


Figure B.1. HSQC spectrum of propionaldehyde functionalized Lignin (PA-lignin).

B.3.2 Quantitative ^{31}P -NMR

Quantitative ^{31}P NMR was performed following a procedure published by Meng et al. working in a nitrogen atmosphere⁸⁶. Briefly, after drying the lignin samples overnight at 45 °C in a vacuum oven, approximately 30 mg of lignin were inserted in a glass vial equipped with a magnetic stir bar and closed with a PTFE-septum sealed cap. To this vial, we added 0.1 mL of a solution of deuterated pyridine and CDCl_3 (1.6:1, v/v) containing chromium (III) acetylacetonate solution (~5.0 mg/mL,) and N-Hydroxy-5-norbornene-2,3-dicarboximide (NHND) as an internal standard (~18.0 mg/mL) with a gas-tight syringe. To the vial were then added 0.5 mL of a solution of deuterated pyridine and CDCl_3 (1.6:1, v/v) and the lignin was let to fully solubilize while stirring. After complete solubilization of the lignin, 0.1 mL of 2-chloro-4,4,5,5-tetramethyl-1,3,2-dioxaphospholane (TMDP) was added dropwise to the solution. The mixture was stirred for an additional hour to achieve complete derivatization and then transferred to an NMR tube previously dried at 120 °C and equipped with a rubber septum. The samples were analysed within 3h of their preparation. The ^{31}P NMR spectra were recorded on a Bruker Avance 600 MHz spectrometer equipped with a 5 mm BBO cryoprobe. The experimental parameters used for the spectra acquisition were: Pulse program=Inverse gated decoupling pulse (zgig), SW=100 ppm, O1P=140 ppm, AQ=0.8 s, D1=10 s, NS=128. The quantified values of hydroxyl groups in the extracted GA-lignin samples are shown in **Table B.2**.

Table B.2. Quantification of aliphatic, phenolic and carboxylic hydroxyl groups of extracted GA-lignins via ^{31}P NMR. Aliph-OH refers to the aliphatic hydroxyl groups, 5-Subst.-OH refers to phenolic groups on aromatic rings substituted at the position 5 (for example Syringol units), G-OH refers to phenolic groups of Guaiacol units, H-OH refers to phenolic groups of Hydroxyphenylpropane units and COOH refers to carboxylic acid groups.

Sample	Aliph-OH [mmol/g]	5-Subst.-OH [mmol/g]	G-OH [mmol/g]	H-OH [mmol/g]	COOH [mmol/g]
1	3.11	0.97	0.41	0.18	0.37
2	3.62	0.71	0.38	0.12	0.46
3	3.04	0.67	0.37	0.11	0.55
4	2.84	0.80	0.36	0.10	0.68

5	2.34	0.71	0.37	0.09	0.89
6	2.50	0.69	0.33	0.06	0.88
7	2.63	0.51	0.29	0.07	0.84
8	1.78	0.31	0.20	0.01	0.86
PA-lignin	1.72	0.70	0.29	0.00	0.13

B.4 Critical Micelle Concentration (CMC) measurements

B.4.1 Sample preparation

GA-lignin solutions at five different concentrations (10, 1, 0.1, 0.01 and 0.001 mg/mL) and three different pH (1, 7 and 14) were prepared in the following manner.

First, a starting solution of 20 mg/mL of GA-lignin at pH 14 was prepared by dissolving 200 mg of lignin in a 10 mL volumetric flask using a 1M NaOH solution. Then, using an autopipette (VWR Signature™ Ergonomic High-Performance Single- Channel Variable Volume Pipettor, 10 mL), 2 mL of solution were transferred to a first vial (Vial 1) and 3 mL of solution to a second vial (Vial 2). The remaining 5 mL were left in the original vial, labelled Vial 3.

To create the five GA-lignin solutions at pH 14, 5 mL of a 1M NaOH solution were first added to Vial 3 using an autopipette. This generated the 10 mg/mL GA-lignin solution, which was then successively diluted with the 1M NaOH solution 4 times using a 10 mL volumetric flask in order to create the 1, 0.1, 0.01 and 0.001 mg/mL solutions of GA-lignin at pH 14.

To create the five GA-lignin solutions at pH 7, the pH in Vial 2 was brought down to 7 using HCl, and then the total volume of the solution was adjusted to 6 mL with deionized water. This 10 mg/mL GA-lignin solution was then successively diluted with deionized water 4 times using a 10 mL volumetric flask in order to create the 1, 0.1, 0.01 and 0.001 mg/mL solutions of GA-lignin at pH 7.

To create the five GA-lignin solutions at pH 1, the pH in Vial 1 was brought down to 1 using HCl, and then the total volume of the solution was adjusted to 4 mL with a 0.1 M HCl solution. This 10 mg/mL GA-lignin solution was then successively diluted with the 0.1 M

HCl solution 4 times using a 10 mL volumetric flask in order to create the 1, 0.1, 0.01 and 0.001 mg/mL solutions of GA-lignin at pH 1.

In addition to these samples, a control was prepared by using 1 mL of deionized water at pH 7 without lignin. A second control sample was prepared with GA-lignin at pH 14 with added NaCl (22.4 mg NaCl/mL of solution) to match the exact amount of salt formed when adjusting the pH from 14 to 7 with HCl 0.1 M.

B.4.2 Surface tension measurements

The water/air surface tension or water/oil interfacial tension of each GA-lignin solution were measured using the pendant drop method. A sample of each solution was inserted in a 1 mL syringe and loaded onto a Krüss DSA 30 drop shape analyzer. The drops were created and visualized using the Krüss Advance software (v.1.6.2.0). Each surface/interfacial tension value was obtained using a standardized procedure. First, a drop was created and expanded until it fell. The volume at which the drop fell was recorded. Then, a second drop was created that had approximately 90% of the volume of the first drop as measured by the Krüss software. The drop was left to stabilize for three min before measuring the surface or interfacial tension value.

B.4.3 Emulsification tests

Either 1 mL of a 10 mg/mL GA-lignin aqueous solution at pH 14, 7 or 1 were added to 0.5 mL of oil phase in a 2 mL glass vial. The GA-lignin solutions at different pH were made by first preparing a 20 mg/mL solution at pH 14, and then either diluting it with 1 M NaOH (for the pH 14 solution) or adjusting the pH to the requisite value with HCl and diluting the resulting solution with deionized water (for the pH 7 solution) or 0.1 M HCl (for the pH 1 solution).

The water and oil phases were then tip sonicated with a Branson 450 Digital Sonifier, using the following parameters: 15 s total sonication time, amplitude of 20%, 2s on/5s off pulse sequence.

B.4.4 Dynamic Light Scattering (DLS) measurements

DLS measurements were made with a Zetasizer Nano-ZS apparatus (Malvern, UK). The analysed solutions were loaded into a plastic UV/visible absorbance spectroscopy cuvette and

inserted into the machine. The data was then processed using the Zetasizer software provided by Malvern (v. 7.02). All solutions had an attenuation factor in the acceptable 6-9 range. Aqueous solutions/colloids of GA-lignin at pH 1, 7 and 14 were analyzed by DLS (**Figure B.2**).

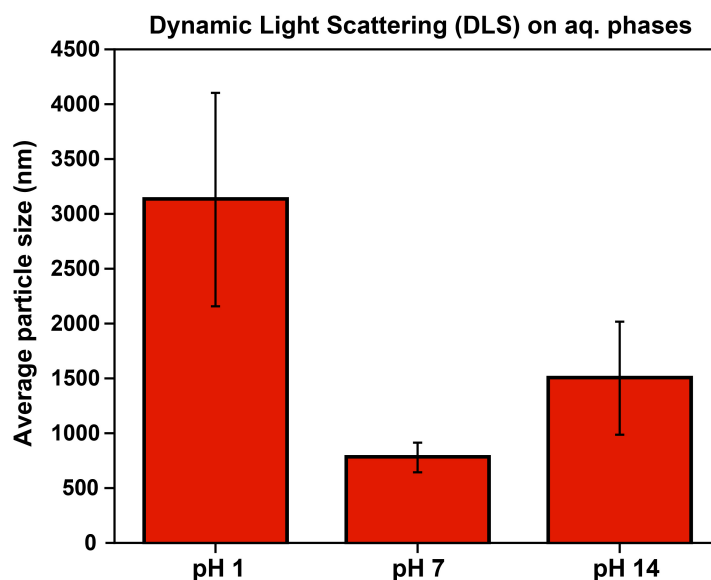


Figure B.2. DLS measurements of lignin in aqueous phases at different pH values.

B.4.5 Microscopy imaging of emulsions and photos of emulsion vials over time

A Nikon Eclipse TS100 Inverted Microscope was used to view the previously described emulsions. Pictures were taken immediately after the emulsification, and every seven days thereafter in order to observe the evolution of the droplets and gauge the stability of the emulsions. Fluorescence images of the emulsion were taken with the same instrument and an example is shown in **Figure B.3**.

Photos of the vials containing the emulsions were taken with an iPhone 11 Pro on the same days as the microscopy images (**Figure B.4**).

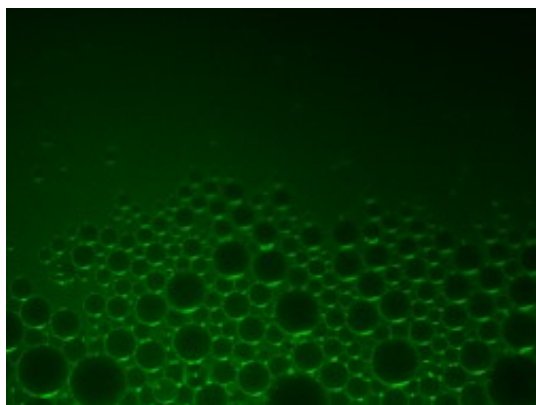


Figure B.3. Fluorescence microscopy image of a cyclohexane/water emulsion. No fluorescence is observed inside the oil droplets confirming that this is an oil in water emulsion (as the autofluorescent lignin is in the water phase, not in the oil phase).

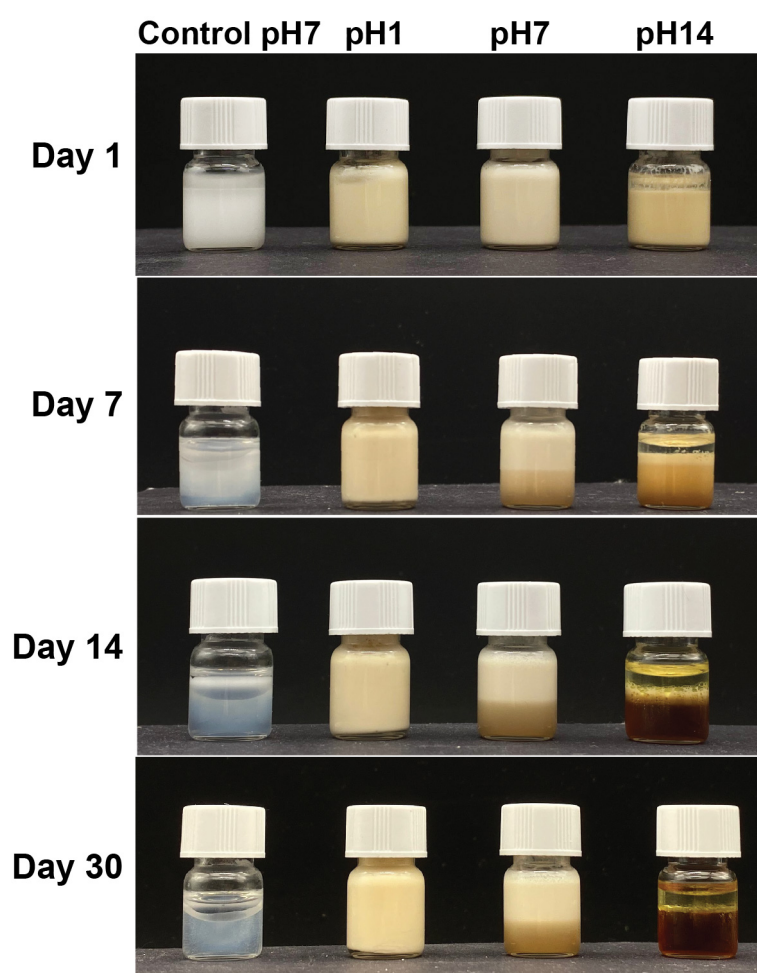


Figure B.4. Pictures of the vials containing the emulsions of water/mineral oil at different pH, taken at day 1, 7, 14 and 30.

B.4.6 Preparation of a hand-cream formulation

The hand cream formulation was prepared by introducing 9 mL of an aqueous solution of GA-lignin at a concentration of 1 wt% at pH 4 into a 20 mL glass vial. To this were added 4.5 mL of mineral oil containing 1 wt% of citral and 100 mg of xanthan gum.

The mixture was then tip sonicated with a Branson 450 Digital Sonifier, using the following parameters: 15 s total sonication time, amplitude of 20%, 2 s on/5 s off pulse sequence.

Two control experiments were also prepared, one without lignin and one by substituting GA-lignin with Kraft lignin at the same concentration.

Appendix C Appendix for Chapter 5

C.1 Chemicals and Materials

All commercial chemicals were of analytical grade and were used without further purification. 2-Chloro-4,4,5,5-tetramethyl-1,3,2-dioxaphospholane 95% (TMDP), sodium hydroxide, terephthalic aldehyde 99% (TALD) and Crystal Violet were purchased from Sigma Aldrich. 1,4-Dioxane was purchased from Carl Roth. Chromium (III) acetylacetonate 97%, pyridine 99.5% and glyoxylic acid monohydrate 98% (GA) were purchased from Acros Organics. Chloroform-d₃ 99,8% (CDCl₃) and dimethylsulfoxide-d₆ (DMSO-d₆) were purchased from Cambridge Isotope Laboratories. *N*-Hydroxy-5-norbornene-2,3-dicarboximide, 97% was purchased from Alfa Aesar. Gelatin type A was purchased from MP Biomedicals, LLC. Hydrochloric acid 37% w/w (HCl) was purchased from Fisher Chemical. Diethyl ether was purchased from Carlo Erba. Birch (*Betula pendula*) wood chips were supplied by Prof. Michael Studer from the Bern University of Applied Sciences, after it was harvested in May 2018 in Solothurn, Switzerland.

C.2 Biomass preparation

The Birch (*Betula pendula*) tree trunk was first debarked, then cut into wood chips and dried at 40 °C for 24 h. The birch wood chips were then transported to EPFL (Lausanne, Switzerland) where they were cleaned from residual bark pieces and leaves. The wood was subsequently milled using a Retsch cutting mill with a 6 mm screen and sieved with a 0.45 mm mesh.

C.3 Lignin Extraction and Simultaneous Functionalization

C.3.1 Terephthalic Aldehyde (TALD)-Glyoxylic Acid (GA) lignin extraction

5 g of birch wood chips (6.09% hydration), terephthalic aldehyde (TALD) and glyoxylic acid (GA) monohydrate (see ratios in **Table C.1**), 0.8 mL of HCl 37 wt% in water, and 25 mL of dioxane were introduced in a 100 mL flat-bottomed flask along with a 30mm-long magnetic stirrer. The cap was closed tightly, and the flask was heated in an oil bath set at 85 °C. The stirring was set to 700 rpm. After 3 h, the flask was removed from the oil bath and allowed to

cool to room temperature. The reaction mixture was then filtered with filter paper (Macherey-Nagel, MN640d) to remove the cellulose-rich solids which were dried overnight in a vacuum oven at 45 °C. The retentate was washed several times with a total of 100 mL of dioxane to remove all soluble compounds. The filtrate, containing the lignin, hemicellulose and residual unreacted TALD and GA, was then concentrated on a rotary evaporator at 45 °C and a pressure of 90-60 mbar until the residual volume was less than 30 mL. For the isolation of TALD/GA lignin, a 1 L flat-bottomed flask was filled with 400 mL of diethyl ether. The diethyl ether was stirred with a 50 mm stir bar at 700 rpm, and the concentrated solution in dioxane was slowly introduced dropwise with a glass pipette, causing the lignin to precipitate as a fine powder. The suspension in diethyl ether was left to stir for 45 min to promote dissolution of all residual carbohydrates and unreacted aldehydes. The mixture was then filtered, and the precipitated lignin was purified overnight with a Soxhlet extractor using diethyl ether as a solvent to remove all impurities. The washed solid was then dried overnight in a vacuum oven at 45 °C to obtain TALD/GA protected lignin.

Table C.1. Ratios of biomass, TALD and GA used during of lignin extractions.

Sample	g dry biomass	g TALD	g GA·H ₂ O	mmol TALD/g dry biomass	mmol GA/g dry biomass	TALD/G A initial ratio
1	4.73	0.00	4.99	0.00	11.46	0.00
2	4.73	0.69	4.56	1.08	10.48	0.10
3	4.73	2.37	3.28	3.74	7.55	0.50
4	4.70	3.59	2.48	5.69	5.72	1.00
5	4.73	4.82	1.70	7.59	3.91	1.94
6	4.75	5.42	1.25	8.51	2.87	2.97
7	4.73	5.85	1.00	9.23	2.30	4.01
8	4.71	6.03	0.86	9.54	1.97	4.83
9	4.72	6.21	0.71	9.80	1.63	6.01
10	4.74	7.13	0.00	11.26	0	n.a.

C.3.2 Preparation of Na⁺ salt of extracted TALD/GA lignins

4 g of TALD/GA lignin were put in a 100 mL round bottomed flask equipped with a magnetic stir bar. 40 mL of an aqueous solution of 1 M NaOH were then added the flask. The lignin was stirred on a magnetic plate until fully dissolved. After complete dissolution, the lignin solution was poured in a 1L flat-bottomed flask containing 400 mL of ethanol and a magnetic stir bar stirring at 500 rpm. The precipitated lignin salt was filtered on a Büchner filter and subsequently dried overnight in a vacuum oven set at 45 °C.

C.4 Lignin Characterization

C.4.1 Diffuse Reflectance Infrared Fourier Transform (DRIFT) spectroscopy

DRIFT spectroscopy was performed on a PerkinElmer Frontier IR instrument. Lignin samples were prepared by mixing approximately 15 mg of lignin and 0.5 g of KBr in a mortar until a homogeneous solid powder was obtained. The DRIFT spectra were collected at room temperature from 500 to 4000 cm⁻¹, with 32 scans. The background of the spectra was recorded by using solid KBr finely ground in a mortar.

C.4.2 Nuclear Magnetic Resonance (NMR)

The NMR characterization of the extracted lignins were performed on Bruker Avance 600 or 800 MHz spectrometers equipped with a 5 mm BBO and TCI cryoprobe respectively. The spectra were processed using the software Bruker TopSpin 3.6.1.

C.4.2.1 Heteronuclear Single-Quantum Coherence-NMR (HSQC-NMR)

HSQC (Heteronuclear Single-Quantum Coherence) spectra of extracted lignins were recorded using standard pulse sequences with some modifications: D1=10 s, NS=8, P1=8 us, TD=65536, O1P (F2, F1)=6.175 ppm, 125 ppm, SW (F2, F1)=13.0186 ppm, 150 ppm.

The central peak of the solvent was used as reference to calibrate the spectra (DMSO-d₆, δ_H/δ_C 2.50/39.50 ppm). The HSQC spectra of lignin GA-lignin (Sample 1) and TALD-lignin (sample 10) are shown in **Figure C.1**.

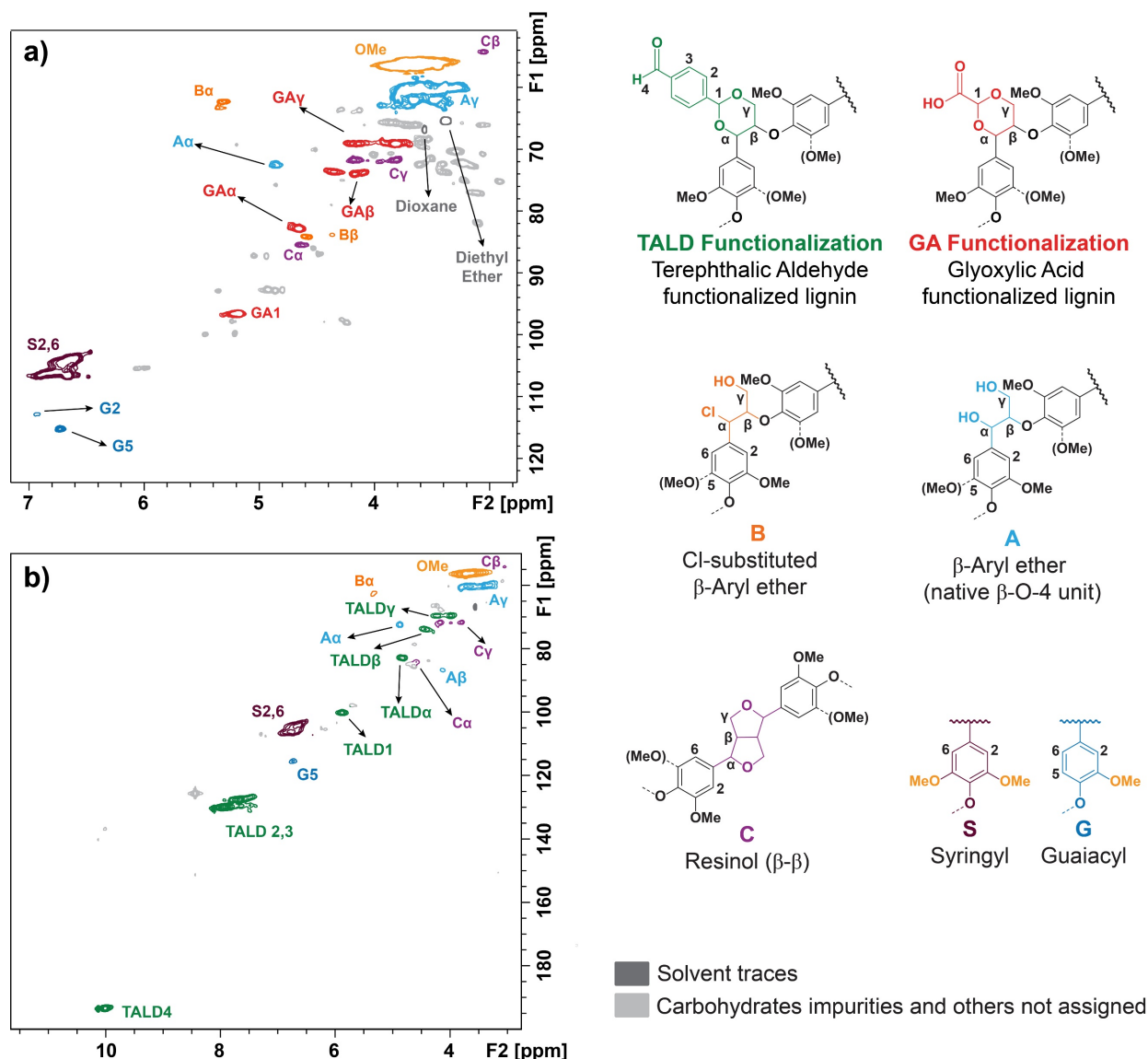


Figure C.1. a) HSQC-NMR spectra of GA-lignin (sample 1) and b) TALD-lignin (sample 10).

C.4.2.2 Quantitative ^1H NMR

The quantification of TALD bound to the extracted lignin samples was performed following a procedure previously published by our research group.¹⁹⁶

Briefly, approximately 50 mg of extracted lignins were weighted in an NMR tube. 100 μL of a solution of 1,4-dinitrobenzene (1,4-DNB) in DMSO-d_6 (~ 0.04 g/g) were then introduced in the NMR tube and weighted. 500 μL of additional DMSO-d_6 were then added. The sample was briefly sonicated, if necessary, until the sample reached full dissolution. The exact quantities used for the quantification of TALD functionalization in extracted lignin samples

are shown in **Table C.2**. The ^1H NMR spectra were recorded with a standard pulse sequence and $D1 \geq 10$ s.

The spectra were then processed, phased and the baseline was corrected with the command ABS in the Bruker TopSpin software. The peak of residual DMSO was used as reference to calibrate the spectra (DMSO- d_6 , δ_{H} 2.50 ppm).

An example of obtained spectrum is shown in **Figure C.2**.

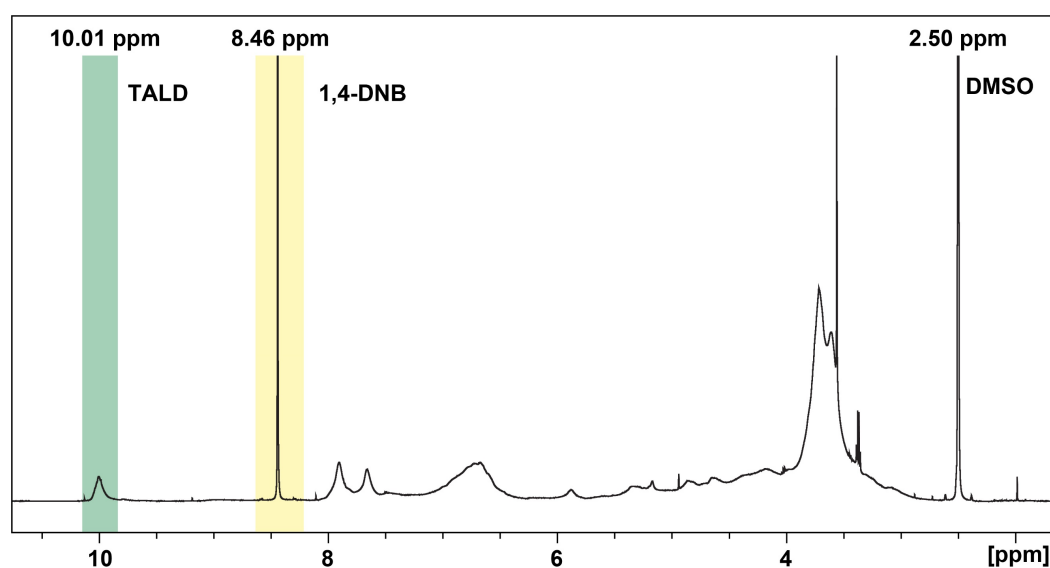


Figure C.2. ^1H NMR spectrum of extracted lignin 4. In green is highlighted the signal of bound TALD, while in yellow is highlighted the signal of 1,4-DNB used for quantification.

The spectra were then integrated as follows. The peak of the internal standard 1,4-DNB at 8.43 ppm (**Figure C.2**, yellow) was calibrated to 4 protons. The integral of the peak assigned to bound TALD at 10.01 ppm (**Figure C.2**, green), and its quantification, was then estimated based on the following equations.

The integrals of the peaks assigned to 1,4-DNB and bound TALD were normalized by the number of protons generating the signals according to **Equation C.1** and **Equation C.2**.

$$\text{Normalized 1,4DNB integral} = (\text{measured I. S. integral})/4$$

Equation C.1. Normalized 1,4-DNB integral.

$$\text{Normalized aldehyde integral} = (\text{measured aldehyde integral})/1$$

Equation C.2. Normalized aldehyde integral.

The number of moles of 1,4-DNB which generated the integral could be calculated using **Equation C.3** by knowing the quantity and purity of the internal standard introduced into the NMR tube.

mmol 1,4DNB in NMR sample

$$= (\text{mg 1,4DNB in NMR tube} * 0.98) / (168.11 \text{ mg / mmol})$$

Equation C.3. mmol of 1,4-DNB in NMR sample.

Where 168.11 mg/mmol is the molecular weight of 1,4-DNB and 98% is the purity of the internal standard that we had available for these measurements.

The number of moles generating the signal of TALD bound to the lignin was then calculated with **Equation C.4**.

mmol TALD in NMR sample

$$\begin{aligned} &= (\text{Normalized TALD integral}) / (\text{Normalized 1,4DNB integral}) \\ &* (\text{mmol 1,4DNB in NMR sample}) \end{aligned}$$

Equation C.4. mmol of TALD in NMR sample.

Finally, the number of moles of free aldehyde bound to the lignin per gram of isolated lignin could be calculated according to the **Equation C.5**.

mmol of TALD in 1g of lignin

$$= (\text{mmol aldehyde in NMR sample})/(\text{mg of lignin in NMR tube}) * 1000$$

Equation C.5. mmol of TALD in 1g of lignin.

The weight of TALD incorporated in 1 g of lignin was finally calculated with **Equation C.6.**

$$\text{g of TALD in 1g of lignin} = \frac{\text{mmol TALD/g lignin}}{1000} * 118.04\text{g/mol}$$

Equation C.6. g of TALD in 1g of lignin.

Where 118.04 g/mol is the molecular weight of a TALD molecule bound to the lignin via acetal formation. Complete data for TALD quantification by ^1H NMR are shown in **Table C.2.**

Table C.2. Data regarding sample preparation and results for ^1H NMR quantification of TALD in extracted lignin samples.

Sample	Int. STD. [0.036 g 1,4- DNB/g]	Lignin weight [g]	mmol in Sample	mmol TALD/g Lignin	g TALD/g Lignin
1	0.119	0.055	0.000	0.00	0.00
2	0.119	0.051	0.008	0.16	0.02
3	0.132	0.058	0.026	0.44	0.05
4	0.121	0.052	0.040	0.78	0.09
5	0.132	0.057	0.049	0.87	0.10
6	0.122	0.048	0.057	1.19	0.14
7	0.119	0.044	0.056	1.28	0.15
8	0.119	0.046	0.060	1.30	0.15
9	0.119	0.044	0.065	1.49	0.18
10	0.120	0.051	0.094	1.81	0.21

C.4.2.3 Quantitative ^{31}P NMR

Quantitative ^{31}P NMR was performed following a recent publication by Meng et al. and working under N_2 atmosphere⁸⁶.

Briefly, extracted lignin samples were dried in a vacuum oven set at 45 °C for 24 h. Approximately 30 mg of lignin were weighted in a 4 mL glass vial equipped with a PTFE septum and containing a small magnetic stirrer. To the same vial were added and weighted 0.1 mL of a solution of deuterated pyridine and chloroform (1.6:1, v/v) containing chromium (III) acetylacetonate solution (~5.0 mg/mL,) and *N*-Hydroxy-5-norbornene-2,3-dicarboximide (NHND) as an internal standard (~18.0 mg/mL). Subsequently, 0.5 mL of a solution composed of pyridine-*d*₅ and CDCl₃ (1.6:1, v/v) was added and the vial was put on a magnetic plate to stir until complete dissolution of the lignin. Upon full dissolution, 0.1 mL of 2-chloro-4,4,5,5-tetramethyl-1,3,2-dioxaphospholane (TMDP) were slowly added to the solution with a gas tight syringe. The mixture was let to stir for approximately 1 h and it was then transferred to an NMR tube which was previously kept dry in an oven at 120 °C. Samples were analysed within 3 h from the addition of TMDP. The ³¹P NMR spectra were recorded on a Bruker Avance 600 MHz spectrometer equipped with a 5 mm BBO cryoprobe. The experimental NMR parameters used were: Pulse program= Inverse gated decoupling pulse (zgig), SW=100 ppm, O1P=140 ppm, AQ=0.8 s, D1=10 s, NS=128.

An example of obtained spectrum is shown in **Figure C.3**.

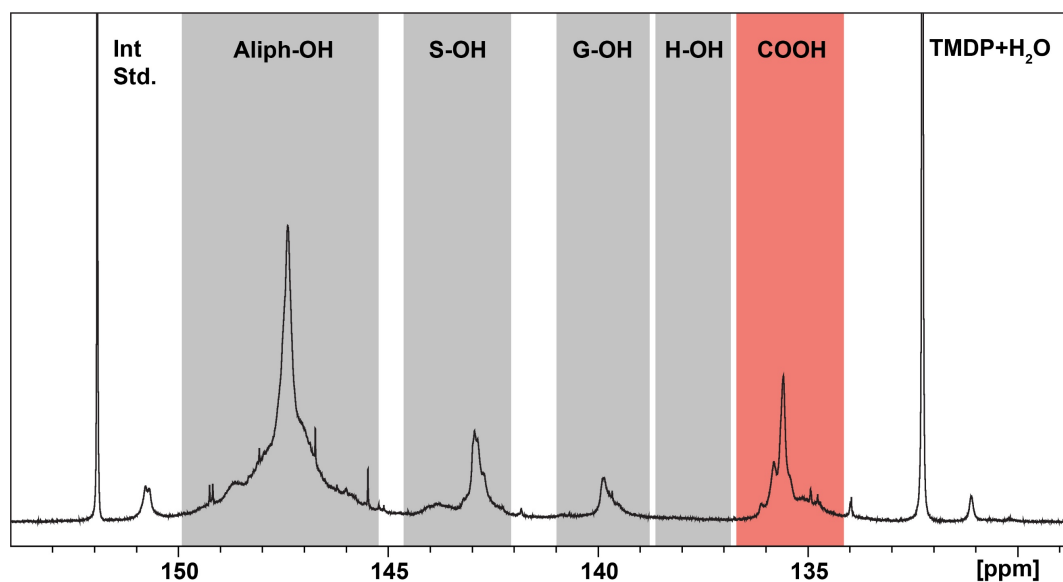


Figure C.3. ³¹P NMR spectrum of extracted TALD/GA lignin (Sample 4). In red is highlighted the signal of bound COOH groups (GA).

The weight of GA covalently bound to the lignin was calculated according to **Equation C.7**, approximating that all COOH groups of the extracted lignins were derived from a bound GA molecule.

$$\text{g of GA in 1g of lignin} = \frac{\text{mmol COOH/g lignin}}{1000} * 58.01\text{g/mol}$$

Equation C.7. g of GA in 1g of lignin.

Where 58.01 g/mol is the molecular weight of a GA molecule bound to the lignin via acetal formation.

The results of the quantification of aliphatic, phenolic hydroxyl groups as well as carboxylic acid groups (GA) for all analysed samples are presented in **Table C.3**.

Table C.3. Quantification of aliphatic hydroxyl, phenolic hydroxyl and carboxylic acid groups on extracted lignins measured via ^{31}P NMR. The results are reported in mmol/g of effective lignin. Aliph-OH indicates the aliphatic hydroxyl groups, S-OH indicates the phenolic groups of Syringol units, G-OH indicates the phenolic groups of Guaiacol units, H-OH indicates the phenolic groups of Hydroxyphenylpropane units and COOH indicates the carboxylic acid groups of GA.

Sample	Aliph.-OH [mmol/g Lignin]	S-OH [mmol/g Lignin]	G-OH [mmol/g Lignin]	H-OH [mmol/g Lignin]	COOH [mmol/g Lignin]	GA [g/g Lignin]
1	3.87	0.45	0.21	0.00	0.97	0.057
2	3.67	0.52	0.24	0.00	0.89	0.052
3	2.95	0.47	0.22	0.00	0.76	0.044
4	2.44	0.55	0.24	0.00	0.63	0.037
5	2.54	0.52	0.23	0.00	0.61	0.035
6	2.60	0.50	0.24	0.00	0.44	0.026
7	2.57	0.39	0.20	0.00	0.30	0.017
8	2.44	0.42	0.21	0.00	0.25	0.015
9	2.53	0.39	0.21	0.00	0.23	0.013
10	3.77	0.67	0.37	0.00	0.18	n.a.

C.5 Solubility Tests of Extracted Lignins

To perform solubility tests of the TALD/GA extracted lignin, 15 mg of lignin were weighted in a glass vial, to which 1 mL of 1 M NaOH in water was added. The vials were thoroughly mixed for 10 min using a Vortex, and the result of the solubility tests were then recorded.

A picture of the vials after completion of the solubility tests is shown in **Figure C.4**.

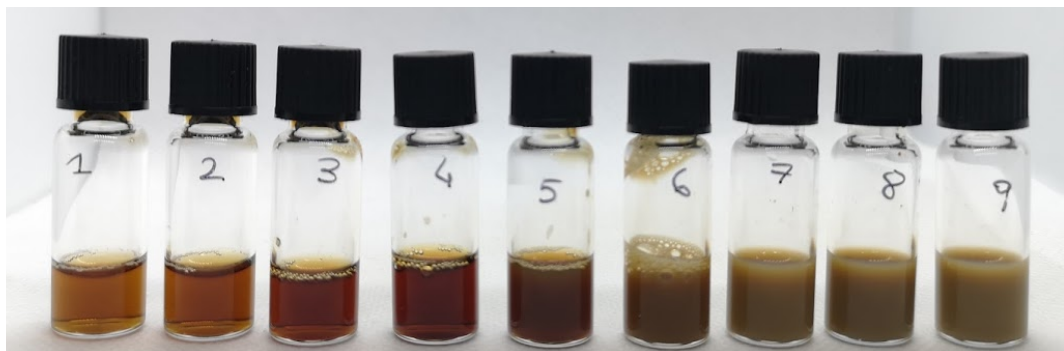


Figure C.4. Picture of the vials containing the extracted lignin after the solubility test.

Table C.4 shows the comprehensive results of the solubility tests.

Table C.4. Result of the solubility test for the extracted TALD/GA lignins.

Sample	Final TALD/GA ratio	Solubility in 1mL 1M NaOH
1	0.00	Soluble
2	0.18	Soluble
3	0.58	Soluble
4	1.23	Soluble
5	1.44	Partially Soluble
6	2.68	Insoluble
7	4.29	Insoluble
8	5.17	Insoluble
9	6.56	Insoluble

C.6 Preparation of Lignin-Gelatin Hydrogels

To prepare the lignin-gelatin hydrogels, gelatin type A was first weighted in a 4 mL vial equipped with a magnetic stir bar (Vial A). Lignin was then weighted in a second vial also

equipped with a magnetic stir bar (Vial B). Finally, the total amount of necessary Phosphate-Buffered Saline (PBS buffer) at pH 7.4 was split and added evenly between Vial A and Vial B. The two vials were placed in a hot plate equipped with an oil bath heating at 37 °C, until full dissolution was reached. When both vials presented a fully solubilized content, they were let to cool to 25 °C. As soon as both vials reached 25 °C, the content of Vial B was quickly transferred with a glass pipette to Vial A, which was then closed and mixed by hand for 10-15 s. The hydrogel precursors, while still in its liquid state, were hence transferred with a glass pipette to PE or PTFE molds and stored in the fridge at 4 °C for at least 15 h before any analysis.

C.7 Characterization of Hydrogels

C.7.1 Gelation Time

The gelation time of the synthesized hydrogels was measured with the Tube Inversion test. In this method, 2 g of hydrogels with lignin:gelatin ratios were prepared in a 4 mL vial equipped with a screw cap, according to Section C.6.

During the preparation, as soon as the solution of lignin was added to the solution of gelatin, a timer was started to record the initial time. The vial was then inverted constantly until the formed hydrogel was not flowing anymore, at which point the timer was stopped and the time elapsed was recorded as gelation time.

A comprehensive graph of the results obtained is shown in **Figure C.5**.

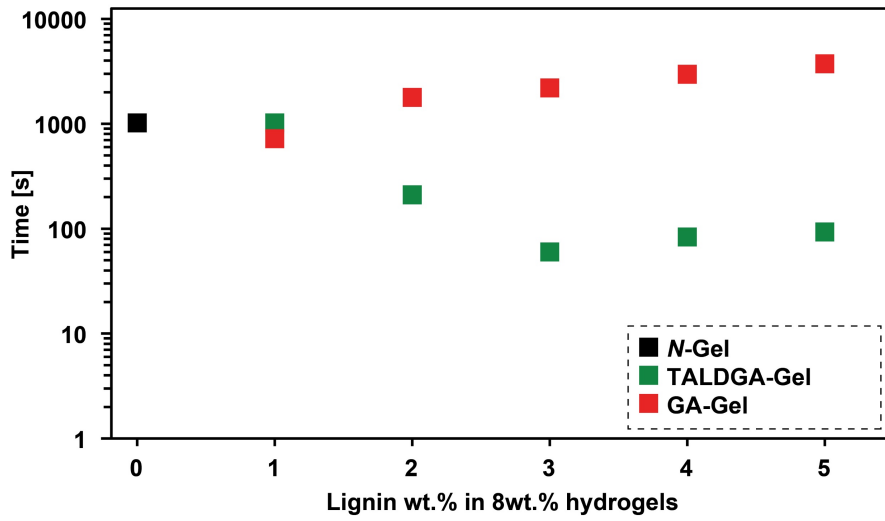


Figure C.5. Gelation Time of hydrogels.

C.7.2 Swelling

Hydrogel samples of cylindrical shape with a diameter of 8 mm and a height of 4 mm were prepared according to Section C.6. 14 hydrogel cylinders of TALDGA-Gel were first weighted and each of them was placed in a 50 mL centrifuge tube filled with 25 mL of PBS, which were stored at 25 °C. As a control, 14 hydrogel cylinders of GA-Gel were also prepared, weighed and placed in 50 mL centrifuge tubes in the same way.

Every day for a week, two TALDGA-Gel samples and two GA-Gel were removed from the PBS buffer, quickly dried of the excess external water with filter paper and weighted to record their swelling, which was calculated according to **Equation C.8**.

$$\text{Swelling [\%]} = \frac{\text{Final hydrogel wt. [g]} - \text{Initial hydrogel weight [g]}}{\text{Initial hydrogel weight [g]}} * 100$$

Equation C.8. Swelling of hydrogels

A comprehensive graph of the results obtained is shown in **Figure C.6**.

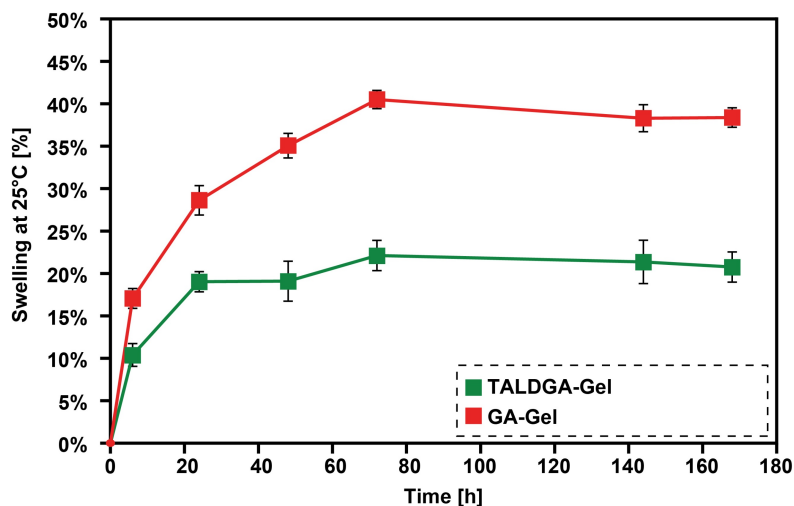


Figure C.6. Swelling of TALDGA-Gel and GA-Gel at 25 °C.

C.7.3 Rheology

Rheological tests were conducted using the parallel-plate geometry of the rheometer (Anton Paar MCR102) with a diameter of 25 mm and a gap between the two plates of 1.0-1.2 mm. Cylindrical shape hydrogel samples with a diameter of 25 mm and a height of 0.7 mm were used for the test.

The linear viscoelastic region (LVR) was determined by identifying the plateau value of the storage moduli (G') curve during the oscillatory amplitude sweep varying the strain between 0.1 and 100% at $1 \text{ rad}\cdot\text{s}^{-1}$ frequency (**Figure C.7**). The evolution in frequency sweep was recorded in oscillatory mode at 1% strain (**Figure C.8**). Subsequently, the storage (G') and loss (G'') moduli were reported from the frequency sweep of each hydrogel.

C.7.3.1 Amplitude Sweep

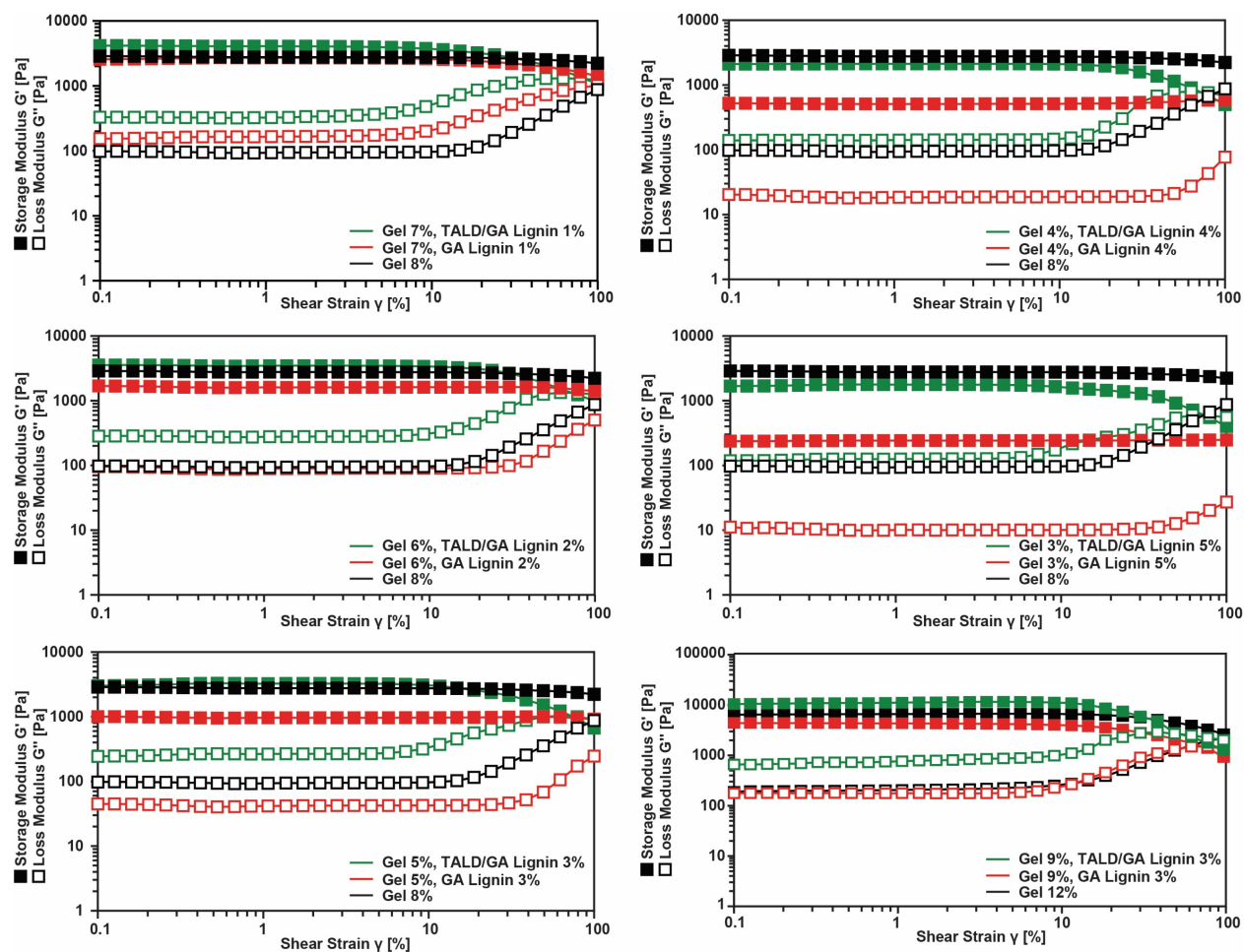


Figure C.7. Amplitude sweep of prepared hydrogels.

C.7.3.2 Frequency Sweep

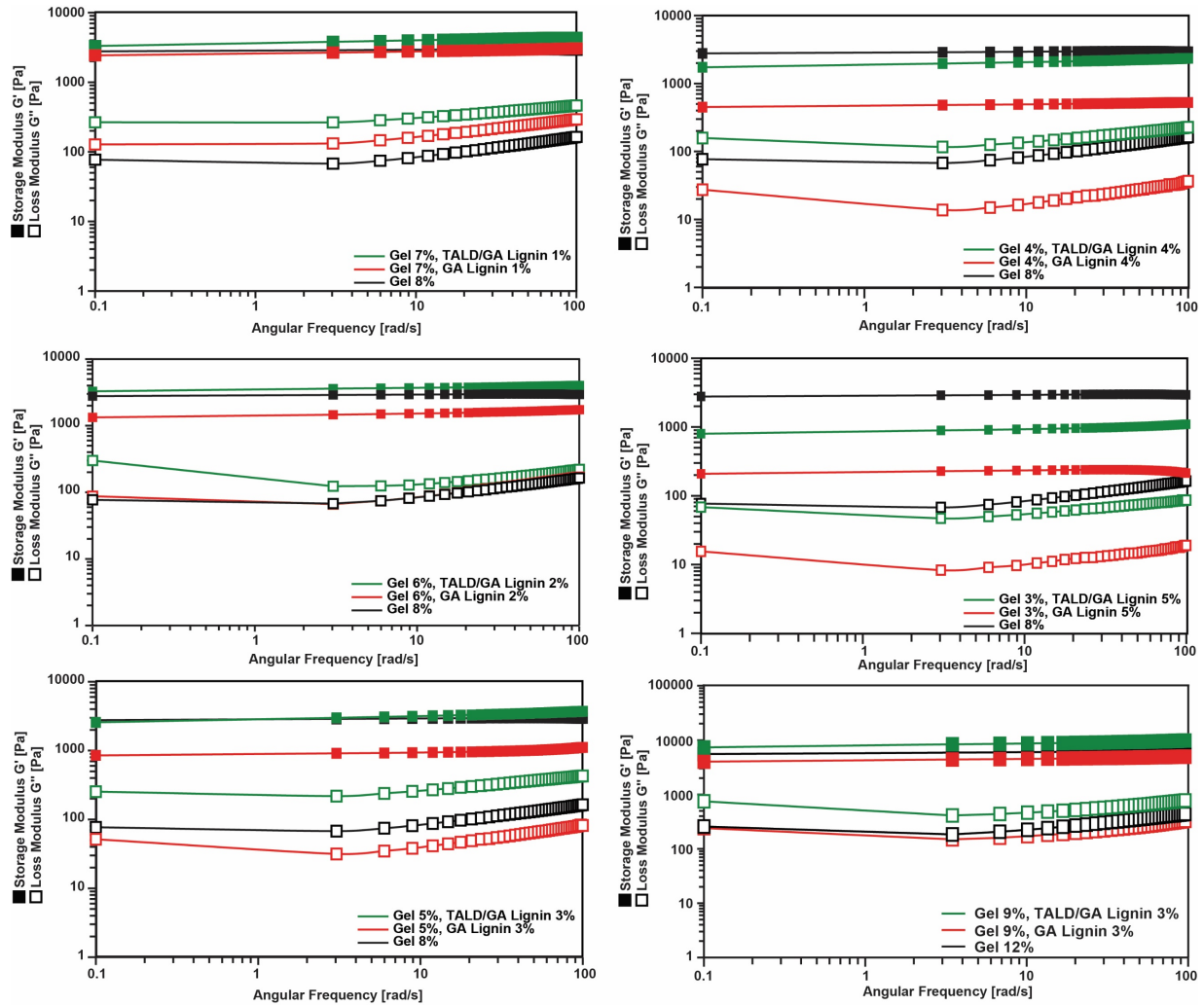


Figure C.8. Frequency Sweep of prepared hydrogels.

C.7.4 Compression and Dissipation

An Instron E3000 linear mechanical testing machine (Norwood, MA, USA) with a 50 N load cell was employed for the analysis. Cylindrical shape hydrogel samples with a diameter of 8 mm and a height of 4 mm were used for the test. The load displacement was recorded at a displacement rate of $0.1 \text{ mm}\cdot\text{s}^{-1}$ where samples were loaded to 50% compressive strain. Finally, the compressive modulus was calculated from the slope of the best linear fit to the stress-strain curve. The bulk energy dissipation of the specimens was measured from the hysteresis loop area in the stress-strain curve during the loading-unloading process ($n \geq 3$).

C.7.5 Lap-Shear Adhesion

The adhesive strength of *N*-Gel, TALDGA-Gel, GA-Gel hydrogels was evaluated using a shear test setup. Briefly, 100 μ l of the hydrogel precursors was applied and cured between the overlap area of two gelatin-coated glass slides with a contact area of 20 mm \times 25 mm. Subsequently, a hydrogel strip was sandwiched between two slides. The adhesion measurements were conducted under shear loading at 1 mm·s⁻¹ using an Instron mechanical machine, as described earlier. The adhesion strength of the samples was measured dividing the maximum load by the contact area ($n \geq 3$).

C.7.6 Scanning Electron Microscopy (SEM)

Scanning electron microscopy (SEM) images of freeze-dried hydrogel samples were recorded by using the InLens detector of GEMINI SEM 300 (Carl Zeiss Germany) at an acceleration voltage of 3 kV. The samples were placed on a dual-sided carbon tape stuck to a holder and coated by 15 nm gold thin film before the analysis.

C.7.7 Cytotoxicity test with eucaryotic cells

The toxicity of the material was examined using MTS 3-(4,5-dimethylthiazol-2-yl)-5-(3 carboxymethoxyphenyl)-2-(4-sulfophenyl)-2H-tetrazolium assay. Vero cell cultures (African green monkey fibroblastoid kidney cells ATCC CCL-81) seeded in 96-well plates were incubated in DMEM (Gibco-BRL, Gaithersburg, MD) supplemented with 2% FBS with 0.7 mg/mL of three tested materials for 24 h. Cell viability was determined by the CellTiter 96 Proliferation Assay Kit (Promega, Madison, WI, USA) according to the manufacturer's instructions. Absorbance was measured using a Microplate Reader (Model 680, BIORAD) at 490 nm. Cells incubated without any material were used as negative control. The effect on cell viability was expressed as percentage of live cells, by comparing the absorbance of treated cells with the one of cells incubated with culture medium.

C.7.8 Toxicity test with bacteria

The toxicity of the material with bacteria was tested on two bacterial strains: Gram-negative *Escherichia coli* BL21 and Gram-positive *Staphylococcus aureus* ATCC 25923. Overnight culture of bacteria was diluted 500 times in PBS buffer and then incubated with 1.1 mg/mL of all three tested materials with mixing at 37 °C for 6 hours. Then, bacterial concentration was

measured by colony count method (at least 6 technical replicates for each dilution). The experiment was done in duplicates.

References

- 1 N. N. Iskander and N. Lowe, *Annu. Rev. Polit. Sci.*, 2020, **23**, 111–131.
- 2 P. N. Stearns, Ed., *The Industrial Revolution in World History*, Routledge, New York, 5th edn., 2020.
- 3 S. Sippel, N. Meinshausen, E. M. Fischer, E. Székely and R. Knutti, *Nat. Clim. Change*, 2020, **10**, 35–41.
- 4 D. J. Frame, S. M. Rosier, I. Noy, L. J. Harrington, T. Carey-Smith, S. N. Sparrow, D. A. Stone and S. M. Dean, *Clim. Change*, 2020, **162**, 781–797.
- 5 D. S. Schmeller, F. Courchamp and G. Killeen, *Biodivers. Conserv.*, 2020, **29**, 3095–3102.
- 6 P. H. Raven and D. L. Wagner, *Proc. Natl. Acad. Sci.*, 2021, 118, e2002548117.
- 7 Masson-Delmotte, V., P. Zhai, A. Pirani, S.L. Connors, C. Péan, S. Berger, N. Caud, Y. Chen, L. Goldfarb, M.I. Gomis, M. Huang, K. Leitzell, E. Lonnoy, J.B.R. Matthews, T.K. Maycock, T. Waterfield, O. Yelekçi, R. Yu, and B. Zhou. IPCC, 2021: Summary for Policymakers. In: *Climate Change 2021: The Physical Science Basis. Contribution of Working Group I to the Sixth Assessment Report of the Intergovernmental Panel on Climate Change*. Cambridge University Press. In Press.
- 8 A. R. G. Heesterman, *Clean Technol. Environ. Policy*, 2020, **22**, 1215–1227.
- 9 R. S'ahel, *Perspect. Glob. Dev. Technol.*, 2016, **15**, 480–496.
- 10 M. Hook and X. Tang, *Energy Policy*, 2013, **52**, 797–809.
- 11 A. J. McMichael, R. E. Woodruff and S. Hales, *The Lancet*, 2006, **367**, 859–869.
- 12 M. C. Urban, *Science*, 2015, **348**, 571–573.
- 13 D. Vogt, Global Carbon Demand for Chemicals and Materials by Sectors (PNG), <https://renewable-carbon.eu/publications/product/global-carbon-demand-for-chemicals-and-materials-by-sectors-png/>, (accessed January 2, 2022).
- 14 V. Smil, *Energy transitions: global and national perspectives*, ABC-CLIO, 2016.
- 15 A. S. Carlsson, *Biochimie*, 2009, **91**, 665–670.
- 16 Y. Liu, B. Dong, A. Hagfeldt, J. Luo and M. Graetzel, *SmartMat*, 2021, **2**, 33–37.

- 17 I. Kougias, G. Aggidis, F. Avellan, S. Deniz, U. Lundin, A. Moro, S. Muntean, D. Novara, J. I. Pérez-Díaz, E. Quaranta, P. Schild and N. Theodossiou, *Renew. Sustain. Energy Rev.*, 2019, **113**, 109257.
- 18 M. Soltani, F. Moradi Kashkooli, A. R. Dehghani-Sanij, A. Nokhosteen, A. Ahmadi-Joughi, K. Gharali, S. B. Mahbaz and M. B. Dusseault, *Int. J. Green Energy*, 2019, **16**, 971–1009.
- 19 A. Tuohy, B. Kaun and R. Enriken, in *Advances in Energy Systems*, John Wiley & Sons, Ltd, 2019, pp. 303–320.
- 20 G. Glenk and S. Reichelstein, *Nat. Energy*, 2019, **4**, 216–222.
- 21 R. Muthuraj and T. Mekonnen, *Polymer*, 2018, **145**, 348–373.
- 22 M. Bui, C. S. Adjiman, A. Bardow, E. J. Anthony, A. Boston, S. Brown, P. S. Fennell, S. Fuss, A. Galindo, L. A. Hackett, J. P. Hallett, H. J. Herzog, G. Jackson, J. Kemper, S. Krevor, G. C. Maitland, M. Matuszewski, I. S. Metcalfe, C. Petit, G. Puxty, J. Reimer, D. M. Reiner, E. S. Rubin, S. A. Scott, N. Shah, B. Smit, J. P. Martin Trusler, P. Webley, J. Wilcox and N. M. Dowell, *Energy Environ. Sci.*, 2018, **11**, 1062–1176.
- 23 Z. Zhang, S.-Y. Pan, H. Li, J. Cai, A. G. Olabi, E. J. Anthony and V. Manovic, *Renew. Sustain. Energy Rev.*, 2020, **125**, 109799.
- 24 D. W. Keith, G. Holmes, D. St. Angelo and K. Heidel, *Joule*, 2018, **2**, 1573–1594.
- 25 S. Lee, D. Kim and J. Lee, *Angew. Chem.*, 2015, **127**, 14914–14918.
- 26 Y. Y. Birdja, E. Pérez-Gallent, M. C. Figueiredo, A. J. Göttle, F. Calle-Vallejo and M. T. M. Koper, *Nat. Energy*, 2019, **4**, 732–745.
- 27 E. Koohestanian, J. Sadeghi, D. Mohebbi-Kalhari, F. Shahraki and A. Samimi, *Energy*, 2018, **144**, 279–285.
- 28 B. Song, B. He, A. Qin and B. Z. Tang, *Macromolecules*, 2018, **51**, 42–48.
- 29 M. Pessarakli, *Handb. Photosynth.*
- 30 Y. M. Bar-On, R. Phillips and R. Milo, *Proc. Natl. Acad. Sci.*, 2018, **115**, 6506–6511.
- 31 S. Zhou, K. Jin and M. J. Buehler, *Adv. Mater.*, 2021, **33**, 2003206.
- 32 J. Amoah, P. Kahar, C. Ogino and A. Kondo, *Biotechnol. J.*, 2019, **14**, 1800494.
- 33 K. Sriroth and K. Piyachomkwan, in *Bioprocessing Technologies in Biorefinery for Sustainable Production of Fuels, Chemicals, and Polymers*, John Wiley & Sons, Ltd, pp. 27–46.
- 34 L. Mesa, Y. Martínez, A. Celia de Armas and E. González, *Renew. Energy*, 2020, **156**, 377–388.

-
- 35 H. Li, P. Lv, Z. Wang, C. Miao and Z. Yuan, *Biomass Convers. Biorefinery*, 2021, **11**, 3053–3060.
- 36 V. Mandari and S. K. Devarai, *Bioenergy Res.*, 2021, 1–27.
- 37 Y. Dahman, K. Syed, S. Begum, P. Roy and B. Mohtasebi, in *Biomass, Biopolymer-Based Materials, and Bioenergy*, eds. D. Verma, E. Fortunati, S. Jain and X. Zhang, Woodhead Publishing, 2019, pp. 277–325.
- 38 M. Naqvi and J. Yan, in *Handbook of Clean Energy Systems*, John Wiley & Sons, Ltd, 2015, pp. 1–18.
- 39 C. De Blasio, in *Fundamentals of Biofuels Engineering and Technology*, ed. C. De Blasio, Springer International Publishing, Cham, 2019, pp. 155–171.
- 40 S. S. Hassan, G. A. Williams and A. K. Jaiswal, *Renew. Sustain. Energy Rev.*, 2019, **101**, 590–599.
- 41 K. Robak and M. Balcerek, *Food Technol. Biotechnol.*, 2018, **56**, 174–187.
- 42 J. Yan, O. Oyedele, J. H. Leal, B. S. Donohoe, T. A. Semelsberger, C. Li, A. N. Hoover, E. Webb, E. A. Bose, Y. Zeng, C. L. Williams, K. D. Schaller, N. Sun, A. E. Ray and D. Tanjore, *ACS Sustain. Chem. Eng.*, 2020, **8**, 8059–8085.
- 43 D. R. Dodds and R. A. Gross, *Science*, 2007, **318**, 1250–1251.
- 44 X. Zhou, W. Li, R. Mabon and L. J. Broadbelt, *Energy Technol.*, 2017, **5**, 52–79.
- 45 D. P. Oehme, M. S. Doblin, J. Wagner, A. Bacic, M. T. Downton and M. J. Gidley, *Cellulose*, 2015, **22**, 3501–3520.
- 46 M. John and S. Thomas, *Carbohydr. Polym.*, 2008, **71**, 343–364.
- 47 G. Bali, X. Meng, J. I. Deneff, Q. Sun and A. J. Ragauskas, *ChemSusChem*, 2015, **8**, 275–279.
- 48 T. Dumitrică, *Carbohydr. Polym.*, 2020, **230**, 115624.
- 49 A. D. French, *Cellulose*, 2014, **21**, 885–896.
- 50 Z. Ling, X. Zhang, G. Yang, K. Takabe and F. Xu, *Ind. Crops Prod.*, 2018, **112**, 541–549.
- 51 M. Hubbe, *BioResources*, 2013, **8**, 4791–4792.
- 52 T. Hemamalini and V. R. Giri Dev, *J. Nat. Fibers*, 2021, **18**, 1823–1833.
- 53 J. Bae, H. Kwon and J. Kim, *Sustainability*, 2018, **10**, 4146.
- 54 T. Li, C. Chen, A. H. Brozena, J. Y. Zhu, L. Xu, C. Driemeier, J. Dai, O. J. Rojas, A. Isogai, L. Wågberg and L. Hu, *Nature*, 2021, **590**, 47–56.
- 55 D. Kundu, S. K. Mondal and T. Banerjee, *J. Chem. Eng. Data*, 2019, **64**, 2601–2617.

- 56 K. Kobetičová and J. Nábělková, *Buildings*, 2021, **11**, 515.
- 57 B. Plancot, B. Gügi, J.-C. Mollet, C. Loutelier-Bourhis, S. Ramasandra Govind, P. Lerouge, M.-L. Follet-Gueye, M. Vicré, C. Alfonso, E. Nguema-Ona, M. Bardor and A. Driouich, *Carbohydr. Polym.*, 2019, **208**, 180–190.
- 58 S. Kishani, F. Vilaplana, W. Xu, C. Xu and L. Wågberg, *Biomacromolecules*, 2018, **19**, 1245–1255.
- 59 L.-Z. Huang, M.-G. Ma, X.-X. Ji, S.-E. Choi and C. Si, *Front. Bioeng. Biotechnol.*, 2021, **9**, 690773.
- 60 D. S. Naidu, S. P. Hlangothi and M. J. John, *Carbohydr. Polym.*, 2018, **179**, 28–41.
- 61 H. Shao, H. Sun, B. Yang, H. Zhang and Y. Hu, *RSC Adv.*, 2019, **9**, 2395–2401.
- 62 W. Farhat, R. Venditti, A. Ayoub, F. Prochazka, C. Fernández-de-Alba, N. Mignard, M. Taha and F. Becquart, *Mater. Des.*, 2018, **153**, 298–307.
- 63 J. Xu, R. Xia, L. Zheng, T. Yuan and R. Sun, *Carbohydr. Polym.*, 2019, **224**, 115164.
- 64 M. Piccini, D. J. Leak, C. J. Chuck and A. Buchard, *Polym. Chem.*, 2020, **11**, 2681–2691.
- 65 M. Piccini, J. Lightfoot, B. C. Dominguez and A. Buchard, *ACS Appl. Polym. Mater.*, 2021, **3**, 5870–5881.
- 66 F. H. Isikgor and C. R. Becer, *Polym. Chem.*, 2015, **6**, 4497–4559.
- 67 B. Ndaba, A. Roopnarain, M. O. Daramola and R. Adeleke, *Sustain. Chem. Pharm.*, 2020, **18**, 100342.
- 68 T. Higuchi, *Wood Sci. Technol.*, 1990, **24**, 23–63.
- 69 R. Vanholme, B. Demedts, K. Morreel, J. Ralph and W. Boerjan, *PLANT Physiol.*, 2010, **153**, 895–905.
- 70 A. K. Sangha, J. M. Parks, R. F. Standaert, A. Ziebell, M. Davis and J. C. Smith, *J. Phys. Chem. B*, 2012, **116**, 4760–4768.
- 71 R. Vanholme, B. Demedts, K. Morreel, J. Ralph and W. Boerjan, *Plant Physiol.*, 2010, **153**, 895–905.
- 72 Y. Tobimatsu and M. Schuetz, *Curr. Opin. Biotechnol.*, 2019, **56**, 75–81.
- 73 R. Vanholme, B. De Meester, J. Ralph and W. Boerjan, *Curr. Opin. Biotechnol.*, 2019, **56**, 230–239.
- 74 A. Voxeur, Y. Wang and R. Sibout, *Curr. Opin. Plant Biol.*, 2015, **23**, 83–90.
- 75 T. R. Mota, D. M. Oliveira, R. Marchiosi, O. Ferrarese-Filho and W. D. Santos, *AIMS Bioeng.*, 2018, **5**, 63–77.

- 76 J. Zakzeski, P. C. A. Bruijninx, A. L. Jongerius and B. M. Weckhuysen, *Chem. Rev.*, 2010, **110**, 3552–3599.
- 77 J. Ralph, K. Lundquist, G. Brunow, F. Lu, H. Kim, P. F. Schatz, J. M. Marita, R. D. Hatfield, S. A. Ralph, J. H. Christensen and W. Boerjan, *Phytochem. Rev.*, 2004, **3**, 29–60.
- 78 R. Rinaldi, R. Jastrzebski, M. T. Clough, J. Ralph, M. Kennema, P. C. A. Bruijninx and B. M. Weckhuysen, *Angew. Chem. Int. Ed.*, 2016, **55**, 8164–8215.
- 79 Y. Li, L. Shuai, H. Kim, A. H. Motagamwala, J. K. Mobley, F. Yue, Y. Tobimatsu, D. Havkin-Frenkel, F. Chen, R. A. Dixon, J. S. Luterbacher, J. A. Dumesic and J. Ralph, *Sci. Adv.*, 2018, 11.
- 80 X. Liu, F. P. Bouxin, J. Fan, V. L. Budarin, C. Hu and J. H. Clark, *ChemSuschem*, 2020, **13**, 4296–4317.
- 81 T.-Q. Yuan, S.-N. Sun, F. Xu and R.-C. Sun, *J. Agric. Food Chem.*, 2011, **59**, 10604–10614.
- 82 R. D. Hatfield, H.-J. G. Jung, J. Ralph, D. R. Buxton and P. J. Weimer, *J. Sci. Food Agric.*, 1994, **65**, 51–58.
- 83 H. Chang, E. B. Cowling and W. Brown, *Holzforsch. - Int. J. Biol. Chem. Phys. Technol. Wood*, 2009, **29**, 153–159.
- 84 E. Capanema, M. Balakshin, R. Katahira, H. Chang and H. Jameel, *J. Wood Chem. Technol.*, 2015, **35**, 17–26.
- 85 F. Lu and J. Ralph, *J. Biobased Mater. Bioenergy*, 2011, **5**, 169–180.
- 86 X. Meng, C. Crestini, H. Ben, N. Hao, Y. Pu, A. J. Ragauskas and D. S. Argyropoulos, *Nat. Protoc.*, 2019, **14**, 2627–2647.
- 87 M. T. Amiri, S. Bertella, Y. M. Questell-Santiago and J. S. Luterbacher, *Chem. Sci.*, 2019, **10**, 8135–8142.
- 88 G. Zinovyev, I. Sulaeva, S. Podzimek, D. Rössner, I. Kilpeläinen, I. Sumerskii, T. Rosenau and A. Potthast, *ChemSusChem*, 2018, **11**, 3259–3268.
- 89 A. S. Bowman, S. O. Asare and B. C. Lynn, *Rapid Commun. Mass Spectrom.*, 2019, **33**, 811–819.
- 90 S. S. Hassan, G. A. Williams and A. K. Jaiswal, *Bioresour. Technol.*, 2018, **262**, 310–318.
- 91 J. C. Carvajal, Á. Gómez and C. A. Cardona, *Bioresour. Technol.*, 2016, **214**, 468–476.
- 92 H. Sixta, *Handbook of Pulp*, Wiley, 1st edn., 2006.

-
- 93 C. Crestini, H. Lange, M. Sette and D. S. Argyropoulos, *Green Chem.*, 2017, **19**, 4104–4121.
- 94 C. Heitner, D. Dimmel and J. A. Schmidt, Eds., *Lignin and lignans: advances in chemistry*, Taylor & Francis, Boca Raton, 2010.
- 95 G. Gellerstedt, A. Majtnerova and L. Zhang, *C. R. Biol.*, 2004, **327**, 817–826.
- 96 M. Yu. Balakshin, E. A. Capanema, Chen and H. S. Gracz, *J. Agric. Food Chem.*, 2003, **51**, 6116–6127.
- 97 P. Tomani, *Cellul. Chem. Technol.*, 2010, **44**, 53–58.
- 98 N. Kvarnlöf and U. Germgård, *BioResources*, 2015, **10**, 3934–3947.
- 99 N. Qureshi, D. B. Hodge and A. Vertes, *Biorefineries: Integrated Biochemical Processes for Liquid Biofuels*, Newnes, 2014.
- 100 Christos Nitsos, Ulrika Rova, and Paul Christakopoulos, *Energies*, 2017, **11**, 50.
- 101 C. S. Lancefield, I. Panovic, P. J. Deuss, K. Barta and N. J. Westwood, *Green Chem.*, 2017, **19**, 202–214.
- 102 Z. Zhang, M. D. Harrison, D. W. Rackemann, W. O. S. Doherty and I. M. O’Hara, *Green Chem.*, 2016, **18**, 360–381.
- 103 A. Das, A. Rahimi, A. Ulbrich, M. Alherech, A. H. Motagamwala, A. Bhalla, L. da Costa Sousa, V. Balan, J. A. Dumesic, E. L. Hegg, B. E. Dale, J. Ralph, J. J. Coon and S. S. Stahl, *ACS Sustain. Chem. Eng.*, 2018, **6**, 3367–3374.
- 104 O. Gordobil, R. Moriana, L. Zhang, J. Labidi and O. Sevastyanova, *Ind. Crops Prod.*, 2016, **83**, 155–165.
- 105 L. Shuai, M. T. Amiri, Y. M. Questell-Santiago, F. Héroguel, Y. Li, H. Kim, R. Meilan, C. Chapple, J. Ralph and J. S. Luterbacher, *Science*, 2016, **354**, 329–333.
- 106 H. L. Trajano, N. L. Engle, M. Foston, A. J. Ragauskas, T. J. Tschaplinski and C. E. Wyman, *Biotechnol. Biofuels*, 2013, **6**, 110.
- 107 N. Giummarella, P. A. Lindén, D. Areskog and M. Lawoko, *ACS Sustain. Chem. Eng.*, 2020, **8**, 1112–1120.
- 108 L. Shuai, M. Talebi Amiri and J. S. Luterbacher, *Curr. Opin. Green Sustain. Chem.*, 2016, **2**, 59–63.
- 109 D. Kun and B. Pukánszky, *Eur. Polym. J.*, 2017, **93**, 618–641.
- 110 J. F. Kadla and S. Kubo, *Compos. Part Appl. Sci. Manuf.*, 2004, **35**, 395–400.
- 111 P. Alexy, B. Košíková and G. Podstránska, *Polymer*, 2000, **41**, 4901–4908.

-
- 112 R. Pucciariello, V. Villani, C. Bonini, M. D'Auria and T. Vetere, *Polymer*, 2004, **45**, 4159–4169.
- 113 M. Canetti and F. Bertini, *Compos. Sci. Technol.*, 2007, **67**, 3151–3157.
- 114 L. B. Tavares, N. M. Ito, M. C. Salvadori, D. J. dos Santos and D. S. Rosa, *Polym. Test.*, 2018, **67**, 169–176.
- 115 G. Stiubianu, M. Cazacu, M. Cristea and A. Vlad, *J. Appl. Polym. Sci.*, 2009, **113**, 2313–2321.
- 116 X. Dong, C. Lu, P. Zhou, S. Zhang, L. Wang and D. Li, *RSC Adv.*, 2015, **5**, 42259–42265.
- 117 M. Tanase-Opedal, E. Espinosa, A. Rodríguez and G. Chinga-Carrasco, *Materials*, 2019, **12**, 3006.
- 118 N. Mandlekar, A. Cayla, F. Rault, S. Giraud, F. Salaün and J. Guan, *Polymers*, 2019, **11**, 180.
- 119 V. Romhányi, D. Kun and B. Pukánszky, *ACS Sustain. Chem. Eng.*, 2018, **6**, 14323–14331.
- 120 S. Yang, Y. Zhang, T.-Q. Yuan and R.-C. Sun, *J. Appl. Polym. Sci.*, 2015, **132**, 42493.
- 121 X. Du, J. Li and M. E. Lindström, *Ind. Crops Prod.*, 2014, **52**, 729–735.
- 122 M. Graglia, J. Pampel, T. Hantke, T.-P. Feller and D. Esposito, *ACS Nano*, 2016, **10**, 4364–4371.
- 123 Z. Wang, J. W. Xue, J. B. Qu and W. X. Liu, 5.
- 124 G.-J. Jiao, Q. Xu, S.-L. Cao, P. Peng and D. She, *BioResources*, 2018, **13**, 1711–1728.
- 125 K. A. Y. Koivu, H. Sadeghifar, P. A. Nousiainen, D. S. Argyropoulos and J. Sipilä, *ACS Sustain. Chem. Eng.*, 2016, **4**, 5238–5247.
- 126 R. Ding, H. Wu, M. Thunga, N. Bowler and M. R. Kessler, *Carbon*, 2016, **100**, 126–136.
- 127 M. Abdollahi, R. Bairami Habashi and M. Mohsenpour, *Ind. Crops Prod.*, 2019, **130**, 547–557.
- 128 Y.-L. Chung, J. V. Olsson, R. J. Li, C. W. Frank, R. M. Waymouth, S. L. Billington and E. S. Sattely, *ACS Sustain. Chem. Eng.*, 2013, **1**, 1231–1238.
- 129 L.-Y. Liu, Q. Hua and S. Renneckar, *Green Chem.*, 2019, **21**, 3682–3692.
- 130 E. Larrañeta, M. Imízcoz, J. X. Toh, N. J. Irwin, A. Ripolin, A. Perminova, J. Domínguez-Robles, A. Rodríguez and R. F. Donnelly, *ACS Sustain. Chem. Eng.*, 2018, **6**, 9037–9046.

-
- 131 X. Liu, H. Yin, Z. Zhang, B. Diao and J. Li, *Colloids Surf. B Biointerfaces*, 2015, **125**, 230–237.
- 132 Y. S. Kim, W.-J. Youe, S. J. Kim, O.-K. Lee and S.-S. Lee, *J. Wood Chem. Technol.*, 2015, **35**, 251–259.
- 133 Y. Xu, L. Yuan, Z. Wang, P. A. Wilbon, C. Wang, F. Chu and C. Tang, *Green Chem.*, 2016, **18**, 4974–4981.
- 134 C. Gupta, M. J. Sverdlöve and N. R. Washburn, *Soft Matter*, 2015, **11**, 2691–2699.
- 135 M. Zhang and A. A. Ogale, *Carbon*, 2014, **69**, 626–629.
- 136 J. Sameni, S. Krigstin and M. Sain, 18.
- 137 H. Jeong, J. Park, S. Kim, J. Lee and J. W. Cho, *Fibers Polym.*, 2012, **13**, 1310–1318.
- 138 P. Buono, A. Duval, P. Verge, L. Averous and Y. Habibi, *ACS Sustain. Chem. Eng.*, 2016, **4**, 5212–5222.
- 139 S. Li, W. Xie, M. Wilt, J. A. Willoughby and O. J. Rojas, *ACS Sustain. Chem. Eng.*, 2018, **6**, 1988–1998.
- 140 Y. Lee, C.-H. Park and E. Y. Lee, *J. Wood Chem. Technol.*, 2017, **37**, 334–342.
- 141 L. Passauer, T. Hallas, E. Bäucker, G. Ciesielski, S. Lebiada and U. Hamer, *ACS Sustain. Chem. Eng.*, 2015, **3**, 1955–1964.
- 142 A. Duval and L. Avérous, *ACS Sustain. Chem. Eng.*, 2016, **4**, 3103–3112.
- 143 L.-Y. Liu, M. Cho, N. Sathitsuksanoh, S. Chowdhury and S. Renneckar, *ACS Sustain. Chem. Eng.*, 2018, **6**, 12251–12260.
- 144 I. Kühnel, J. Podschun, B. Saake and R. Lehnen, *Holzforschung*, 2014, **69**, 531–538.
- 145 R. J. Li, J. Gutierrez, Y.-L. Chung, C. W. Frank, S. L. Billington and E. S. Sattely, *Green Chem.*, 2018, **8**.
- 146 J. C. de Haro, C. Allegretti, A. T. Smit, S. Turri, P. D'Arrigo and G. Griffini, *ACS Sustain. Chem. Eng.*, 2019, **7**, 11700–11711.
- 147 M. Alinejad, C. Henry, S. Nikafshar, A. Gondaliya, S. Bagheri, N. Chen, S. K. Singh, D. B. Hodge and M. Nejad, *Polymers*, 2019, **11**, 1202.
- 148 D. Mahata, M. Jana, A. Jana, A. Mukherjee, N. Mondal, T. Saha, S. Sen, G. B. Nando, C. K. Mukhopadhyay and R. Chakraborty, *Sci. Rep.*, 2017, **7**, 1–16.
- 149 I. Panovic, J. R. D. Montgomery, C. S. Lancefield, D. Puri, T. Lebl and N. J. Westwood, *ACS Sustain. Chem. Eng.*, 2017, **5**, 10640–10648.
- 150 Y. Han, L. Yuan, G. Li, L. Huang, T. Qin, F. Chu and C. Tang, *Polymer*, 2016, **83**, 92–100.

-
- 151 H. Sadeghifar, R. Venditti, J. Jur, R. E. Gorga and J. J. Pawlak, *ACS Sustain. Chem. Eng.*, 2017, **5**, 625–631.
- 152 J. Podschun, A. Stücker, B. Saake and R. Lehnen, *ACS Sustain. Chem. Eng.*, 2015, **3**, 2526–2532.
- 153 S. Yang, J.-L. Wen, T.-Q. Yuan and R.-C. Sun, *RSC Adv.*, 2014, **4**, 57996–58004.
- 154 C. Gioia, G. Lo Re, M. Lawoko and L. Berglund, *J. Am. Chem. Soc.*, 2018, **140**, 4054–4061.
- 155 W. Lan, M. T. Amiri, C. M. Hunston and J. S. Luterbacher, *Angew. Chem. Int. Ed.*, 2018, **57**, 1356–1360.
- 156 G. R. Dick, J. Luterbacher, S. Bertella. European Patent EP19202957.7. Filed in October **2019**.
- 157 M. Talebi Amiri, G. R. Dick, Y. M. Questell-Santiago and J. S. Luterbacher, *Nat. Protoc.*, 2019, **14**, 921–954.
- 158 C. S. Lancefield, H. L. J. Wienk, R. Boelens, B. M. Weckhuysen and P. C. A. Bruijninx, *Chem. Sci.*, 2018, **9**, 6348–6360.
- 159 S. Kalami, N. Chen, H. Borazjani and M. Nejad, *Ind. Crops Prod.*, 2018, **125**, 520–528.
- 160 J. Li, J. Zhang, S. Zhang, Q. Gao, J. Li and W. Zhang, *Polymers*, 2017, **9**, 428.
- 161 M. Lettner, F. Hesser, B. Hedeler, P. Schwarzbauer and T. Stern, *J. Clean. Prod.*, 2020, **256**, 120520.
- 162 A. Tribot, G. Amer, M. Abdou Alio, H. de Baynast, C. Delattre, A. Pons, J.-D. Mathias, J.-M. Callois, C. Vial, P. Michaud and C.-G. Dussap, *Eur. Polym. J.*, 2019, **112**, 228–240.
- 163 M. Ghorbani, F. Liebner, H. W. G. van Herwijnen, L. Pfungen, M. Krahofer, E. Budjav and J. Konnerth, *BioResources*, 2016, **11**, 6727–6741.
- 164 M. Wang, M. Leitch and C. Xu, *Eur. Polym. J.*, 2009, **45**, 3380–3388.
- 165 S. Bertella and J. S. Luterbacher, *Trends Chem.*, 2020, **2**, 440–453.
- 166 F. Taleb, M. Ammar, M. ben Mosbah, R. ben Salem and Y. Moussaoui, *Sci. Rep.*, 2020, **10**, 11048.
- 167 M. Zhou, H. Shi, C. Li, X. Sheng, Y. Sun, M. Hou, M. Niu and X. Pan, *Ind. Eng. Chem. Res.*, 2020, **59**, 14296–14305.
- 168 J. Podschun, B. Saake and R. Lehnen, *Eur. Polym. J.*, 2015, **67**, 1–11.
- 169 G. R. Dick, A. O. Komarova and J. S. Luterbacher, *Green Chem.*, 2022, **24**, 1285–1293.

- 170 K. A. Goulas, M. Shiramizu, J. R. Lattner, B. Saha and D. G. Vlachos, *Appl. Catal. Gen.*, 2018, **552**, 98–104.
- 171 G. Foyer, B.-H. Chanfi, D. Virieux, G. David and S. Caillol, *Eur. Polym. J.*, 2016, **77**, 65–74.
- 172 D. S. Zijlstra, A. de Santi, B. Oldenburger, J. de Vries, K. Barta and P. J. Deuss, *J. Vis. Exp.*, 2019, 58575.
- 173 S. Wang, W.-X. Li, Y.-Q. Yang, X. Chen, J. Ma, C. Chen, L.-P. Xiao and R.-C. Sun, *ChemSusChem*, 2020, **13**, 4548–4556.
- 174 M. M. Abu-Omar, K. Barta, G. T. Beckham, J. S. Luterbacher, J. Ralph, R. Rinaldi, Y. Román-Leshkov, J. S. M. Samec, B. F. Sels and F. Wang, *Energy Environ. Sci.*, 2021, **14**, 262–292.
- 175 M. Wang, M. Leitch and C. (Charles) Xu, *Eur. Polym. J.*, 2009, **45**, 3380–3388.
- 176 M. Sultania, J. S. P. Rai and D. Srivastava, *Eur. Polym. J.*, 2010, **46**, 2019–2032.
- 177 V. G. Kontogianni, P. Charisiadis, A. Primikyri, C. G. Pappas, V. Exarchou, A. G. Tzakos and I. P. Gerothanassis, *Org. Biomol. Chem.*, 2013, **11**, 1013–1025.
- 178 X. Huang, J. M. Ludenhoff, M. Dirks, X. Ouyang, M. D. Boot and E. J. M. Hensen, *ACS Catal.*, 2018, **8**, 11184–11190.
- 179 W. Yang, L. Jiao, X. Wang, W. Wu, H. Lian and H. Dai, *Int. J. Biol. Macromol.*, 2021, **166**, 1312–1319.
- 180 L. Granado, R. Tavernier, S. Henry, R. O. Auke, G. Foyer, G. David and S. Caillol, *ACS Sustain. Chem. Eng.*, 2019, **7**, 7209–7217.
- 181 A. E. Vithanage, E. Chowdhury, L. D. Alejo, P. C. Pomeroy, W. J. DeSisto, B. G. Frederick and W. M. Gramlich, *J. Appl. Polym. Sci.*
- 182 W. Boerjan, J. Ralph and M. Baucher, *Annu. Rev. Plant Biol.*, 2003, **54**, 519–546.
- 183 N. Alwadani and P. Fatehi, *Carbon Resour. Convers.*, 2018, **1**, 126–138.
- 184 S. A. Gundersen and J. Sjöblom, *Colloid Polym. Sci.*, 1999, **277**, 462–468.
- 185 C. Xu and F. Ferdosian, in *Conversion of Lignin into Bio-Based Chemicals and Materials*, eds. C. Xu and F. Ferdosian, Springer, Berlin, Heidelberg, 2017, pp. 81–90.
- 186 A. K. Soares, D. A. Gatto, W. L. E. Magalhães, X. Erdocia, M. A. U. Gutiérrez, R. A. Delucis and A. L. Missio, *J. Wood Chem. Technol.*, 2021, **41**, 199–209.
- 187 J. Ruwoldt, *Surfaces*, 2020, **3**, 622–648.
- 188 J. Ruwoldt, J. Planque and G. Øye, *ACS Omega*, 2020, **5**, 15007–15015.

-
- 189 J. Zhang, Y. Ge, L. Qin, W. Huang and Z. Li, *J. Dispers. Sci. Technol.*, 2018, **39**, 1140–1143.
- 190 N. Ghavidel and P. Fatehi, *Langmuir*, 2021, **37**, 3346–3358.
- 191 Z. Zhang, Y. Zhang, Z. Lin, A. Mulyadi, W. Mu and Y. Deng, *Chem. Eng. Sci.*, 2017, **165**, 55–64.
- 192 J. Ou, Z. Kong, R. Yang and Z. Dai, *J. Dispers. Sci. Technol.*, 2021, **0**, 1–8.
- 193 C. Gupta and N. R. Washburn, *Langmuir*, 2014, **30**, 9303–9312.
- 194 S. Gharehkhani, N. Ghavidel and P. Fatehi, *ACS Sustain. Chem. Eng.*, 2019, **7**, 2370–2379.
- 195 Y. M. Questell-Santiago, R. Zambrano-Varela, M. Talebi Amiri and J. S. Luterbacher, *Nat. Chem.*, 2018, **10**, 1222–1228.
- 196 S. Bertella and J. S. Luterbacher, *Green Chem.*, 2021, **23**, 3459–3467.
- 197 A. I. Benítez-Mateos, S. Bertella, J. Behaghel de Bueren, J. S. Luterbacher and F. Paradisi, *Chemsuschem*, 2021, **14**, 3198–3207.
- 198 D. S. Zijlstra, C. W. Lahive, C. A. Analbers, M. B. Figueirêdo, Z. Wang, C. S. Lancefield and P. J. Deuss, *ACS Sustain. Chem. Eng.*, 2020, **8**, 5119–5131.
- 199 N. Ghavidel and P. Fatehi, *ChemSusChem*, 2020, **13**, 4567–4578.
- 200 A. Moreno, M. Morsali, J. Liu and M. H. Sipponen, *Green Chem.*, 2021, **23**, 3001–3014.
- 201 X. Ouyang, L. Ke, X. Qiu, Y. Guo and Y. Pang, *J. Dispers. Sci. Technol.*, 2009, **30**, 1–6.
- 202 N. Delgado, F. Ysambertt, G. Chávez, B. Bravo, D. E. García and J. Santos, *Waste Biomass Valorization*, 2019, **10**, 3383–3395.
- 203 C. Shi, S. Zhang, W. Wang, R. J. Linhardt and A. J. Ragauskas, *ACS Sustain. Chem. Eng.*, 2020, **8**, 22–28.
- 204 N. Migliore, D. S. Zijlstra, T. G. Van Kooten, P. J. Deuss and P. Raffa, *ACS Appl. Polym. Mater.*, 2020, **2**, 5705–5715.
- 205 Z. Zhao, W. Wang, J. Xiao, Y. Chen and Y. Cao, *Nanomaterials*, 2020, **10**, 1068.
- 206 A. N. Evdokimov, A. V. Kurzin, O. V. Fedorova, P. V. Lukanin, V. G. Kazakov and A. D. Trifonova, *Wood Sci. Technol.*, 2018, **52**, 1165–1174.
- 207 E. Schuler, M. Demetriou, N. R. Shiju and G.-J. M. Gruter, *ChemSusChem*, 2021, **14**, 3636–3664.
- 208 K. Isobe, *Biosci. Biotechnol. Biochem.*, 1995, **59**, 576–581.

- 209 L. Manker, G. Dick, A. Demongeot, M. Hédou, C. Rayroud, T. Rambert, M. Jones, I. Sulaeva, Y. Leterrier, A. Potthast, F. Maréchal, V. Michaud, H.-A. Klok and J. Luterbacher, ChemRxiv, 2021. This content is a preprint and has not been peer-reviewed.
- 210 S. Bertella and J. S. Luterbacher, *Trends Chem.*, 2020, **2**, 440–453.
- 211 J. Sternberg, O. Sequerth and S. Pilla, *Prog. Polym. Sci.*, 2021, **113**, 101344.
- 212 K. Y. Lee and D. J. Mooney, *Chem. Rev.*, 2001, **101**, 1869–1880.
- 213 P. Karami, C. S. Wyss, A. Khoushabi, A. Schmocker, M. Broome, C. Moser, P.-E. Bourban and D. P. Pioletti, *ACS Appl. Mater. Interfaces*, 2018, **10**, 38692–38699.
- 214 M. Suneetha, K. M. Rao and S. S. Han, *ACS Omega*, 2019, **4**, 12647–12656.
- 215 Y. Li, J. Rodrigues and H. Tomás, *Chem Soc Rev*, 2012, **41**, 2193–2221.
- 216 R. Naomi, H. Bahari, P. M. Ridzuan and F. Othman, *Polymers*, 2021, **13**, 2319.
- 217 S. Giraudier, D. Hellio, M. Djabourov and V. Larreta-Garde, *Biomacromolecules*, 2004, **5**, 1662–1666.
- 218 Z. Yang, S. Chaieb and Y. Hemar, *Polym. Rev.*, 2021, **61**, 765–813.
- 219 A. Ehrmann, *Polymers*, 2021, **13**, 1973.
- 220 C. S. Wyss, P. Karami, A. Demongeot, P.-E. Bourban and D. P. Pioletti, *Soft Matter*, 2021, **17**, 7038–7046.
- 221 T. Huang, Z. Tu, X. Shangguan, X. Sha, H. Wang, L. Zhang and N. Bansal, *Trends Food Sci. Technol.*, 2019, **86**, 260–269.
- 222 Y. Liu, S. Cheong NG, J. Yu and W.-B. Tsai, *Colloids Surf. B Biointerfaces*, 2019, **174**, 316–323.
- 223 M. Balakshin and E. Capanema, *J. Wood Chem. Technol.*, 2015, **35**, 220–237.
- 224 A. M. Sisso, M. O. Boit and C. A. DeForest, *J. Biomed. Mater. Res. A*, 2020, **108**, 1112–1121.
- 225 R. Kale and A. Bajaj, *J. Young Pharm. JYP*, 2010, **2**, 90–94.
- 226 P. Karami, N. Nasrollahzadeh, C. Wyss, A. O’Sullivan, M. Broome, P. Procter, P.-E. Bourban, C. Moser and D. P. Pioletti, *Macromol. Rapid Commun.*, 2021, **42**, 2000660.
- 227 C. F. Guimarães, L. Gasperini, A. P. Marques and R. L. Reis, *Nat. Rev. Mater.*, 2020, **5**, 351–370.
- 228 R. Kaur, S. K. Uppal and P. Sharma, *Sugar Tech*, 2017, **19**, 675–680.
- 229 J. Behaghel de Bueren, F. Héroguel, C. Wegmann, G. R. Dick, R. Buser and J. S. Luterbacher, *ACS Sustain. Chem. Eng.*, 2020, **8**, 16737–16745.

Curriculum Vitae

Contact Information

Address Rue des Amis 7, 1018 Lausanne, Switzerland

Email stefania.bertella@epfl.ch

Languages

Italian Mother Tongue

English Advanced

French Intermediate

Swedish Elementary

Education

April 2018 **PhD in Chemistry and Chemical Engineering**

June 2022 École polytechnique fédérale de Lausanne (EPFL). Route Cantonale, 1015 Lausanne, Switzerland

October 2012 **Master's Degree in Chemistry**

July 2015 University of Parma, Department of Chemistry
Parco Area delle Scienze 17/A, 43124, Parma, Italy

September 2009 **Bachelor's Degree in Chemistry**

October 2012 University of Parma, Department of Chemistry
Parco Area delle Scienze 17/A, 43124, Parma, Italy

September 2004 **High School Diploma**

July 2009 Liceo Classico "Rinaldo Corso"
Via Roma, 15, 42015, Correggio (RE), Italy

Employment history

May 2016 **R&D Laboratory Engineer**

March 2018 Stora Enso AB, Innovation Centre for biomaterials.
Fannys Väg 1, 13104, Nacka, Sweden

September 2015 **R&D Laboratory Assistant**

April 2016 Rexnord FlatTop Europe s.r.l.
Via dell'Industria 4, 42015, Correggio (RE), Italy

February 2014 **Master Student Researcher**

August 2014 University of Jyväskylä, Department of Chemistry,
P.O. Box 35, FI-40014, Jyväskylä, Finland

Scientific Publications

- **S. Bertella**, V. Kumar Rana, P. Karami, Ł. Richter, F. Stellacci, D. Pioletti, J. Luterbacher, Extraction of bi-functionalized lignin for controlling properties of gelatin-based hydrogels, *manuscript in preparation*.
- **S. Bertella**, M. Bernardes Figueirêdo, G. De Angelis, M. Mourez, C. Bourmaud, E. Amstad, J. Luterbacher, Extraction and Surfactant Properties of Glyoxylic Acid Functionalized Lignin, *ChemSusChem*, **2022**.
- **S. Bertella**, J. Luterbacher, Simultaneous extraction and controlled chemical functionalization of hardwood lignin for improved phenolation, *Green Chem.*, **2021**, 23, 3459.
- **S. Bertella**, J. Luterbacher, Lignin Functionalization for the Production of Novel Materials, *Trends in Chemistry*, **2020**, 2, 440.
- A.I. Benítez-Mateos, **S. Bertella**, J. Behaghel de Bueren, J. Luterbacher, F. Paradisi, Dual revalorization of lignin through its use as a versatile and renewable matrix for enzyme immobilization and (flow) bioprocess engineering, *ChemSusChem*, **2021**, 14, 3198-3207.
- M. T. Amiri, **S. Bertella**, Y. M. Questell-Santiago and J. S. Luterbacher, Establishing Lignin Structure-Upgradeability Relationships Using Quantitative ^1H - ^{13}C Heteronuclear Single-Quantum Coherence Nuclear Magnetic Resonance (HSQC-NMR) Spectroscopy, *Chem. Sci.*, **2019**, 10, 8135.
- F. Pan, N.K. Beyeh, **S. Bertella**, K. Rissanen, Anion Binding and Exchange Properties of Trifluoroacetate and Triflate Salts of N-Alkyl Ammonium Resorcinarenes, *Chem. Asian J.*, **2016**, 11, 782.

Patents

- **S. Bertella**, A. Komarova, S. Sun, J. Luterbacher, Biobased surfactants. European Patent EP22167726.3. Filed in **April 2022**.
- G. R. Dick, J. Luterbacher, **S. Bertella**, Production of fragments of lignin with functional groups. European Patent EP19202957.7. Filed in **October 2019**.
- L. P. Manker, J. Luterbacher, **S. Bertella**, G. R. Dick, Renewable monomer and polymer thereof. European Patent EP19203000.5. Filed in **October 2019**.

Conferences and presentation

- 2019** NRG2019: Energy Systems: managing the transition to renewables, Champéry (Switzerland). Poster presented: New materials from functionalized lignin oligomers.
- 2020** SCS Fall Meeting, online conference. Oral presentation: Simultaneous extraction and controlled chemical modification of polymeric lignin from hardwood.
- 2020** Virtual AIChE Annual Meeting, online conference. Oral presentation: Simultaneous extraction and controlled chemical modification of lignin from hardwood.
- 2021** ACS Fall National Meeting, online conference. Oral presentation: Single-step extraction of multifunctionalized lignins from biomass.
- 2021** AIChE Annual Meeting, Boston, MA. Oral presentation: One-step extraction of

multifunctionalized lignins from biomass.

- 2022** Lignin Conference GRC, Easton, MA. Poster presented: Unlocking the potential of lignin in material applications through its simultaneous isolation and multifunctionalization.

Awards

- SCNAT / SCS Chemistry Travel Awards 2022 (1000 CHF)
- NASA Space App Challenge 2018, Local People's Choice winner (Lausanne) and Global Finalist nominee for the most inspirational idea

Teaching and Mentoring

- 2020-2021** Supervisor of Anna Bosch Rico in her Master project in Molecular & Biological Chemistry at EPFL (6 months)
- 2021** Supervisor of Malcolm Mourez in his Master project in Molecular & Biological Chemistry at EPFL (6 months)
- 2021** Teacher Assistant in Chemical Engineering lab & Project at EPFL (80h)
- 2020** Teacher Assistant in Heterogeneous Reaction Engineering at EPFL (42h)
- 2020** Teacher Assistant in Chemical Engineering lab & Project at EPFL (144h)
- 2019** Teacher Assistant in Chemical Engineering lab & Project at EPFL (130h)
- 2018** Teacher Assistant in Chemical Engineering lab & Project at EPFL (130h)
- 2015** Student Tutor in the Chemistry Department at the University of Parma
- 2015** Assistant in Organic Chemistry laboratory course at the University of Parma

Institutional Responsibilities

- 2018-2022** Safety Delegate (COSEC) of the Laboratory of Sustainable and Catalytic Processing at EPFL
- 2016-2018** Safety and Work Environment representative at the Innovation Centre for biomaterials at Stora Enso
- 2014-2015** Student delegate in the Council of the Department of Chemistry at the University of Parma
- 2014-2015** Student delegate in the Council of the School of Chemistry at the University of Parma
- 2014-2015** Member of the Committee for Self-evaluation of the teaching activities of the master's degree in chemical science at the University of Parma

Main Technical Skills

- Traditional and inert atmosphere organic synthesis
- Operating glass batch reactors up to 10 L for process scale-up.
- Operating and troubleshooting batch and continuous-flow high-pressure reactors
- Rheological and mechanical testing of materials

- Analytical techniques: GC, GC-MS and HPLC, FT-IR, NMR
- Softwares: Microsoft Office 365 (Word, PowerPoint, Excel etc..), Adobe (Photoshop, Illustrator, Premiere Pro), TopSpin for NMR data analysis, ChemDraw

Interests and other extracurricular activities

- Composer and musician (guitar, banjo, keyboard, percussions and voice)
- Guitarist at Rockin'1000. Player at the concerts in Commerzbank Arena (Frankfurt, 2019) and Linate Airport (Milan, 2019). Holder of the world record for "largest performing rock band" certified by Rekord-Institut für Deutschland in Frankfurt on July 7th, 2019.
- Member of the EPFL association "The Catalyst" since 2018. Musician at improvisation theater shows.
- Organizers of the Scientific Film Hackaton (SciFilmIt) event at the EPFL/UNIL campus in July 2021. Musician and composer for the produced short movies.